Phase transitions and adjacent phenomena in simple atomic systems

R S Berry, B M Smirnov

Contents

Abstract. Clusters and bulk systems of bound atoms with pairwise interactions have two types of excitations: configurational, due to a change in the atomic arrangement in space, and thermal, associated with atomic vibrations. The configurational excitation is responsible for phase transitions in such systems and can be considered as a transition from the global minimum of the atomic potential energy surface in a multidimensional space of atomic coordinates to some other, higher-energy local minima. From this standpoint, various aspects of aggregate states of atomic clusters are considered, including coexistence of the liquid and solid cluster phases, the freezing point as the temperature of transition from the metastable liquid state to the unstable state, the glassy states as unstable configurationally excited states with long lifetimes, and the phase transition under high pressures when the crystal lattice for the distribution of atoms is no longer the most stable form for the solid state. The concept of voids as elementary internal configurational excitations of a macroscopic atomic system, which are connected with local minima of the potential energy surface, allows us to consider the glassy – solid transition and processes of the growth of nuclei of a new phase as a result of void transport. The degrees of deviation from traditional macroscopic thermodynamics for clusters and bulk systems near a phase transition is analyzed. It is shown that the thermal motion of atoms makes a significant contribution to the entropy jump at the phase transition, which allows us to use the Lindemann criterion for the phase transition and other criteria which use parameters of thermal motion of atoms, even though the inherent nature of the phase transition is determined by configurational excitation.

R S Berry Department of Chemistry, University of Chicago,
5735 South Ellis Av., Chicago, IL 60637, USA,
Tel. 01 773 702 7021
Fax 01 773 834 4049
E-mail: berry@uchicago.edu
B M Smirnov Institute for High Temperatures,
Russian Academy of Sciences
Izhorskaya ul. 13/19, 127412 Moscow, Russian Federation
Tel./Fax (7-095) 190 42 44
E-mail: smirnov@oivtran.iitp.ru

1. Introduction

The subjects of this discussion are large simple clusters, i.e., ensembles of units consisting of a large number of bound atoms with pairwise interactions between them, and the related bulk systems of bound atoms that can be considered as clusters with arbitrarily large numbers of atoms. We will analyze the aggregate states of such systems of bound atoms and phase transitions in these clusters. Computer simulation of clusters has deepened our understanding of the phase

transitions and allowed us to consider the microscopic nature of this phenomenon and adjacent phenomena. At first we note that from the standpoint of classical thermodynamics [1 – 6], the solid – liquid phase transition in a bulk system of bound atoms proceeds at a characteristic temperature by a jump and is a first-order phase transition according to the thermodynamic classification. That is, the transition involves a nonzero change of energy and entropy as the system goes from one phase to the other. Computer simulations of clusters reveal coexistence of the solid and liquid phases [7 – 10] over some temperature range that makes the phase transition richer than that of bulk matter and seems to lie outside the traditional thermodynamic classification of phase transitions in order, depending on what thermodynamic quantities display discontinuities. Classical thermodynamics [1 – 6] divides phase transitions into (at least) two fairly well separated classes, first-order and second-order, according to the behavior of parameters such as entropy, enthalpy, and heat capacity at the transition temperature. However, the distinction between these, and even the nature of the phase change itself, becomes a much richer subject for small systems.

In considering large clusters and bulk systems of bound atoms from a general standpoint, and basing our interpretations on computer simulations of clusters, we use the same concepts and description for both these systems. Then we retain some traditional concepts and parameters for cluster description such as the entropy, temperature, and thermodynamic potentials, but omit others, such as the surface tension. As a result, one can understand the character of transition from finite clusters to infinite (or very large) systems and understand peculiarities of the microscopic nature of the phase transition. In particular, although atoms are complex particles with a shell structure, they cannot exhibit phase transitions, but phase changes do take place in many sorts of clusters. The reason for this follows from the analysis that we will give below.

We concentrate on clusters consisting of classical atoms, such as clusters of Ne, Ar, Kr, and Xe. One can consider these clusters in terms of atomic motion in any of the potential wells that result from atomic interactions. This approach opened the study of the behavior of such clusters; it was first revealed in computer calculations of the cluster energy [11, 12]. In order to find the minimum of a cluster's internal energy and the optimal configuration of its atoms, one can start from an arbitrary atomic configuration, calculate the cluster's energy for this configuration, and then move to a new atomic configuration with lower energy. In this manner, one can hope to reach the global minimum of the cluster's effective potential energy which must relate to the optimal atomic configuration at zero temperature. But this approach is not easily realized because a typical cluster potential energy surface has many local minima. For example, the Lennard-Jones cluster consisting of 13 atoms (a cluster with the Lennard-Jones interaction potential between atoms) was characterized by 988 local minima on its potential energy surface [11, 12]; a later, more detailed analysis [13] found 1478 local minima and 17357 saddle points of the potential energy surface for just the same Lennard-Jones cluster of 13 atoms. The number of geometrically distinct local minima increases at least exponentially with the number of particles in the cluster [14, 15]. The number of permutational isomers for each of these increases approximately as the factorial of the number of atoms comprising the cluster. Of course, the neighboring local minima of the multidimensional potential

energy surface are separated by barriers characterized by saddle points.

Understanding the behavior of such a classical cluster is a natural subject for simulation by molecular dynamics or Monte Carlo methods. The evolution of this system consists of the passage of atoms from the vicinity of certain local minima of the potential surface to neighboring minima [10, 16 – 19]. Studying the corresponding saddle-crossing dynamics [20] is a convenient method for analyzing cluster evolution. Assuming the dwell time of a system near one minimum of the potential surface is long compared with the time required to thermalize atomic vibrations in that local minimum, we can divide the atomic energy into two parts [21]. The first part is the thermal energy of atomic vibrational (and rotational) motion, while the second, configurational, part is that of the local minimum of the potential surface in whose region the system resides. At zero temperature, the only energy of the (classical) system is the configurational energy of the system at its global minimum on the potential surface. (Here, we do not treat clusters of helium atoms or of very cold neon atoms, which must be analyzed in quantum-mechanical terms.)

The possibility of dividing the atomic energy into a thermal, vibrational energy and configurational excitation opens a powerful way to approach many-body dynamics. One can explain the nature of a phase transition for a system of bound atoms within the framework of this concept, using a lattice model [3, 22 – 24], with the atoms located at the sites of a lattice. The model becomes particularly straightforward to use if one assumes that only nearest-neighbor atoms interact. We demonstrate this fact in Fig. 1 where atoms are located at sites of the square lattice. This model shows two different kinds of atomic distributions: the compact ordered state in which the total binding energy of atoms is maximum, and a disordered atomic distribution in which atoms may be anywhere on the lattice. The latter state is characterized by a lower binding energy than the ordered state, but there are many ways to achieve such a distribution, so the statistical weight of the disordered distribution and, hence, its entropy are large. Therefore, at a certain temperature such a system can exhibit an order – disorder phase transition, and for a system of a large number of atoms this transition appears as a jump in the internal energy or enthalpy and in the entropy at a certain temperature at which the free energies of the two forms are equal. Thus, the lattice model exhibits the nature of the first-order phase transition in a system of a large number of bound atoms; this order – disorder transition models the solid – liquid transition in real systems.
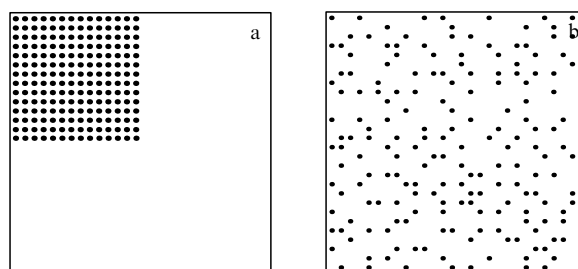

Figure 1. Distributions of particles over sites of the square lattice within the framework of the lattice model [24]. (a) The ordered (compact) distribution of atoms, and (b) the disordered (random) distribution of atoms.

As an elementary configurational excitation we examine a void [25] or empty lattice site; we may think of this as a perturbed (or relaxed) vacancy, but in contrast to a vacancy in a solid, a void has an indefinite volume and shape that change in time. Therefore, from the standpoint of saddle-crossing dynamics, each configurationally excited state corresponds to a certain number of voids. The concept of an average void is useful when configurational excitation of atoms can be separated from the vibrational excitation associated with an increase in the kinetic energy of the atoms. We then define the cluster's aggregate state as a set of its configurations in the multidimensional space of atomic coordinates near the relevant local minima of the potential surface, with their nearby thermal excitation energies. This aggregate state can be thought of as the collection of all the configurational states in a chosen energy band, together with the vibrational excitations of those configurations. This differs from the concept of 'state' in traditional thermodynamics in which the phase is characterized by a uniform (mean) spatial distribution of atoms, i.e., an excited aggregate thermodynamic state includes many elementary configurational excitations. In the cluster case, the liquid aggregate state can contain even one elementary excitation (which can migrate, of course), and hence uniformity (in the sense of inclusiveness) is not a requirement for the cluster aggregate state. Within the framework of the void concept, one can describe coexistence of the solid and liquid phases in a cluster as a result of the formation and decay of voids. Hence, the hierarchy of times for the establishment of thermal equilibrium, the lifetimes of aggregate states, and typical times of cluster interaction with an environment must be allowed for in analyzing cluster phase transitions, and we give some examples of this below.

By separating configurational excitation from thermal, and introducing an elementary configurational excitation, we transform basic thermodynamic concepts of the phase or the aggregate states of clusters to a larger, more flexible mode. Simply because its behavior is not dominated by very large numbers of particles, a cluster is more complex than a bulk system and can exhibit several aggregate states, but in many cases only two aggregate states may be of importance in a given temperature range. (Ensembles of homogeneous clusters of a single size may, for example, exhibit more than two phases in equilibrium [10].) Hence, we will keep the approach of two aggregate states, and the phase transition can be described by the same parameters as in classical thermodynamics, i.e., the cluster's melting point T_m, the change of the cluster energy ΔE, and the entropy ΔS characterize the cluster phase transition. In this work, by T_m we mean the temperature at which the free energies of the solid and liquid clusters are equal. These cluster parameters can be determined on the basis of cluster simulations by methods of molecular dynamics or can be taken from the experiment.

Of course, a more detailed description of cluster excitations can lead to apparent contradictions with a traditional thermodynamic description of the phase transitions. As an illustration we refer to one specific criterion of a phase transition. According to a widely used Lindemann criterion [26, 27], bulk melting proceeds at a temperature at which the ratio of the mean atomic oscillation amplitude to the distance between nearest neighbors reaches a certain value, typically $10 - 15\%$. Development of numerical methods for computer cluster simulation gave new criteria of cluster melting on the basis of the Etters – Kaelberer parameter [28 – 30] or the

closely related Berry parameter [9, 31] which bases this fluctuation on pair correlations in the positions of atoms. These parameters also experience a jump when a system melts, and, along with the Lindemann criterion, they directly reflect the change in thermal atomic motion under melting, while the melting results from configurational excitation of an ensemble that opens the system to mobility and large-amplitude motions of the atoms. Hence, there is an apparent disconnection between the origin of the melting transition in ensembles of bound atoms due to configurational excitation and practical criteria that indicate the onset of this transition based on the thermal motion of atoms. Below, we analyze this paradox within the framework of the void concept of configurational excitation of clusters and find that the entropy jump ΔS as a result of the phase transition includes, in addition to its configurational contribution, a thermal part, because the transition from the compact solid state to the loose liquid state allows thermal motion of atoms to make a more significant contribution to the entropy jump ΔS at the melting point, and the magnitude of this effect increases with increasing temperature. This justifies applying the melting criteria based on the thermal motion of atoms, but we need to be aware of the connection between the thermal and configurational degrees of freedom in the melting transition.

The void concept of configurational excitation allows us to analyze the phase transition in condensed inert gases from the standpoint of void formation [32 – 36]. This enables us to interpret various aspects of a given phase transition. In particular, the liquid curve of the dependence of the internal energy on the temperature terminates at the point at which the liquid state's *local minimum* in this curve disappears; this is analogous to the low-temperature spinodal point, well below the classical point of equilibrium of the two phases [37]. Below this temperature the metastable liquid aggregate state does not exist. One can see an analogy of configurationally excited cluster states at low temperatures with glassy states [38]. This allows us to analyze glassy states in inert gases at low temperatures and in clusters [36, 39, 40]. The transport of voids also determines the character of transport phenomena in liquid bulk systems of bound atoms; this is especially conveniently studied using systems with pairwise atomic interactions. Displacement of an individual atom results from its transition to a neighboring minimum of the potential energy surface, and this displacement is on the order of the interatomic distance. Therefore, any atomic displacement over large distances has the nature of a diffusion. This process is closely connected with nucleation phenomena, because growth of a new phase in the old one may be considered a result of void transport. Hence, considering the liquid state as a configurationally excited state of an ensemble of bound atoms, the state that, in turn, results from the formation of voids inside the system, we can analyze from a general standpoint a circle of properties and processes in a configurationally excited ensemble of bound atoms. Such an analysis is a goal of this review.

2. Structures of solid clusters

2.1 Configurations of atoms in solid clusters with pairwise atomic interactions

In considering a cluster as a system of bound atoms, we base our approach on the concept that two types of cluster excitations, configurational and vibrational, are separable.

Indeed, each local minimum on the potential energy surface of this cluster in a space of atomic coordinates corresponds to a specific atomic configuration, i.e., to a certain configurational state of the cluster, with its own excitation energy. Along with this, atoms execute a vibrational motion near each local minimum of the potential energy surface, and the amplitudes of these vibrations characterize the degree of thermal excitation of cluster atoms. We assume an equilibrium for the thermal motion of atoms and describe a thermal cluster state by a certain translational (transverse) temperature of cluster atoms. This means that thermal equilibrium is established rapidly compared with transition to another local minimum of the cluster's potential energy. Thus, we suppose that we can separate the configurational and vibrational excitations and characterize the latter by a definite temperature.

We focus below on a pairwise interaction between atoms as the simplest case of interactions in a system of bound atoms. In this case one can express the cluster's energy parameters in terms of parameters of the interaction potential of two isolated atoms. If we proceed to the limit of zero temperature in the sense of zero energy of thermal excitation, only configurational excitation of the cluster takes place; we will analyze the configurational excitation of the cluster in this manner. In considering clusters with pair interactions between atoms, we will be guided by clusters of inert gases for which the interaction potential between neighboring atoms is small compared to the typical energy of the electronic excitation in the atom. Because of the weakness of interaction between these atoms, we ignore three-body and many-body interactions. This simplifies the problem and allows one to ascertain the influence of short-range and long-range interactions on the properties of a system of many bound atoms.

At zero and low temperatures, clusters form regular structures, some of which can be found in bulk crystalline solids. One can construct such clusters by cutting them out of a bulk crystal. Altogether there are 230 space groups of symmetry for crystalline lattices [41], and hence clusters can have any one of these depending on the character of interaction inside the system. Clusters have their greatest stability at sizes corresponding to completed structures composed of 'magic numbers' of atoms. Magic numbers of solid clusters may be recognized from local maxima in the mass spectra of clusters [42–48]. The optimal cluster structures themselves for these magic numbers have been determined from electron diffraction experiments [49–54], although the interpretation of electron diffraction spectra of clusters is associated with some challenges [55, 56]. Magic numbers are reflected in other cluster properties, in particular, in ionization spectra [57–59]. Magic numbers are important in the way they influence various cluster properties: the binding energy of a surface atom, the ionization potential, the electron affinity, and other cluster parameters have local maxima at magic numbers of atoms, at which a cluster has the greatest stability. Magic numbers disappear in the liquid aggregate states because these exhibit monotonic dependence of their parameters on their size. This effect is used for determining the cluster melting point [60, 61].

Below, we restrict our discussion to two close-packed crystal structures that result from a pair interaction potential, when the short-range interaction dominates a system of many bound atoms. These are of course the face-centered cubic and hexagonal crystal lattices. In these, each internal atom of the lattice has 12 nearest neighbors, i.e., the maximal possible number of nearest neighbors. We now examine these structures and analyze their energy parameters.

Guided by this pairwise interaction model, we also consider the limiting case in which there is no long-range interaction between atoms. Since only nearest neighbors interact in this case and all the distances between nearest neighbors are identical in ensembles with close-packed structures, the total binding energy of atoms E_b in such clusters at zero temperature is proportional to the total number k of bonds between nearest neighbors [62, 33]:

$$E_b = kD,\qquad(2.1)$$

where D is the bond dissociation energy. Since the total energy of such a cluster is $E = -E_b$, one can introduce the surface energy of such a cluster consisting of n atoms in the following way:

$$E_{sur} = E + 6nD.\qquad(2.2)$$

When a long-range interaction is present, the binding energy per atom ε_0 exceeds that $(6D)$ in the case of a short-range interaction of atoms, and formula (2.2) takes the form

$$E = -\varepsilon_0 n + E_{sur}.\qquad(2.3)$$

In the limit of large clusters (with $n \to \infty$), for which the cluster surface energy is proportional to the cluster surface which, in turn, is proportional to $n^{2/3}$, formula (2.3) becomes the asymptotic form

$$E = -\varepsilon_0 n + An^{2/3},\qquad(2.4)$$

where A is the specific surface energy. This formula is an expansion of the cluster energy in terms of a small parameter $n^{-1/3}$ [63] for a large cluster ($n \gg 1$), when the number of surface atoms is small compared to the total number of atoms. Their ratio appears as a small parameter of the theory.

In reality, $E(n)$ has a nonmonotonic dependence on n due to the varying structures of incomplete cluster shells. One can ascribe this to the surface energy and define in this manner the function $A(n)$ as a nonregular function in accordance with formula (2.4). With such a definition, we have

$$A(n) = \frac{\varepsilon_0 n + E}{n^{2/3}}.\qquad(2.5)$$

Like crystalline particles whose optimal shape is determined by the character of atomic interactions, the configuration of cluster atoms is determined by parameters of the pair interaction potential in the case under consideration. Atoms of a solid cluster are distributed over cluster shells or layers, and joining new atoms to a cluster proceeds through filling such shells or layers. In contrast to bulk particles, edge and vertex atoms make a nonnegligible contribution to the cluster energy. Optimal atomic configurations correspond to closed cluster shells, layers, or facets; these are the configurations that correspond to magic numbers of atoms.

Bulk particles and clusters of a given crystalline structure can form different geometric figures. Which one is optimal depends on the parameters of the pair interaction. The energy parameters of a cluster with open shells are sensitive to the filling of certain shells or layers. The optimal cluster structure results from competition among several cluster shapes even when only one crystalline structure is realized. The competi-

tion among cluster shapes for close-packed structures is the focus of the analysis we make next.

2.2 Clusters of the face-centered cubic structure

Clusters of a given structure can be cut off from a crystal lattice of this structure. Considering a cluster with the face-centered cubic (fcc) structure, we use as a basis the fcc crystal lattice. If we take an atom of the fcc lattice or the middle of an elementary cell as an origin of the reference frame and place some atoms on the axes of this reference frame, the fcc crystal will possess the corresponding symmetry, so that this crystal lattice is conserved as a result of the following transformations

$$x \longleftrightarrow y \longleftrightarrow z; \quad x \longleftrightarrow -x; \quad y \longleftrightarrow -y; \quad z \longleftrightarrow -z, \tag{2.6}$$

where x, y, z are the coordinates of atoms. Note that we have two types of fcc crystal lattices, depending on the position of the origin of a reference frame. The origin can be placed either in the center of an elementary cell or at an atom of the lattice. Thus, there are two types of fcc clusters, with and without a central atom.

Taking planes {100} (in accordance with a general notation [41]) as the planes of the reference frame, we obtain the 12 nearest neighbors of a test atom with coordinates x, y, z, whose coordinates are

$$x, y \pm \frac{a}{\sqrt{2}}, \quad z \pm \frac{a}{\sqrt{2}}, \quad \text{or} \quad x \pm \frac{a}{\sqrt{2}}, \quad y, z \pm \frac{a}{\sqrt{2}},$$
$$\text{or} \quad x \pm \frac{a}{\sqrt{2}}, \quad y \pm \frac{a}{\sqrt{2}}, \quad z, \tag{2.7}$$

where a is the distance between nearest neighbors. It is convenient to introduce reduced values for atomic coordinates, expressing them in units of $a/\sqrt{2}$. Then the coordinates z, x, y of each an atom are integers, and the 12 nearest neighbors of an atom with coordinates x, y, z have the following reduced coordinates:

$$x \pm 1, \quad y \pm 1, z; \quad x \pm 1, y, z \pm 1; \quad x, y \pm 1, z \pm 1. \tag{2.8}$$

If we choose an atom to be at the origin, then the 12 neighbors combine into the three sets of four atoms lying at the centers of the four square faces surrounding the central atom, in each of the three mutually perpendicular 100 planes.

We define a cluster shell of a system of atoms whose positions go over into one another as a result of transformations (2.6). Thus, the coordinates of atoms of one shell differ by the sign of one or more coordinates and by the transposition of coordinates z, x, y. We see that the maximum number of atoms in one shell is equal to $6 \times 2 \times 2 \times 2 = 48$. Next, a shell is closed if any transformation (2.6) transfers a test atom into an initially occupied position. The number of atoms that gives a cluster a closed outer atomic shell is a magic number.

Let us formulate a method for constructing a cluster of the fcc structure with the maximum binding energy for a given number of cluster atoms with a short-range interaction potential [33, 62, 64, 65]. The optimal configuration of atoms at zero temperature corresponds to a maximum number of bonds according to formula (2.1). There are problems in determining the optimal configuration of cluster atoms by computer simulation because of the large number of local minima on the potential surface, but for clusters with

short-range interaction, a simple algorithm allows one to find the optimal atomic configuration by comparing the cluster energies for a restricted number of favorable configurations. It is clear that the maximum number of bonds corresponds to compact atomic configurations and filled atomic shells. Therefore, the most favorable atomic configurations are based on a spherical core with closed shells and appended atoms outside these shells, so that the optimal atomic configuration follows from comparison of the cluster energies at different positions of a supplementary atom. This method gives both the most favorable configuration of atoms for a given number of atoms and the sequence of filling the atomic shells.

One can illustrate this method with an example [33] where a cluster has a symmetrical core consisting of 79 atoms that contains the atomic shells 000(1), 011(12), 002(6), 112(24), 022(12), and 013(24). The total number of atoms in each shell is given in parentheses. We here define a shell by atomic coordinates z, x, y of one representative atom from that shell, whose coordinate set is given by positive numbers satisfying the inequality $z \leqslant x \leqslant y$. Thus, such an atom characterizes its shell, and other atoms of this shell can be obtained with transformations (2.6). Nearest neighbors of a test atom in the course of filling next shells are determined by formula (2.8) and are given in Table 1. One can see that the optimal character of cluster growth at this stage consists of filling individual blocks, so that each block contains 1 atom of the shell 222, and 6 atoms of the shell 123. In this manner, the filling of separate facets of the cluster in the direction {111} proceeds one after the other.

Table 1. Nearest neighbors of newly joined atoms in the course of cluster growth.

Shell	Nearest neighbors			Binding energy
222	**211**	**121**	**112**	3
	213	123	132	
	231	321	312	
	233	323	332	
123	**112**	**022**	**013**	4−6
	114	024	033	
	132	**222**	*213*	
	134	224	233	

Note. Nearest neighbors from previous shells are indicated in bold text, and nearest neighbors from the shell being filled are indicated in italics.

The manner of growth of an fcc cluster with a central atom is evident from Table 2, if only nearest neighbors interact in this cluster. The same information for fcc clusters without a central atom is contained in Table 3. Note that the sum of reduced coordinates $z + x + y$ for clusters with a central atom is even, and for clusters without a central atom is odd. These two types of clusters are different, and it is necessary to consider them separately. We focus on an example [33] in which a noncentered fcc cluster with closed outermost shells 122, 113, and 023 consists of 116 atoms (see Table 3). The surface energy of this cluster is 180 (we reduce it to the units of the energy spent on breaking one bond). We now construct an fcc cluster with a central atom of a given size; the spherical core of such a cluster contains 79 atoms (see Table 2). Adding to this core five blocks of 7 atoms from the 222 and 123 shells and two atoms from the shell 114 in such a manner that these atoms join filled blocks, we obtain the surface energy of an

Table 2. The sequence of growth of fcc clusters with a central atom for a short-range interaction of atoms [33, 62, 64, 65].

Shells being filled	n	E_{sur}	Block being filled
011	$2-13$	—	—
002(4)	$13-19$	$42-54$	—
112(3−5) + 022(5)	$19-55$	$54-114$	110
013(4)	$55-79$	$114-138$	100
222(3) + 123(4−6)	$79-135$	$138-210$	111
035(5) + 004(4) + 114(5) + 024(6)	$135-201$	$210-258$	100
233(3−5) + 224(5) + 134(5−6)	$201-297$	$258-354$	111
015(4−6) + 125(5−6)	$297-369$	$354-402$	100
044(5) + 035(6)	$369-405$	$402-414$	110
006(4) + 116(5) + 026(6)	$405-459$	$414-450$	100
334(3−5) + 244(5) + 235(5−6) + 145(5−6) + 226(5) + 136(6)	$459-675$	$450-594$	111
055(5) + 046(6)	$675-711$	$594-606$	110
017(4−6) + 127(5−6) + 037(6)	$711-807$	$606-654$	100
008(4) + 118(5) + 028(6)	$807-861$	$654-690$	100
444(3) + 345(4−6) + 255(5) + 336(5) + 246(6) + 156(5−6) + 237(5−6) + 147(6)	$861-1157$	$690-858$	111

Note. The figures in parentheses mean the number of nearest neighbors for the shell filled.

Table 3. The sequence of growth of fcc clusters without a central atom for a short-range interaction of atoms [33, 62, 64, 65].

Shells being filled	n	E_{sur}	Block being filled
001	$1-6$	—	—
111(3)	$6-14$	$24-48$	111
012(3−6)	$14-38$	$48-84$	110
003(4)	$38-44$	$84-96$	100
122(3−5) + 113(5) + 023(5−6)	$44-116$	$96-180$	110
014(4−6)	$116-140$	$180-204$	100
223(3−5) + 133(5) + 124(5−6) + 034(5−6)	$140-260$	$204-312$	111
005(4) + 115(5) + 025(6)	$260-314$	$312-348$	100
016(4−6)	$314-338$	$348-372$	100
333(3) + 234(4−6) + 225(5) + 144(5) + 135(6) + 126(5−6)	$338-538$	$372-516$	111
045(5−6) + 036(6)	$538-586$	$516-528$	110
007(4) + 117(5) + 027(6)	$586-640$	$528-564$	100
018(4−6)	$640-664$	$564-588$	100
344(3−5) + 335(5) + 245(5−6) + 236(5−6) + 155(5) + 146(6) + 227(5) + 137(6)	$664-952$	$588-756$	111
056(5−6) + 047(6)	$952-1000$	$756-768$	110
128(5−6) + 038(6)	$1000-1072$	$768-792$	100

Note. The figures in parentheses indicate the number of nearest neighbors in the shell filled.

fcc atom-centered cluster $138 + 5 \times 9 + 2 \times 2 = 187$ (see Table 2). Another structure of an fcc atom-centered cluster consists of a core of 79 atoms, four added blocks of 7 atoms, six atoms of the 033 shell, two atoms from the 123 shell, and one additional atom from the 222 shell. These atoms add themselves to the above blocks. In this case, the cluster's surface energy reaches 186, i.e., this structure of the atom-centered cluster is more stable than the previous one, but an atom-noncentered cluster with a given number of atoms is preferable to an atom-centered one. Note that an atom-centered cluster identical to the above atom-noncentered cluster of 116 atoms with closed shells includes a core of 55 atoms, and outside this, 20 atoms from the 013 shell, 24 atoms from the 113 shell, 4 atoms from the 222 shell, 4 atoms from the 033 shell, 1 atom from the 004 shell, 4 atoms from the 114 shell, and 4 atoms from the 024 shell. As follows from Table 2, obtaining such an atomic configuration requires the displacement of many internal atoms, and, hence, such a configuration of atoms does not include atom-centered clusters in our scheme of construction. This means that the schemes for assembling atom-centered and atom-noncentered clusters are different. Thus, assuming the optimal cluster configuration be close to the spherical one and constructing the cluster around a given center, we obtain

two schemes of construction of fcc clusters, depending on the position of the central atom around which the cluster is assembled.

Analyzing the data in Tables 2 and 3, we conclude that the optimal cluster configurations in the course of cluster growth proceed through an addition to the blocks consisting of atoms of different shells. Comparing the energies of cluster structures with a central atom and without it allows us to choose the energetically optimal structure for a given size of fcc cluster. It follows from the data of Tables 2 and 3 that the cluster blocks added in the course of cluster growth are elements of plane facets. Magic numbers of clusters correspond to the addition of individual blocks to a spherical core.

Thus, one can formulate the method of assembling an fcc cluster with short-range atomic interaction. The main goal of this cluster construction is to analyze compact atom configurations and to choose, for a given number of atoms, the configuration that corresponds to the maximum number of bonds between nearest neighbors. Because such an idealized growing cluster has almost spherical form, the number of shells being filled is restricted for moderately large clusters. In reality, growth of an fcc cluster with a short-range atomic interaction proceeds through growth of individual facets, and magic numbers correspond to the filling of each cluster facet.

The same method of cluster construction may be used if a long-range atomic interaction is present. However, this additional interaction can change intermediate magic cluster numbers.

In considering clusters with pairwise atomic interaction, we take as a basis a short-range interaction of atoms that corresponds to interaction between nearest neighbors. When a long-range interaction is included, the short-range atomic interaction still makes the dominant contribution to the total binding energy, so that it is convenient to represent the total binding energy E_b in the form [66]

$$E_b = E_{nn} + E_{nnn} + E_{str} \,. \tag{2.9}$$

Here, E_{nn} refers to the interaction between nearest neighbors and is given by formula (2.1), E_{nnn} represents the interaction between nonnearest neighbors, and E_{str} is the strain energy due to tensions inside the cluster which is equal to

$$E_{str} = E_b(a) - E_b(R_e) \,,$$

where R_e is the equilibrium distance for the pair interaction potential, and a is the distance between nearest neighbors. In particular, in the case of the Lennard-Jones interaction between atoms, we have for a crystal of the fcc structure [33, 67]:

$$\frac{E_b}{n} = 8.61D, \quad \frac{E_{nn}}{n} = 6D, \quad \frac{E_{nnn}}{n} = 2.39D, \quad \frac{E_{str}}{n} = 0.22D \,, \tag{2.10}$$

where n is again the number of cluster atoms; interaction between nearest neighbors dominates in this case.

2.3 Regular clusters with close-packed structures
In the course of growth, a cluster passes through closed-shell structures; now we consider the geometric figures that can be realized for clusters with pairwise interactions. Regular figures of close-packed structures can have either fcc or hexagonal (hcp) structures. In the case of the fcc structure, the corresponding geometric figure possesses cubic symmetry O_h [68]. This means that any one of transformations (2.6) transfers a test atom of the cluster to a position that is occupied by another atom (or by this one). In the case of the hexagonal structure, the geometric figure possesses a lower symmetry, whose atomic configuration is conserved as a result of transformations

$$z \leftrightarrow -z, \quad \Phi \to \Phi \pm \frac{\pi}{3} \,. \tag{2.11}$$

Here, we take a plane {111} in which each atom has 6 nearest neighbors as a basis of the hexagonal lattice. The z-axis is directed perpendicular to this plane, and Φ is the polar angle with respect to that z-axis. According to this symmetry, the maximum number of atoms in one shell is equal to $2 \times 6 = 12$ for a cluster with the hexagonal structure, as with the fcc structure. Optimal configurations of atoms in solid hexagonal clusters may be found by the same method [64, 71], as we described above for the fcc solid clusters.

In order to construct geometric figures of solid clusters that are restricted by plane facets, we first consider planes which can be formed for a close-packed structure. In the case of the fcc structure, there are three types of planes, namely, {100}, {110}, and {111}. We use standard notation for these planes [41] expressed as the coordinates of a line passing

through the origin that is perpendicular to this plane. There are 6 different planes of the {100} type, 12 planes of the {110} type, and 8 planes of the {111} type. Thus, the maximum number of simple, low-order plane facets of an fcc crystalline particle equals 26. This determines the variety of geometric figures for clusters of the fcc symmetry. The planes of the fcc crystal lattice are displayed in Fig. 2 [33]. Note that according
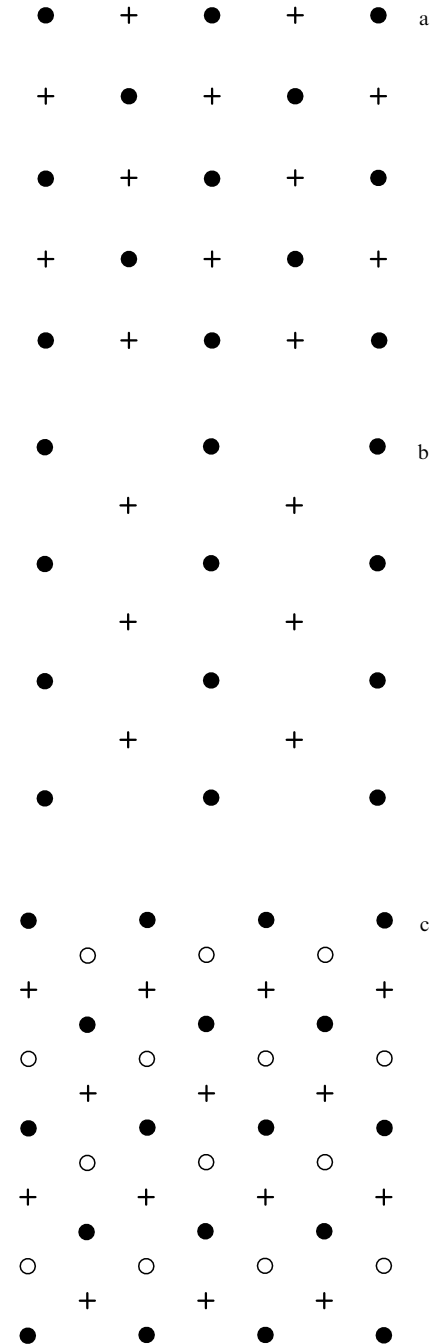
Figure 2. The structures of fcc-planes. Positions of atomic centers of the surface layer are indicated by black circles, centers of atoms of the preceding layer are marked by crosses, and centers of atoms of the next layer are shown by white circles. (a) A {100}-plane; the distance between neighboring lines of atoms in the plane is a, and the distance between neighboring planes is $a\sqrt{2}$; (b) a {110}-plane; the distance between neighboring lines of atoms in the plane is $a\sqrt{2}$, and the distance between neighboring planes is $a/\sqrt{2}$; (c) a {111}-plane; the distance between neighboring lines of atoms in the plane is $a\sqrt{3}/2$, and the distance between neighboring planes is $a\sqrt{2/3}$.

Table 4. Parameters of the families for geometric figures of clusters with close-packed structures and a short-range interaction between atoms. In the case of an icosahedral cluster, the truncated Lennard-Jones potential is used, i.e., the Lennard-Jones interaction potential specifies the interaction between nearest neighbors, and is zero for all other interatomic distances.

Figure	n	E_{sur}/D	E_b/D	A_∞/D
Octahedron	$(2/3)m^3 + 2m^2 + (7/3)m + 1$	$6m^2 + 12m + 6$	$4m^3 + 6m^2 + 2m$	7.86
Cuboctahedron	$(10/3)m^3 + 5m^2 + (11/3)m + 1$	$18m^2 + 18m + 6$	$20m^3 + 12m^2 + 4m$	8.07
Trunc. octahedron	$n^{oct} - k(k+1)(2k+1)$	$E_{sur}^{oct} - 6k(k+1)$	$E_b^{oct} - 12k^2(k+1)$	—
Reg. trunc. octahedron	$16m^3 + 15m^2 + 6m + 1$	$48m^2 + 30m + 6$	$6m(16m^2 + 7m + 1)$	7.56
Hexahedron	$4m^3 + 6m^2 + 4m - 7$	$21m^2 + 21m - 12$	$24m^3 + 15m^2 + 3m + 5$	8.33
Trunc. hexahedron	$28m^3 + 21m^2 + 6m + 1$	$72m^2 + 36m + 6$	$168m^3 + 90m^2$	7.81

to Tables 2 and 3, growth of clusters with fcc structures results from the filling of facets of the three orientations {100}, {110}, and {111}.

Let us evaluate the number of nearest neighbors for a surface atom of each plane of the fcc structure. Each surface atom of a {100}-plane has 4 nearest neighbors from the surface layer and 4 nearest neighbors from the preceding, more interior one, i.e., a surface atom of a {100}-plane has 4 nearest neighbors. In the same manner we find that each surface atom of a {110}-plane has 4 nearest neighbors, and each surface atom of a {111}-plane has 9 nearest neighbors. From this it follows that geometric figures with surface facets of directions {111} and {100} are energetically more stable for bulk fcc crystalline particles with pair interactions. Hence, below we restrict ourselves to geometric figures whose facets are directed along these planes (see Fig. 3).

One can construct families of identical figures, which differ by size. Taking the edge length of this figure to be ma, where a is the distance between nearest neighbors, we call m the figure number in the series. We start from the octahedral cluster (Fig. 3a) whose surface consists of 8 regular triangles; an octahedral cluster can be either atom-centered or atom-noncentered. The 6 vertex atoms of such a cluster have the coordinates $0, 0, m$ or can be obtained from these as a result of transformations (2.6). Table 4 contains formulas for a number of atoms in this cluster, depending on the number m of the series and the surface energy E_{sur} of this cluster and the total binding energy E_b of cluster atoms [33, 65, 69] in the case of a short-range interatomic interaction. The total cluster energy is connected with its surface energy by formula (2.2). The surface of the cuboctahedral figure (Fig. 3b) consists of 6 squares and 8 equilateral triangles, and Table 4 lists its parameters for a short-range interaction [33, 65, 69]. In contrast to octahedral clusters, all the cuboctahedral clusters have a central atom.

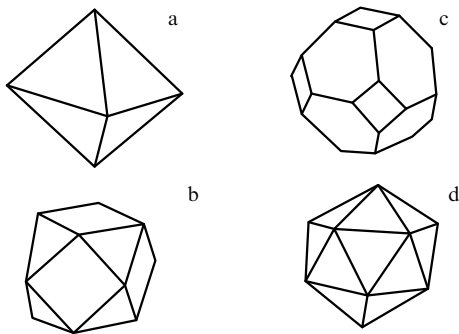The truncated octahedral structure (Fig. 3c) is formed from the octahedron by cutting off 6 regular pyramids from

Figure 3. Regular structures of atomic clusters: (a) octahedron, (b) cuboctahedron, (c) truncated octahedron, and (d) icosahedron.

Table 5. Parameters of filled structures of fcc clusters with short-range interatomic interaction within the framework of the structure of a truncated octahedron. The asterisk marks the minimum of $A(n)$ as a function of magic numbers.

n	A	m, k	n	A	m, k
201*	7.519	6.2	1000	7.680	—
260	7.659	7.3	1072*	7.561	11.3
314*	7.533	7.2	1126	7.650	11.2
338	7.666	7.1	1139	7.647	12.5
369	7.814	—	1157	7.785	—
405	7.563	8.3	1289*	7.548	12.4
459*	7.562	8.2	1385	7.581	12.3
538	7.801	—	1504	7.587	13.5
586*	7.540	9.3	1654*	7.550	13.4
640	7.594	9.2	1750	7.602	13.3
664	7.699	9.1	1804	7.693	13.2
675	7.719	—	1865	7.643	—
711	7.607	10.4	1925	7.561	14.5
807*	7.545	10.3	2075*	7.561	14.4
861	7.624	10.2	2171	7.622	14.3
885	7.746	10.1	2190	7.614	15.6
952	7.812	—	2225	7.710	14.2
976	7.561	11.4	2406*	7.552	15.5

its vertices. A so-formed cluster is characterized by the index m, the number of the octahedron in its family, and by the index k, the number of atoms on the pyramid's edge. Parameters of this figure for a short-range interatomic interaction are given in Table 5 [33, 65, 69], and the parameters n^{oct}, E_{sur}^{oct}, E_b^{oct} relate to the octahedral cluster of the m-th series. The regular truncated octahedron is the optimal structure for a short-range interaction. Its surface consists of 8 regular hexagons and 6 squares and contains 36 edges of the identical size. For the family of regular truncated octahedrons we have $m = 3k$, and the parameters of this figure are presented in Table 4 [33, 65, 70, 71]. Furthermore, Fig. 4a displays the dependence of the specific surface energy for fcc clusters on the cluster size in the conditions of interatomic interactions involving nearest neighbors, while maximum values of the specific surface energy relate to the structure of a regular truncated octahedron.

Favorable structures of fcc clusters with a short-range interaction possess the structure of a truncated octahedron, and Table 5 gives closed structures of such fcc clusters in the course of their growth. Almost all these structures consisting of hundreds of atoms constitute truncated octahedrons. The regular truncated octahedron is also an optimal cluster structure if long-range interaction is important [70]. Note that the specific surface energy A given by formulas (2.4) and (2.5) is characteristic of the energetics of a solid cluster. For optimal structures, this quantity has minimal values. This parameter is listed in Table 4 for infinite clusters with the structures under consideration. For the truncated octahe-
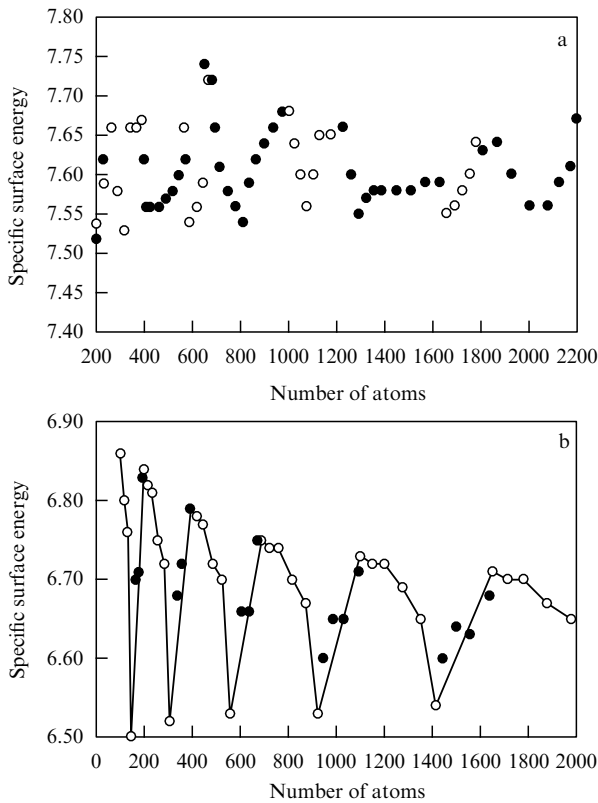
Figure 4. The specific surface energy for optimal atomic configurations of fcc clusters (a) and icosahedral clusters (b) [33]. In the case of fcc clusters, black circles correspond to clusters with a central atom, and white circles to atom-noncentered clusters.

dron, this quantity is equal to [33]

$$A_\infty = 3 \times (18)^{1/3} \frac{(1 - k^2/m^2)}{(1 - 3k^3/m^3)^{2/3}} . \qquad (2.12)$$

As follows from Table 4, the regular truncated octahedron is the optimal figure for large clusters with the fcc structure.

The hexagonal structure is the other close-packed structure in which each internal atom of the lattice has 12 nearest neighbors. This structure may be analyzed for clusters in the same manner [33, 62, 71] as was done for clusters of the fcc structure. We illustrate this structure by constructing the cuboctahedral cluster involving 13 atoms. Indeed, taking a plane in the direction {111} as a base for this cluster, we place a regular hexagon of atoms with a central atom on this plane. The edge of this pentagon measures a, the equilibrium distance for a pair atomic interaction. Next, three atoms are located in a layer parallel to and at a distance $a\sqrt{2/3}$ from the basic one, and the same kind of layer is constructed below the basic layer. Atoms are placed in these layers in hollows of triangles and form regular triangles such that atoms of new layers form a regular triangle whose edge length equals a. There are two possibilities for the relative location of atoms in the upper and lower layers. If the projections of atoms from the upper and lower layers onto the central layer plane do not coincide, these atoms form a cuboctahedron. Such a cluster has the fcc structure and it is conserved as a result of transformations (2.6). If the atomic projections of the first and third layer coincide, the figure formed is a hexahedron.

This cluster possesses hexagonal symmetry and is conserved under transformations (2.11).

Clusters of the hexagonal structure contain a central atom in a basic layer and a system of regular hexagons is formed around a common center located at the central atom. Atoms of next layers are located in the hollows of triangles formed by atoms of preceding layers, and the distance between nearest layers measures $a\sqrt{2/3}$, as in the above case of the simplest hexagonal cluster involving 13 atoms. Taking a system of regular hexagons in the basic layer and placing atoms of a new layer in hollows between three atoms of the preceding layer, we obtain a hexahedron that is conserved under transformations (2.11). Parameters of the family of hexahedrons [33, 71] are presented in Table 4. We also construct a truncated hexahedron by removing some layers from the hexahedron. For the parameters of Table 4, we take a $2m$-th hexahedron and remove m upper and lower layers. From this it follows that a large truncated hexahedron is a more favorable figure, but the energetics of large hexagonal clusters is worse than that for fcc clusters because of the former's lower symmetry. Next, in contrast to fcc clusters in which all the surface atoms are located on the plane facets, atoms of lateral sides of hexagonal clusters do not form planes.

Thus, the hexagonal cluster structure competes with the fcc structure in the case of small clusters for which the icosahedral structure is more favorable, and therefore this competition is not significant for small clusters [33, 71]. Because of their higher symmetry, the fcc cluster surfaces are more favorable for large cluster sizes than the hexagonal ones, and therefore large clusters of the fcc structure are characterized by a higher binding energy of atoms than hexagonal clusters. The competition of the hexagonal and fcc structures becomes stronger for bulk clusters or crystals when the surface effects are not dominant and the competition depends on the character of interatomic interactions. In particular, in the case of the Lennard-Jones crystal, the hexagonal structure is favorable [72], although the difference in the sublimation energies per atom is small ($\sim 0.2\%$). In reality, inert gas crystals have the fcc structure [41, 67, 73, 74].

2.4 Competition among icosahedral and close-packed structures

The number of ordered cluster structures is greater than the number of types of crystal lattices. Clusters with a pair interaction of atoms, including clusters of inert gas atoms, demonstrate this fact vividly. Indeed, clusters with short-range interaction, like bulk systems of bound atoms, can have a close-packed structure that corresponds to the fcc or hexagonal crystal lattices, but such clusters also permit the icosahedral structure that is not realized for bulk crystals. Thus, clusters with pair interatomic interactions give a convenient example for understanding the structural and energetic parameters of clusters.

The icosahedral cluster structure (see Fig. 3d) can be related to close-packed structures because, like fcc and hcp crystals, each internal atom has 12 nearest neighbors. But in the close-packed lattice structures, all the distances between nearest neighbors in a bulk system are identical, whereas in the case of the icosahedral structure there may be two different distances between nearest neighbors. This is one reason why the icosahedral structure cannot compete with the close-packed structures at the limit of a bulk atomic system, and this structure cannot be realized in a bulk crystal lattice. The other reason is that it does not correspond to a translationally

invariant lattice, but rather to a structure with a specific center. But the icosahedral structure is nonetheless compact enough to yield stable clusters, because all 20 surface triangles of the icosahedral cluster with closed shells are {111}-planes with the maximum number of nearest neighbors for surface atoms. Hence, the icosahedral structure is energetically favorable for small and moderate sizes of clusters.

An icosahedral cluster as a geometric figure has 12 vertices located at identical distances from the center [75]. The icosahedron possesses a high symmetry Y_h [68] characterized by 6 five-fold axes passing through the icosahedron's center and two opposite vertices located at opposite poles of a sphere, and rotation of the icosahedron by the angle $2\pi/5$ around any symmetry axis conserves its figure. Along with this, the icosahedron is conserved as a result of turning by an angle $\pi/5$ around one of these axes and reflection with respect to the plane perpendicular to the axis and passing through the icosahedron center. Another symmetry of the icosahedron corresponds to the inversion operations $x \leftrightarrow -x$, $y \leftrightarrow -y$, and $z \leftrightarrow -z$. Next, the icosahedron possesses a symmetry of reflection with respect to any plane that passes through a given symmetry axis and two vertices of pentagons. This is also valid for any axis of the icosahedron. Thus, the icosahedron constitutes a geometric figure of very high symmetry.

In order to construct the simplest icosahedral cluster consisting of 13 atoms, we place one atom in the center and construct around this atom a sphere of a radius R, where the other 12 atoms are located in the following way. Two atoms are placed at the sphere's poles, so that they are connected by a line that passes through the center. The other 10 atoms form two pentagons whose planes are perpendicular to this line. The pentagons are inscribed in circles that are sections of planes and the sphere, and the pentagon's vertices are rotated by an angle of $\pi/5$ with respect to each other. These circles form a cylinder whose axis is the icosahedral axis. Joining the nearest vertices of the icosahedron, we obtain 20 equilateral surface triangles. This means that the distances between nearest neighbors on the sphere are identical, and each surface atom has 5 nearest neighbors on the sphere. Nearest neighbors of polar atoms on the sphere are the atoms of the nearest pentagon, and each atom of a pentagon has as nearest neighbors on the sphere one atom of the nearest pole, two nearest atoms of its own pentagon, and two atoms of the neighboring pentagon. The distance R_0 between nearest neighbors on the sphere and the distance R from the center to surface atoms are connected through the relation

$$R = \sqrt{\frac{\sqrt{5}}{8} \left(1 + \sqrt{5}\right)} \, R_0 = 0.951 R_0 \,. \tag{2.13}$$

All the atoms in this cluster are equivalent, apart from the central atom. Let us find the specific binding energy of atoms for a bulk icosahedral cluster in the case of atomic interactions between nearest neighbors. The method of determining the cluster binding energy [33, 76–78] leans upon the fact that the equilibrium distance R_e for the pair interaction potential is close to distances R_0 and R between cluster nearest neighbors, so that the total binding energy can be expanded in powers of a corresponding small parameter. We demonstrate this method for a bulk icosahedral cluster with the interaction between nearest neighbors only, when the cluster binding energy per internal atom is given by

$$\varepsilon = -3U(R) - 3U(R_0) \,, \tag{2.14}$$

where $U(R)$ is the interaction potential of two atoms at a distance R between them. We make use of the fact that each internal atom has 6 nearest neighbors of the same layer at a distance R_0, 3 nearest neighbors of the preceding layer and 3 nearest neighbors of the next layer at a distance $R = 0.951R_0$, and we take into consideration the fact that each bond is shared between two atoms. Expanding this specific energy near the equilibrium distance R_e, we obtain from formula (2.14) the following relationship

$$\varepsilon = 6D - \frac{1}{2} U''(R_e) \left[(R_e - R)^2 + (R_e - R_0)^2\right]$$

and, by optimizing this energy, we arrive at the equation

$$R_e - R + \frac{\partial R_0}{\partial R} \, (R_e - R_0) = 0 \,.$$

From the last relationship it follows that $R = 0.974R_e$, and $R_0 = 1.024R_e$, so that the asymptotic expression for the specific binding energy has the form [33]

$$\varepsilon_0 = 6D - 0.00189 U''(R_e) \,. \tag{2.15a}$$

The surface energy per atom for a short-range interaction is $\varepsilon_{sur} = -(3/2)U(R)$. The number of surface atoms in an icosahedral cluster equals $10m^2$, where m is the number of filled layers in the closed icosahedral cluster, and the total number of cluster atoms in this approximation reaches $n = 10m^3/3$. From this we obtain the cluster surface energy

$$E_{sur} = -15m^2 U(R) = -15 \times (0.3n)^{2/3} U(R) \,,$$

with the result for the cluster's specific surface energy [33]:

$$A = 15 \times (0.3)^{2/3} \left[D - \frac{1}{2} \, (R - R_e)^2 U''\right]$$
$$= 6.72D - 0.0022 U'' \,. \tag{2.15b}$$

The popular pair interaction potential of atoms, which contains simultaneously short-range and long-range parts, is the Lennard-Jones interaction potential which has the form [79, 80]

$$U(R) = D\left[\left(\frac{R_e}{R}\right)^{12} - 2\left(\frac{R_e}{R}\right)^{6}\right] \,. \tag{2.16}$$

Here, R is the distance between atoms; the parameters D and R_e are, respectively, the depth of the potential well and the equilibrium distance between atoms. It is convenient to use the truncated Lennard-Jones interaction potential as a short-range interatomic potential; this interaction potential is given by formula (2.16), if two atoms are nearest neighbors, and is zero for two atoms that are nonnearest neighbors. In the case of the truncated Lennard-Jones interaction potential, we find the following parameters from formulas (2.15) for a bulk icosahedral cluster with filled layers [33, 77]:

$$\varepsilon_0 = 5.86D, \quad A = 6.56D \,. \tag{2.17}$$

Let us compare these parameters with parameters of the optimal fcc structure and regular truncated hexahedron, for which we obtain in the limit $n \to \infty$, according to Table 5: $\varepsilon_0 = 6D$, $A = 7.55D$. Distances between nearest neighbors for a cluster of the icosahedral structure are in close agreement, and a number of bonds between nearest neighbors is more for

the icosahedral structure than that for a close-packed one. Figure 4b depicts the size dependence for the specific surface energy of the icosahedral cluster with atomic interactions involving nearest neighbors only. It demonstrates the preference of filled cluster shells. The comparison of fcc and icosahedral structures shows that for very large clusters the fcc structure is energetically favored, whereas the optimal cluster structure is the icosahedral one for not-so-large clusters. The transition between these structures occurs in the range of several hundred atoms, and there is indeed a range of sizes for this transition, in which increasing the cluster size by one atom may result in passing to the most favorable structure. It is also important to recognize here that these are purely energetic comparisons, so they relate to stability at zero temperature and not necessarily at higher temperatures.

Because the distances between nearest neighbors in the icosahedral cluster are nearly identical, and an icosahedral cluster is more compact than clusters with close-packed lattices, the icosahedral structure can be more favorable for large but not very large clusters. Let us demonstrate this for the Lennard-Jones cluster consisting of 13 atoms. Taking into consideration the cluster structure, we represent the total binding energy of atoms in the form [67]

$$\frac{E_{\mathrm{b}}}{D} = 2C_6 \left(\frac{R_{\mathrm{e}}}{R}\right)^6 - C_{12}\left(\frac{R_{\mathrm{e}}}{R}\right)^{12} . \qquad (2.18)$$

Table 6 lists the parameters of this formula for the cuboctahedral, hexahedral, and icosahedral clusters, where k is the total number of bonds between nearest neighbors, a is the optimal distance between nearest neighbors, E_{b} is the total binding energy of atoms for the optimal atomic configuration, and these parameters are given by formulas

$$a = R_{\mathrm{e}}\left(\frac{C_{12}}{C_6}\right)^{1/6} , \quad E_{\mathrm{b}} = \frac{C_6^2}{C_{12}} . \qquad (2.19)$$

As follows from Table 6, the icosahedral structure for a 13-atom cluster is preferred over the close-packed structures because of the larger number of bonds between nearest neighbors in the icosahedral cluster. In addition, the icosahedral Lennard-Jones cluster shrinks more than the cuboctahedral or hexahedral structures under a long-range interaction. The interaction between nearest neighbors makes the main contribution to the total binding energy of clusters in all these cases. Comparing structures with close packing of atoms, one can see that the hexahedral structure is moderately favorable, but the distinction between the two close-packed structures is small.

Comparison of the energies of the cuboctahedral and icosahedral structures is convenient because these structures are characterized by the same number of atoms in their closed geometric figures, and therefore such a comparison allows the competition between the fcc and icosahedral structures [53,

Table 6. Energy parameters for different structures of Lennard-Jones clusters involving 13 atoms.

Structure	k	C_6	C_{12}	E_{b}/D	a/R_{e}
Cuboctahedron	36	38.48	36.22	40.88	0.990
Hexahedron	36	38.56	36.23	41.04	0.990
Icosahedron	42	35.59	28.57	44.34	0.964

81–83]. This comparison of closed structures with the Lennard-Jones interaction potential shows that the cuboctahedral structure becomes more stable for sizes starting from about 10^4 atoms in a cluster. But the cuboctahedral structure is not optimal among the fcc structures, and hence comparison of the energies of the cuboctahedral and icosahedral structures does not allow us to draw conclusions about competition of the fcc and icosahedral structures. Nevertheless, on the basis of comparison between the atomic binding energies for the cuboctahedral and icosahedral structures, one can ascertain the character of atomic interactions in these structures. In particular, in the case of the truncated Lennard-Jones interaction potential, we have for the total binding energies of a cuboctahedral and an icosahedral cluster the corresponding values $7476D$ and $7474D$ at zero temperature [33], if these clusters have 7 filled layers or 1415 atoms (D is the binding energy per bond). In the case of 8 filled layers or 2057 atoms in the cluster, these values are $11040D$ and $11005D$, respectively, whereas for clusters containing 6 filled layers or 923 atoms, these total binding energies of atoms at zero temperature are $4776D$ and $4793D$ for the cuboctahedral and icosahedral clusters (see Ref. [33]). One can see a weak dependence (a small increase) of the mean binding energy per atom on the number of cluster atoms. We add to this that the difference in the binding energies of two structures is a nonmonotonic function of the number of atoms, so one can infer that there is a wide range of competition among these structures. In particular, this was demonstrated in Refs [84, 85] by the competition among the fcc and icosahedral cluster structures for the Morse interaction potential between atoms, for which the binding energies of cluster atoms and the optimal cluster structure depend on the Morse parameter value. Figure 4a contains values of the specific surface energies for fcc clusters with a short-range interaction of atoms, and Fig. 4b gives the same value for icosahedral clusters with a truncated Lennard-Jones interaction potential, when only nearest neighbors interact. These data testify to the competition between these cluster structures.

Comparison of the cuboctahedral and icosahedral filled cluster structures is also useful in order to ascertain the role of a long-range interaction. For the Lennard-Jones interaction potential, the binding energies of atoms in clusters of these structures consisting of 1415 atoms (or 7 closed layers) are $10309D$ and $10232D$ for the icosahedral and cuboctahedral structures, respectively [82, 83]. Comparing them with those for the truncated Lennard-Jones pair interaction potential, when nearest neighbors only interact, for which the values are $7474D$ and $7476D$, respectively, we find that the character of the structure competition depends on the shape of the pair interaction potential. Indeed, the structure is determined primarily by the number of bonds between nearest neighbors, but the difference in these values for competing structures is relatively small throughout the range of competition. Hence, the smaller contributions, notably from non-nearest neighbors, can play a determining role in the competition. For example, the number of bonds between nearest neighbors is 4902 for the icosahedral cluster consisting of 923 atoms, whereas the optimal fcc cluster of this size contains 4814 bonds between nearest neighbors [86, 87], and the number of these bonds is 4776 for the corresponding cuboctahedral cluster. Therefore, the favorable structure is sensitive to the shape of the pair interaction potential in the competition range [66, 85]. In addition, the number of bonds

between nearest neighbors varies in a nonregular manner with an increase in the number of atoms for the icosahedral structure as a cluster layer is filling [77, 78], a consideration that intensifies the structure competition. This fact follows also from the energy calculations [88] for the icosahedral Lennard-Jones clusters in the course of increasing the number of atoms up to $n = 147$. This leads to expansion of the range of structure competition. We note also that the hexagonal structure is not important for the structure competition. Indeed, at small cluster sizes where fcc and hexagonal structures compete, the icosahedral structure is favorable, whereas at moderate and large cluster sizes, where icosahedral and fcc structures compete, the hexagonal structure is not favorable [33, 71].

Still another peculiarity in the competition among cluster structures consists in structure mixing. In the case of close-packed structures, the mixed structure of the crystal lattice may simultaneously contain elements of face-centered cubic and hexagonal structures, resulting in dislocations and twinning (see, for example, Refs [65, 89]). Such structural defects can be important for transitional structures of clusters [56]. In clusters with a pair interaction, new possibilities for mixing of structures arise due to competition between the icosahedral and fcc structures. The most important mixing of these structures [51, 52, 88] relates to the filling of cluster layers when the icosahedral structure is favored, so that a growing cluster has an icosahedral core. In the first stage of filling, the new layers have the fcc structure, but it then transforms into the icosahedral structure [77]. Indeed, an atom being joined goes onto the cluster surface in a hollow between three surface atoms, and the number of such positions for the surface of an fcc-structure is more than that for the icosahedral structure which requires places for edge atoms. For the cluster with m filled layers, the number of positions above each triangle is $m(m-1)/2$ for the fcc layer structure, and is only $(m-1)(m-2)/2$ for the icosahedral layer structure. Comparison of these surface structures shows [77] that at the first stage of the filling of a new layer the fcc structure of the layer is favored, and after filling 8 surface triangles, the icosahedral structure of the layer being filled provides the maximum binding energy of cluster atoms.

Thus, the analysis of clusters with a pair interaction of atoms demonstrates the variety of cluster structures that can be realized. Even for this simple character of interaction, clusters can possess face-centered cubic, hexagonal, or icosahedral structures, or their mixtures, and each structure gives rise to different cluster shapes. At low temperatures, when a cluster is solid, one can find the optimal configuration of cluster atoms that leads to the maximum binding energy of cluster atoms. Even for large clusters one can observe a size range with alternation, with cluster size, of optimal structures, so that a change in the number of cluster atoms by one can change the optimal cluster structure. In addition, the optimal configuration of cluster atoms in a range of competition can contain elements of different structures.

2.5 Solid clusters of inert gases

In considering clusters with pair interactions, we are guided by both clusters and macroscopic solids of inert gases. Parameters of the interaction potential for two inert gas atoms can be found from the analysis of physical properties that depend on those atomic interactions. These quantities are the differential and total elastic scattering cross sections of two atoms, the second virial coefficients of inert gases, the

Table 7. Parameters of the pair interaction potential for inert gas atoms and the reduced parameters for systems consisting of interacting atoms of inert gases.

Parameter	Ne	Ar	Kr	Xe
R_e, Å	3.09	3.76	4.01	4.36
D, meV	3.64	12.3	17.3	24.4
D, K	42	143	200	278
m, a.m.u.	20.18	39.95	83.80	131.3
$p_0 = D/R_e^3$, MPa	20.2	37.1	43.0	47.1
$\rho_0 = m\sqrt{2}/R_e^3$, g cm^{-3}	1.606	1.764	3.051	3.718
γ	7.6	8.1	7.7	5.9
R_0, Å	2.07	2.85	2.99	3.18

diffusion coefficients of atoms in their parent inert gas, the thermal conductivity and viscosity coefficients, spectra of excitation for dimers of inert gas atoms, and some parameters of solid and liquid inert gases. As a result of measurements of these quantities and their treatment, very reliable and precise parameters of the interaction potential for two atoms of inert gases have been determined [90–93]. Table 7 contains the parameters R_e, the equilibrium distance for the diatomic molecule consisting of interacting atoms, and D, the depth of the interaction potential well. Based on these parameters, we accept the short-range interaction as the dominant part of the interatomic interaction in condensed inert gases [65, 76, 94]. This character of scaling implies the classical character of atomic motion in condensed inert gases, which is valid so long as a typical vibrational energy $\hbar\omega$ is small compared with the binding energy of the atoms. This criterion assumes the form $\hbar\omega \ll D$, i.e., the vibrational energy $\hbar\omega$ is small relative to the dissociation energy D, and can be rewritten for a diatomic molecule as

$$D^2 \gg \frac{\hbar^2}{m} U'', \tag{2.20}$$

where m is again the atomic mass, $U(R)$ is the interaction potential of two atoms, and the derivative is taken near the bottom of the potential well. This criterion is not well met for many vibrational levels of the diatomic molecules of neon and argon, but for an assembly of many interacting atoms it is satisfactory and a classical model is valid for clusters of all inert gases except helium. (There are modest quantitative deviations for neon in the region of solid–liquid coexistence [95, 96].)

Repulsion of interacting atoms at small interatomic distances is determined by the exchange interaction potential due to overlapping of atomic electron shells. The corresponding interaction potential varies sharply with the variation of the distance R between atoms, so that the pair interaction potential is often approximated by the formula

$$U(R) = U(R_0)\left(\frac{R_0}{R}\right)^{\gamma}, \tag{2.21}$$

with $\gamma \gg 1$. (An exponential form, rather than a power-law relation, is also frequently used; see the next section.) Table 7 collates the parameters of the repulsive interaction potential for inert gas atoms [97], if $U(R_0) = 0.3$ eV. Since in reality $\gamma \gg 1$, the collision of two inert gas atoms corresponds moderately well to the hard sphere model, where atoms are modelled by hard balls. (Note, however, that the Lennard-Jones potential sets the exponent of the repulsive term to 12, significantly larger than the values in Table 7).

Table 8. Parameters of solid inert gases and the reduced parameters near the triple point [65, 76, 94, 107].

Parameter	Ne	Ar	Kr	Xe	Average
a, Å	3.156	3.755	3.992	4.335	—
a/R_e	1.02	1.00	0.99	1.01	1.005 ± 0.013
$\rho(0)/\rho_0$	1.06	1.00	0.99	0.98	1.01 ± 0.04
ρ_{sol}, g cm^{-3}	1.444	1.623	2.826	3.540	
T_{tr}, K	24.54	83.78	115.8	161.4	
T_{tr}/D	0.581	0.587	0.578	0.570	0.579 ± 0.007
p_{tr}, kPa	43.3	68.8	73.1	81.6	
$p_{tr}R_e^3/D$, 10^{-3}	2.2	1.9	1.7	1.7	1.9 ± 0.2
ε_{sub}, meV	22	80	116	164	
ε_{sub}/D	6.1	6.5	6.7	6.7	6.5 ± 0.3
ε_{sol}, meV	22.5	80.2	112	158	
ε_{sol}/D	6.2	6.5	6.5	6.5	6.4 ± 0.2
$\varepsilon_{sol}/\varepsilon_{sub}$	0.98	1.00	1.04	1.04	1.02 ± 0.03
p_0, MPa	1800	4600	5600	4900	
$p_0 R_e^3/D$	89	124	130	104	110 ± 20

Because a variable of any dimensionality may be composed from three dimensional parameters (see, for example, Refs [98–100]), we use the parameters D, R_e, and m for the inert gas atoms given in Table 7 in order to compose parameters for condensed inert gases. Table 8 [101–106] contains measured parameters of solid inert gases and their reduced values [65, 76, 94, 107], whose coincidence confirms the validity of the similarity law for condensed inert gases and, correspondingly, the dominant pairwise character of atomic interactions in these systems. Here, a is the distance between nearest neighbors in the crystal lattice at zero temperature, $\rho_0 = \sqrt{2}m/R_e^3$, m is the atomic mass, $\rho(0)$ is the crystal density at zero temperature, ρ_{sol} is the density of the solid inert gas at its triple point, T_{tr} and p_{tr} are the temperature and pressure at the triple point, and ε_{sub} is the binding energy per atom for the solid inert gas at the melting point. Note that under commonly encountered conditions, solid inert gas crystals have a face-centered cubic structure [41, 67, 73, 74]. The hexagonal structure of solid inert gases is observed in films formed on a special substrate [108–110]. Along with the sublimation energy, we present in Table 8 the atomic binding energy ε_{sol} in the crystal, obtained on the basis of the Clapeyron–Clausius formula [4, 6], according to which the equilibrium pressure of saturated vapor $p_{sat}(T)$ over a plane solid surface is given by

$$p_{sat}(T) = p_0 \exp\left(-\frac{\varepsilon_{sol}}{T}\right) \qquad (2.22)$$

at a temperature of T. (Note that throughout this article, we express the temperature in energy units.) Coincidence of reduced parameters for different inert gases characterizes the accuracy of the scaling law for condensed inert gases, the law that says that the properties of all inert gases are almost the same when they and the conditions for them are expressed in 'reduced units', the units scaled to the conditions at the triple point of each substance. Equivalently, the scaling law says that the properties of the rare gases are essentially the same if they are scaled as in Table 8.

One can compare condensed inert gases with models based on simple versions of the pair interaction potentials. In the case of the Lennard-Jones interaction potential (2.16), the parameters of a solid crystal are [67]: $a = 0.971R_e$, and $\varepsilon_{sub} = 8.61D$ [see formula (2.11)], while in the case of a short-range interaction, when only nearest neighbors interact, we have $a = R_e$, and $\varepsilon_{sub} = 6D$. Comparing these values with the data from Table 8, one can conclude that interaction in real solid inert gases is close to that modelled by a short-range interatomic interaction.

2.6 Bulk ensembles of repelling atoms

A bulk ensemble of atoms with a purely repulsive pair interaction potential does not form a crystal lattice as do atoms bound by a short-range attractive interaction. Even at low temperatures, repulsive atoms do not form a crystal lattice, so that the number q of nearest neighbors for a test internal atom of this system differs from the value 12, characteristic of a crystal with a close-packed structure. Because the exchange interaction potential between atoms at small distances is determined by the extent of overlapping of their electron shells, it is frequently represented by a sharp exponential dependence on the interatomic distance. Alternatively, a model of hard spheres [24, 111, 112] can be applied effectively to describing the system of repelling atoms, the model that is valid if $\gamma \gg 1$ in formula (2.21).

It is convenient to characterize the distribution of spheres in space by the packing density [38] given by the formula

$$\varphi = \frac{4\pi}{3n} r^3 N, \qquad (2.23)$$

where r is the sphere's radius, N is the density of spherical particles, n is the number of atoms inside the sphere, and the packing density φ is the fraction of the space occupied by hard spheres. Evidently, the maximum value of this parameter for hard spheres corresponds to a close-packed crystal lattice when the packing density is given by

$$\varphi_{cr} = \frac{\pi\sqrt{2}}{6} = 0.74. \qquad (2.24)$$

The packing density φ for an ensemble of hard spheres follows from simple experiments based on filling a container with hard balls [113–115] and on system simulations with hard spheres [116–118]. The observed value $\varphi_d = 0.64$ [114] accords with a more precise value obtained from computer simulations for the packing density of this system [117]:

$$\varphi_d = 0.644 \pm 0.005. \qquad (2.25)$$

This means that an ensemble of hard spheres does not form a close-packed crystal lattice. Using the connection of the mean coordination number q with the corresponding atomic density ρ [76], namely

$$q = 12\frac{\rho_{cr}}{\rho}, \qquad (2.26)$$

where ρ_{cr} is the crystal density, and taking $q = 12$ for the close-packed structure, we have on the basis of Eqns (2.23) and (2.24):

$$q = 12\frac{\varphi}{\varphi_{cr}} = 16.2\varphi, \qquad (2.27)$$

and formulas (2.25) and (2.27) give $q = 10.4 \pm 0.1$ that is close to the coordination number of liquid inert gases at low pressures, in which atoms are bonded due to attractive forces, and for which $q = 10.1 \pm 0.1$ [33, 76].

Additional information follows from applying the virial theorem [24, 119] to a system of repelling atoms. According to the virial theorem, the higher the average number of nearest

neighbors for an internal atom, the greater the total energy of particles for a system of repelling particles. Therefore, the crystal structure of repelling atoms is unstable with respect to a decrease in the number of nearest neighbors, if this compact system is supported by an external pressure. Indeed, the crystal distribution of atoms at high pressures and low temperatures is characterized by a higher energy than the atomic distribution that does not have the regular, close-packed structure of the crystal lattice. Because the entropy of the less regular distribution is higher than that of the crystal distribution, the crystal distribution of atoms at high pressures and low temperatures is unstable towards a structure of lower density.

Note that the system of repelling atoms at high pressures is governed by a pair interaction between atoms, since repulsion of interacting atoms is determined by the overlapping of the wave functions of valence electrons. Consequently, this interaction is created by the electron distribution near the axis joining the interacting atoms, and the exchange interaction potential of two atoms does not depend on the positions of other atoms. Next, the interaction potential of two atoms is small compared to a typical value of an electronic excitation or ionization of an atom (the atomic ionization potential) that restricts the range of pressures for which the foregoing discussion is valid. For xenon, in particular, metallization is expected at pressures of about 150 GPa [120 – 122]. Hence, the pressure range under consideration here lies below this limit; for other inert gases, this phase transition proceeds at higher pressures. Note that the absence of the stable crystal lattice for a system of repelling atoms does not mean the absence of two aggregate states which are similar to the solid and liquid aggregate states for a system of bound atoms. Below, we consider both these aggregate states.

Thus, as demonstrated by modelling an ensemble of repelling atoms by hard balls filling a container [38, 113 – 115], and by computer simulation of the system of hard, repelling spheres [116 – 118], the system of strongly repelling atoms does not form a crystalline lattice at high pressures and low temperatures. Reliable information is also available from X-ray diffraction investigations of compressed inert gases at low temperatures. If we start from the crystalline state of an inert gas and increase the pressure, a stacking instability [123, 124] develops in some pressure range that is reported to induce a transition from the face-centered lattice to the hexagonal lattice. For xenon at low temperatures, in particular, a stacking disorder starts to appear at a pressure of about 4 GPa ($p \approx 100p_0$). At pressures above 70 ± 5 GPa ($p \approx 2000p_0$), high-resolution X-ray diffraction studies show the presence of only the hexagonal close-packed structure for the system of repelling atoms [125]. But such measurements highlight only one aspect of the atomic structure, namely, that the correlation in positions of nearby atoms corresponds to the hexagonal structure. Simultaneously, a pressure increase reduces the long-range order of the structure, even while nearby atoms remain correlated. This results in some resonance-like maxima in the high-resolution X-ray diffraction pattern, but nevertheless the correlation length is comparable to the distance between nearest atoms. Hence, this does not prove that atoms form a regular hexagonal crystal lattice.

On the basis of such investigations one can suggest that the system of repelling atoms at high pressures consists of individual domains — that is, solid clusters of fcc and hexagonal structures (or one of these structures). These clusters are presumably oriented randomly, with neighboring clusters connected by fixed 'bonds'. Voids or vacancies at the boundaries between neighboring clusters lower the average number q of nearest neighbors in comparison with that for the close-packed crystal for which $q = 12$. At high pressures and very low temperatures, the average number of nearest neighbors run into $q = 10.4$; this picture is not consistent with one set of computer simulations by molecular dynamics of xenon at high pressures [126]; however, for those calculations, a regular, body-centered cubic structure was assumed. Since the number of nearest neighbors is precisely $q = 8$ for a body-centered crystal, the assumption of this structure is in disagreement with our results and seems incompatible with the evidence now available. Whether a bcc structure would have enough local stability to be observed is an open question at the present time.

The domain structure of an ensemble of repelling atoms at high pressures, following from the results of computer simulation and experiments, and the behavior of hard balls in a container, means that some degree of order (probably with some long-range character) in a hexagonal structure is established, at least temporarily, for each test atom. For estimating the length of this correlation at high pressures, we compare this structure with an ensemble of noninteracting clusters with the hexagonal structure, for which the magic number of atoms $n = 946$ for the optimal hexagonal structure — that is, a truncated hexahedron corresponding to the average coordination number $q = 10.5$ [33, 65]. This coincides with the coordination number $q = 10.4$ of nearest neighbors for an ensemble of repelling atoms at high pressures. Hence, the number of correlating atoms in a line that links a test atom with its neighbors measures $4 – 5$, and the total number of correlating atoms, we can infer, is several hundred.

Thus, one can describe the character of evolution of the solid inert gas structure resulting from compression in the following way. At low pressures $p \ll p_0 = D/R_e^3$, the crystal has the fcc structure ($q = 12$); an increase in the external pressure leads to a stacking instability which starts from $p \sim p_0$. As a result of this instability, regions of hexagonal structure develop inside the crystal, at first for layers and later for domains or small clusters. The random distribution in cluster orientations produces a decrease of the packing density φ and of the mean coordination number q for this system due to the formation of voids on boundaries of structured clusters. Together with this, pairwise interactions fix neighboring clusters. As a result, solid inert gases at high pressures consist of small solid domains — clusters — so that a bulk solid containing a large number of such domains has an amorphous structure. Since interaction of adjacent domains may be characterized in significant part by interaction of non-nearest atoms (depending on the specific interatomic potential), their structure can be sensitive to the details of that interaction potential. Consequently, the parameters of strongly compressed rare gases at low temperatures can be very different for various inert gases. Hence, the solid system of strongly repelling atoms is characterized by order on the scale of typical sizes of individual clusters, but it is amorphous on large scales. Thus, in spite of the simple character of the approximate model for interaction, the structure of solid systems of repelling atoms is not so simple as one might expect from general, simplistic considerations.

Additional information about the polycrystalline structure of a particle ensemble with a strong repulsion follows

from investigations of colloid solutions. One can utilize a solution with particulate material such that spherical particles of virtually identical radius (up to 5%) are formed under given conditions. This follows from the character of particle charging that restricts their growth in the solution and selects a certain particle size when they reach a critical degree of mutual repulsion. This method, in particular, is used to produce fractal aggregates consisting of solid monomers of identical size by changing the acidity of the solution in which solid colloid particles are formed (for example, gold colloids) [127–133]. Studies of crystallization in colloid solutions [134–136] concerned with colloid particles of 170 nm radius, allowing one to detect the particle structure by light scattering. It was confirmed that, for the packing parameter values $\varphi < 0.494$ common to the colloid solution, the distribution of particles is random, whereas for $\varphi > 0.545$ the colloid solution consists of a large number of randomly oriented crystallites of size ~ 100 μm. At the same time, the density of individual crystallites exceeds 10^6 cm^{-3} [136], corresponding to a number of monomers in an individual crystallite on the order of 4×10^7.

These crystallites also demonstrate a random transition between the hexagonal and fcc structures [136] that corresponds to the onset of stacking instability in strongly compressed inert gases. But gravitational forces and rates of nucleation are important for formation and relaxation of crystal structures in colloid solutions. This leads to an additional value ($\varphi = 0.58$) of the packing parameter for which stability is seen in colloid solutions, which corresponds to the so-called glass transition. This is the parameter value above which a long-lived amorphous phase is stable, at least locally, in a colloid solution. In addition, nucleation processes giving rise to more structured forms start the freezing process significantly at these values of the packing parameter. However, under the gravitation-free conditions of a cosmic experiment [137], crystallization of a colloid solution is substantially enhanced at large packing parameters.

Thus, in spite of the simplicity of the representation of the interatomic interaction we used initially, the structure of solid systems of repelling atoms is not so simple as one might expect from that convenient but approximate model. In considering the ensemble of repelling atoms, we assume it to be sustained under external pressure, and that the transition between two aggregate states proceeds at a constant pressure. Under these conditions, the crystal lattice does not form at low temperatures. But this result may be different under other external conditions. In particular, this conclusion does not hold true for a dusty plasma in which micron-sized charged particles may be captured by a trap made of a gas discharge, as was observed in experiments [138–141] and was analyzed in some reviews (see, for example, Refs [142–146]). This electric trap for charged particles may be the near-cathode region of a high-frequency discharge or striations in a glow discharge; in this case, the charged macroscopic particles interact with each other through the Yukawa interaction potential. The Yukawa potential comprises short-range interactions and long-range screened Coulomb parts; with the strong screening of charges in a plasma (or large distances between nearest particles), the long-range part makes a small contribution to the total particle interaction, so that an ensemble of micron-sized particles in a plasma trap becomes virtually identical to a system of hard particles. Under certain conditions, this ensemble is analogous to saturated solutions of charged colloidal particles.

In contrast to an ensemble of repelling atoms, the particles in a dusty plasma can form a crystal lattice under certain conditions. Moreover, the phase transition between the solid and liquid states in a dusty plasma can proceed in the form of a wave [147], whereas in usual ensembles of interacting particles the phase transition results from the growth of nuclei of a new phase inside an old one [38]. One can roughly explain the difference in behavior of these systems in terms of the conditions under which they are found. The ensembles of repelling atoms under consideration here are kept at constant pressure, whereas an ensemble of charged particles in a dusty plasma is best described as being in a potential well created by an external source, whose parameters are determined partially by the self-consistent field of charged particles. Hence, in the latter case, we have more complicated boundary conditions which may allow the pressure to change in the course of the phase transition. As for the phase transition wave, it can occur under a high degree of metastability (overcooling of a liquid or overheating of a solid) that is possible in a dusty plasma.

We note also the distinction between the aggregate states at low temperatures for the ensemble of hard spheres and for a system of particles interacting through the Yukawa potential. The latter [148–154] can have crystal structures at low temperatures and small screening length, although in this limit one can expect the behavior of the system of Yukawa particles to be similar to that of the ensemble of hard spheres. Possible, this contradiction should be resolved by computer simulation simultaneously for both interaction potentials.

Thus, both a dusty plasma and a collection of Yukawa particles can be considered representatives of simple ensembles of interacting particles, and the analysis of their aggregate states together with transitions between these aggregate states may be joined in a general scheme. The apparent contradictions or paradoxes just described can be overcome with a more detailed analysis that will deepen our understanding of the physics of aggregate states.

3. Phase transitions in simple systems of bound atoms

3.1 The lattice model for the order–disorder phase transition

The nature of the phase transition between two aggregate states in a condensed system of atoms has been interpreted on the basis of the lattice model. Within the framework of this model, we place atoms at sites of a crystal lattice, as shown for the square lattice in Fig. 1. Denoting by n_1 the number of atoms at lattice sites, and by n the total number of sites, we consider the limit of a large number of atoms ($n_1 \to \infty$), when the atomic concentration is $c = n_1/n$. We consider the Bragg–Williams approximation [3, 22, 23], a simple version of the lattice model accounting for interaction of nearest neighbors only. In the limit under consideration, when $n \to \infty$, one can extract two types of atomic distributions over the lattice sites, so that in the first the binding energy is maximal; a random distribution with higher entropy corresponds to the second type. In the first case, for a compact atomic distribution, we obtain the total binding energy of the system, $q n_1 \varepsilon_0 / 2$, where ε_0 is the binding energy per bond, and q is the number of nearest neighbors for an internal atom.

Analyzing the random distribution of atoms over the sites, the average number of nearest neighbors for a test atom is

determined to be qc, and the average binding energy is $qcn_1\varepsilon_0/2 = qnc^2\varepsilon_0/2$. Therefore, the energy change as a result of transition from the compact or ordered distribution of atoms to a random distribution reaches

$$\Delta E = \frac{q}{2}\,nc\varepsilon_0 - \frac{q}{2}\,nc^2\varepsilon_0 = \frac{q\varepsilon_0}{2}\,nc(1-c)\,. \tag{3.1}$$

In addition to this, the entropy of the random distribution of atoms is equal to

$$S = \ln\frac{n!}{n_1!(n-n_1)!} = -n\big[c\ln c + (1-c)\ln(1-c)\big]\,, \tag{3.2}$$

and the change in the free energy ΔF as a result of the transition between the ordered and disordered states is

$$\Delta F = \Delta E - TS = \frac{q\varepsilon_0}{2}\,nc(1-c)$$
$$+ Tn\big[c\ln c + (1-c)\ln(1-c)\big]\,, \tag{3.3}$$

where we applied the Stirling formula and the condition $n_{1,2} \gg 1$. This gives the temperature T_c of the phase transition according to the relation $\Delta F(T_c) = 0$:

$$T_c = \frac{q\varepsilon_0}{2}\left[\frac{\ln(1/c)}{1-c} + \frac{\ln\big(1/(1-c)\big)}{c}\right]^{-1}. \tag{3.4}$$

We note that in this treatment the concentration of atoms c was fixed, but the number of unoccupied sites is a free parameter of the problem. Since this parameter is not connected with any specific properties of an ensemble of bound atoms, the lattice model allows us to make qualitative conclusions about the nature of the phase transition. Therefore, we draw general conclusions from this analysis. Indeed, we have two distributions of bound atoms in a loosely confined space: a compact (or ordered) distribution of atoms with a large total binding energy, and a random distribution with a large entropy (or statistical weight). Competition between these two forms leads the system to equilibrate to the more thermodynamically stable state. From this it follows that the phase transition is possible only under conditions in which the aggregate state with the lower binding energy is characterized by a large statistical weight. From this standpoint, one can analyze and contrast atoms (as well as small molecules) and clusters. Both systems possess shell structures, but the excited states of atoms and small molecules are sparse, so the statistical weights of their excited states is not large, and therefore phase transitions are impossible in such systems. This contrasts with the cluster case. (It is possible, however, that ensembles of heavy atoms with open electronic shells could show order–disorder transitions at temperatures high enough to produce a variety of excited electronic states.)

One more conclusion from this treatment is the stepwise character of the phase transition for an ensemble of many bound atoms. Indeed, the ratio of the probabilities for the ensemble to be found in the disordered and ordered state is characterized by the factor $\exp(-\Delta F/T)$, where T is the current temperature, and ΔF is the free energy difference for the ordered and disordered aggregate states. The temperature range in which the ordered and disordered states coexist (i.e., the probabilities for these states are comparable) is given by

$$\frac{\delta T}{T_c} \sim \frac{T_c}{\Delta E} \sim \frac{1}{n}\,, \tag{3.5}$$

i.e., the width of the transition range is inversely proportional to the number of atoms. In the limit $n \to \infty$, we obtain a stepwise transition.

3.2 Structural transitions in solid clusters

The lattice model exhibits the character of the phase transition between two states, so that the higher-energy state has the larger statistical weight or greater entropy at temperatures at which it is accessible. Consequently, at a certain temperature an excited state becomes thermodynamically favorable, and then the phase transition proceeds. Since a large statistical weight of an aggregate excited state is required for the phase transition, this process is the consequence of transitions involving many particles of the system. For this reason, a phase transition is impossible in small systems because each atomic shell contains relatively few electrons, but it is possible for large clusters in which many atoms can be located in a shell or layer. The simplest phase transition takes place between two solid cluster structures. In particular, we consider here the structural transition between the face-centered cubic structure and the icosahedral structure of clusters with a pair interaction of atoms. Above, we analyzed the general basis for the competition of these structures and established that for large clusters any of these structures may be thermodynamically favorable, depending on the pair interaction potential and cluster size.

Let us consider such a cluster for which the binding energies of cluster atoms are similar for these two structures at zero temperature, and the lower-energy structure is characterized by its closed atomic shells. In this treatment, we will be guided by a cluster of 923 atoms whose lower-energy state has icosahedral structure with a closed outer shell, and the excitation energy of the fcc structure is comparable to the binding energy of one atom. Because an fcc cluster of this size exhibits unfilled shells, it has a large statistical weight $g_0 = 5544$ at zero temperature for an fcc cluster of 923 atoms [86, 87]. This is just the number of places where the vacancies can be. The pairwise binding energies of the two cluster structures are similar. For example, if we invoke Morse interactions between atoms, the pair interaction potential of the atoms is

$$U(R) = D\Big\{\exp\big[2\alpha(R-R_e)\big] - \exp\big[\alpha(R-R_e)\big]\Big\}\,, \tag{3.6}$$

where R_e is the equilibrium distance, and α is the Morse parameter. Then the energies of the close-packed and icosahedral structures coincide at $\alpha R_e = 7.1$ [84, 85]. Hence, in the case under consideration $\alpha R_e \leqslant 7.1$, so that in this range the icosahedral structure generally has lower energy, but the energy gap between structures is not large, and a transition between these structures occurs at temperatures well below the melting point $T_m = 0.44D$ [155]. Variation of αR_e allows the control of the conditions of this cluster's structural phase change, thus helping us to understand the nature of structural phase transitions in solids.

When two structures compete, one can construct the cluster's partition function Z on the basis of these two structures:

$$Z = Z_{\text{ico}} + Z_{\text{fcc}}\,, \tag{3.7}$$

where Z_{ico} and Z_{fcc} are the partition functions for the icosahedral and fcc structures, respectively. Taking the statistical weight of the lower icosahedral state to be one, we

have the connection between these partition functions:

$$Z_{\text{fcc}} = Z_{\text{ico}} \, g \, \exp\left(-\frac{\Delta}{T}\right), \tag{3.8}$$

where Δ is the difference in the ground state energies for these structures, and g is the statistical weight of the fcc cluster. The temperature at which the two phases have equal free energies, which is the precise analog of the temperature of the bulk phase transition T_{tr} between the two solid structures, is determined from the condition of equality of the partition functions for the two phases: $Z_{\text{fcc}} = Z_{\text{ico}}$. If the energy difference Δ for the ground states of these structures is small enough, the statistical weight g corresponds to the ground configuration state of the fcc cluster and comprises 5544. In this limiting case, the transition temperature for the cluster of 923 atoms is equal to (we make use of the relation $Z_{\text{fcc}} = Z_{\text{ico}} = Z/2$)

$$T_{\text{tr}} = \frac{\Delta}{\ln g + \ln(Z_{\text{fcc}}/Z_{\text{ico}})} = 0.104\Delta \,. \tag{3.9}$$

Let us find the dependence of the structural transition on thermodynamic parameters of the cluster. We concentrate on the cluster's heat capacity under conditions that the configurational excitation is in equilibrium with thermal vibrations of cluster atoms, i.e., these degrees of freedom are characterized by the identical temperature T. Evidently, the configurational part of the cluster's heat capacity has a resonant-like structure — that is, it exhibits a maximum. We will focus on this aspect, relating the partition function (3.7) to configurational excitation and representing it in the form

$$Z = \sum_i g_i \exp\left(-\frac{\varepsilon_i}{T}\right), \tag{3.10}$$

where ε_i and g_i are the excitation energy and statistical weight of a given configurational excitation of the cluster, respectively, and the configurational part of the heat capacity is given by

$$C = \frac{\partial E}{\partial T} = \frac{\partial}{\partial T}\left(\frac{1}{Z} \sum_i \varepsilon_i Z_i\right) = \frac{\overline{E^2}}{T^2} - \left(\frac{\overline{E}}{T}\right)^2, \tag{3.11}$$

where $\overline{E}$ and $\overline{E^2}$ are the average and mean square values of the configurational excitation energy of a cluster, respectively. Separating configurational excitation for the icosahedral and fcc structures and substituting formula (3.10) into formula (3.11), we represent the cluster's heat capacity in the form [86, 87]

$$C = \frac{Z_{\text{ico}}}{Z} C_{\text{ico}} + \frac{Z_{\text{fcc}}}{Z} C_{\text{fcc}} + \frac{1}{T^2} \frac{Z_{\text{ico}} Z_{\text{fcc}}}{Z^2} \left(\overline{\varepsilon_{\text{ico}}} - \overline{\varepsilon_{\text{fcc}}} - \Delta\right)^2. \tag{3.12}$$

Here, Z_{ico} and Z_{fcc} are the total partition functions for the corresponding cluster structures, Z is the total partition function according to Eqn (3.7), and C_{ico} and C_{fcc} are the heat capacities for each cluster structure, when the other cluster structure is absent. In the last term, $\overline{\varepsilon_{\text{ico}}}$ and $\overline{\varepsilon_{\text{fcc}}}$ are the average excitation energies for a given cluster structure in which the ground configuration of this structure corresponds to zero energy. The last term possesses a resonant structure near the transition temperature (3.9) at which formula (3.12)
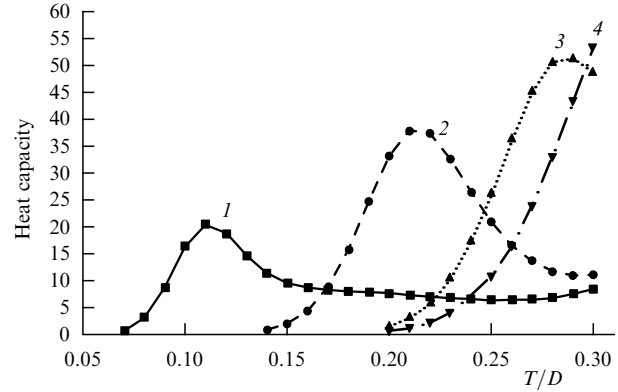

Figure 5. The heat capacity of a solid cluster consisting of 923 atoms as a function of the temperature [86, 87]. The ground state of this cluster at zero temperature corresponds to the closed icosahedral structure, and Δ, the excitation energy of the ground state of the fcc structure, is equal to (in units of breaking one bond): 1 (*1*), 2 (*2*), 3 (*3*), 4 (*4*).

takes the form

$$C_{\text{max}} = \frac{1}{2}(C_{\text{ico}} + C_{\text{fcc}}) + \left(\frac{\Delta}{2T_{\text{tr}}}\right)^2 \exp\left[-\alpha(T - T_{\text{tr}})^2\right],$$
$$\alpha = \left(\frac{\Delta}{2T_{\text{tr}}^2}\right)^2, \tag{3.13}$$

and the 'resonance' corresponds to $Z_{\text{ico}} = Z_{\text{fcc}} = Z/2$. Defining the resonance width as $\Delta T = (1/\alpha)^{1/2}$, we obtain

$$\Delta T \equiv \frac{2T_{\text{tr}}^2}{\Delta}\,. \tag{3.14}$$

In particular, for a cluster consisting of 923 atoms and a small difference Δ between the energies of the two structures, we obtain $\Delta T/T_{\text{tr}} = 0.2$.

Although we are guided here by small Δ, when the maximum in the heat capacity is observed at low temperatures, one can extend this approach to larger Δ, but to do that, we must take into account configurationally excited cluster states for each structure. This step was made in Refs [86, 87]. Figure 5 exhibits the behavior of the configurational heat capacity in the temperature range, below the melting point [86]. In this temperature range a restricted number of cluster configurations are excited. Clearly, the maximum heat capacity increases with an increase in Δ.

The structural transition also influences other thermodynamic properties of the cluster. The entropy undergoes an abrupt change associated with the structural transition as it passes from its value for the first structure to that for the other. Because an excited structure is characterized by a higher entropy, the structural transition as a result of a temperature elevation leads to an entropy increase in a stepwise manner. In particular, if we return to the case of a cluster with 923 atoms and with a small energy gap between its two relevant structures, the abrupt change in entropy as a result of the transition from the icosahedral cluster structure to the fcc structure is $\Delta S = \ln g = 8.6$. This entropy jump must increase with an increase in the energy gap Δ, but its order of magnitude is conserved, i.e., $\Delta S \sim 10$.

Thus, we find that the structural transition leads to a maximum in the cluster's heat capacity and to an abrupt change in the cluster's entropy. Of course, corresponding

changes occur in the other thermodynamic parameters as well. Let us compare these changes with the thermodynamic parameters due to atomic vibrations in the cluster. In the Debye approximation, in particular, the cluster entropy at moderate temperatures is given by [6]

$$S_{\mathrm{vib}} = 3n \left(\ln \frac{T}{\hbar \omega_{\mathrm{D}}} - 1 \right), \quad T \gg \hbar \omega_{\mathrm{D}}, \qquad (3.15)$$

where ω_{D} is the Debye frequency (the maximum or cut-off frequency in the model), and n is again the number of cluster atoms. In particular, for a cluster of 923 atoms, this formula gives $S_{\mathrm{vib}} \sim 1000$. One can see that this value significantly exceeds the entropy jump due to a structural transition. However, the vibrational entropy does not change very much at all in the transition, typically increasing only slightly as a few modes drop in frequency as the system goes to the high-temperature phase, due to void spaces that soften local vibrational modes. This is a general result for large clusters. Any phase transition in a cluster influences its thermodynamic parameters through the appearance of resonance-like maxima and abrupt changes at the phase transition temperature. But if one looks only at the configurational contributions directly associated with the transition process and neglects the thermal motion of atoms, it is easy to overlook the fact that the changes in the cluster's thermodynamic parameters due to the phase transition are small in comparison with their total values due primarily to the thermal motion of the atoms. The analysis of the structural transition in a cluster consisting of 923 atoms [86, 87] confirms this statement. Nonetheless, because the phase transition itself is a reflection of *changes* predominantly in configurational properties, the vibrational contribution to the changes in thermodynamic properties is typically less important than the configurational part.

The importance of the structural transition in large clusters decreases with cluster size because such a transition requires spontaneous reconstruction of the cluster's structure at low temperatures. Under those conditions, reconstruction proceeds extremely slow, so that conditions of thermodynamic equilibrium can be violated for a very long time. It follows that the structural transitions in very large solid clusters are usually not especially important.

3.3 Phase transitions in a system of strongly repelling atoms

An ensemble of repelling atoms constitutes a system with pairwise atomic interactions that models the behavior of inert gases at high pressures. In considering such systems at low temperatures, we deduced that the symmetric, crystalline distribution of atoms is not realized at thermodynamic equilibrium. Nevertheless, a solid – liquid phase transition does occur in these systems, so that a general statement by Stishov [156] may be fulfilled, namely that the melting curve in the pressure – temperature phase diagram of this system need not terminate at a critical point, but may continue up to high temperatures and pressures. At high pressures, the phases that this curve separates are not the crystal and liquid states as it does at low pressures. Rather, both states of this phase transition correspond to disordered distributions of atomic particles; they are states of dense and loose packing structures [38]. This enables us to describe the phase transition in a bulk system of repelling atomic particles on the basis of the changes in density and coordination number

q, the number of nearest neighbors for an internal test atom. The extent of short-range order in each of these phases is, at present, unknown.

Information about the phase transition in a bulk ensemble of repulsing atoms may be extracted from experimental data [123, 157 – 162] for compressed inert gases and from computer simulation [116 – 118, 163, 164]. Analyzing computer simulation, we are guided by the pair interaction potential (2.21) whose parameter γ characterizes its steepness. The passage to the limit $\gamma \to \infty$ corresponds to the hard sphere model, and within the framework of this model the phase transition between the states of dense random packing structure (dr) and loose random packing structure (lr) corresponds to the following values of the packing density [116 – 118] given by formulas

$$\varphi_{\mathrm{dr}} = 0.545, \quad \varphi_{\mathrm{lr}} = 0.494. \qquad (3.16)$$

On the basis of formula (3.16), we find that $q_{\mathrm{dr}} = 8.8$ is the number of nearest neighbors of a test atom in the dense random packing state in the melting curve, and $q_{\mathrm{lr}} = 8.0$ for the loose random packing state. If we construct the melting curve for various pressures for a condensed system such as a condensed inert gas, we move with increasing pressure from the crystalline solid state to the dense random packing structure which must lie on the dense portion of the melting curve. Therefore, although crystalline order is absent in the dense random structure, it starts from the ordered state. At the present time, it is not clear whether the transition from crystalline to dense random packing structure is a continuous transition or involves an abrupt change, in effect a first-order structural transition, from crystalline to a state with a definite finite degree of disorder. In contrast to the dense random state, the loosely packed random structure starts from a disordered state at low pressures, typically liquid. Hence, it is convenient to connect the dense random packing structure with the close-packed crystal structure, and the loose random packing structure with the liquid state in which there is no periodic long-range order and one can describe the system in terms of its average continuous homogeneity. In addition, if we move at high pressures from zero temperature to the melting point, the number of nearest neighbors decreases from $q = 10.4$ to $q_{\mathrm{dr}} = 8.8$.

An additional understanding of the structures of the particle ensemble with a strong repulsion follows from the study of colloid solutions involving particles of almost identical sizes and, correspondingly, of almost identical charges. Then, for $\varphi < 0.494$, a random distribution of colloid particles is observed that corresponds to the liquid aggregate state, whereas for $\varphi > 0.545$ the colloid solution consists of a large number of randomly oriented crystallites, each of them including a large number of colloidal particles. In an intermediate range of packing parameters, the colloid solution consists of amorphous and polycrystal phases which are separated by sharp boundaries [134, 136].

For finite values of the parameter γ in the interaction potential (2.21), the values of various parameters in the melting curve may be estimated on the basis of a typical length d that follows from the relation $U(d) \sim T$ and is given by

$$d = \left(\frac{A}{T} \right)^{1/\gamma}, \qquad (3.17)$$

Table 9. Parameters of the phase transition between the solid or dense random packing state (index dr) and liquid or loose random packing state (index lr) for a system of repelling atoms (taken from Ref. [164]).

γ	4	6	8	12	∞
$T/(pV_{\text{dr}})$	0.011	0.026	0.036	0.053	0.091
$V_{\text{dr}}\sqrt{2}/d^3$	0.254	0.641	1.030	1.185	1.359
$V_{\text{lr}}\sqrt{2}/d^3$	0.255	0.649	1.060	1.230	1.499
$\Delta V/V_{\text{dr}}$	0.005	0.013	0.030	0.038	0.103
$p\Delta V/T$	0.45	0.50	0.63	0.72	1.16
ΔS	0.80	0.75	0.84	0.90	1.16

where T is the temperature in the melting curve. Introducing the pressure p, the volumes per atom for the dense random packing (solid) and loose random packing (liquid) states V_{dr} and V_{lr}, respectively, the change of the reduced volumes ΔV upon melting ($\Delta V = V_{\text{dr}} - V_{\text{lr}}$), and the entropy change per atom ΔS, we obtain the scaling law for the melting curve [156]:

$$p \sim \frac{T}{d^3}, \quad \Delta V \sim V_{\text{dr}} \sim V_{\text{lr}} \sim d^3, \quad \Delta S \sim 1. \quad (3.18)$$

Table 9 gives the parameters in the melting curve for a system of atomic particles with the interaction potential (2.21) for various γ, obtained on the basis of numerical calculations [164]; the equation connecting the pressure p and temperature T in the melting curve is, of course, the usual equation for phase coexistence. From the data in Table 9, it follows that the volume change between dense and loose random states, $\Delta V = V_{\text{dr}} - V_{\text{lr}}$, is small compared with each term of the expression. Next, also from Table 9, the packing densities in the coexistence curve in the limit $\gamma \to \infty$ coincide with those in formulas (3.16).

Experimental approaches to constructing the melting curve for inert gases at high pressures are based on the method of the diamond-anvil cell containing an inert gas compressed by a laser beam. The laser beam heats the inert gas inside the diamond cell through its metal substrate, and is used to measure the inert gas pressure and temperature in the course of its heating. The melting point is found from a change in the optical properties of the compressed, condensed inert gas. This method allows us to analyze pressures up to 100 GPa, two orders of magnitude higher than those available to classical methods of gas compression (see, for example, Refs [157–160] covering the case of argon).

Even at the highest pressures, the kinetic energy of atoms in the melting curve is small compared to the electronic excitation energy or the ionization potential of these atoms. Hence, thermal electronic excitation and ionization of atoms in the melting curve under consideration is small and does not influence the phase transition. At very high pressures, compression of inert gases creates such strong overlap of the wave functions of valence electrons that it can induce a transition from the insulating state to the metallic state. This effect is especially strong for xenon, for which the transition to the metallic conductivity is expected at $130–150$ GPa [120–122]. In reality, this transition proceeds over a wide pressure range and evidently depends on the temperature. This effect can, of course, affect the behavior of the melting curve. Moreover, one can expect that the observed decline of the melting curve $T(p)$ for xenon at pressures above 15 GPa, and for krypton at pressures above 25 GPa, can also be attributed to this effect.

In order to escape the influence of metallization at high pressures on the behavior of the melting curve, we consider
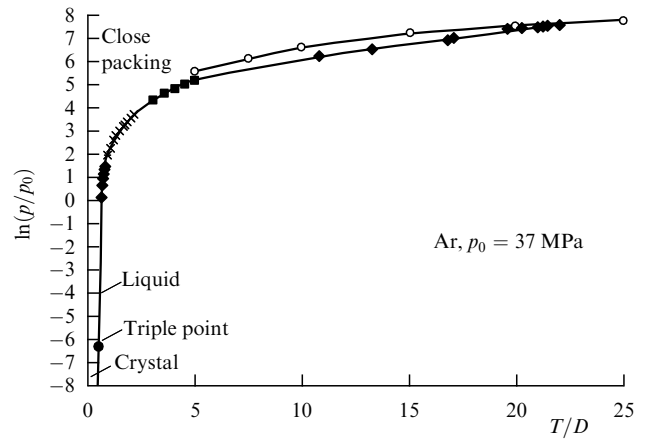

Figure 6. The melting curve for condensed argon. Experimental data: black diamonds, squares, and crosses [123, 161, 162]. The black circle is the triple point, and the solid curve is constructed on the basis of these data, and its derivative is given by formula (3.19). White circles correspond to calculations according to the data from Table 9 with the interaction potential (2.21) whose parameters are given in Table 7.

the melting curve of compressed argon (Fig. 6). This figure is based on experimental data [123, 161, 162] which are approximated by the following expression for the argon melting curve:

$$\frac{\mathrm{d}p}{\mathrm{d}T} = 4 + a\left[\left(\frac{T}{T_{\text{tr}}}\right)^k - 1\right]. \quad (3.19)$$

In this formula, the derivative $\mathrm{d}p/\mathrm{d}T$ is measured in MPa K^{-1}, and $T_{\text{tr}} = 83.8$ K is the argon triple point. We take this derivative at T_{tr} to be 4 MPa K^{-1}, as follows from the Clapeyron–Clausius and Simon equations for argon [94]. The parameters of formula (3.19) are $a = 2.1$, and $k = 0.78$. One can see that this derivative varies by one order of magnitude (from 4 up to 37 MPa K^{-1}), when the temperature along the melting curve varies over the temperature (or pressure) range under consideration, from T_{tr} up to 3400 K. The melting curve for argon is given in Fig. 6 at high pressures, as constructed from the data in Table 9. We see that this theoretical curve is located above and close to the melting curve that approximates experimental results.

Let us now analyze the behavior of compressed inert gases up to the highest pressure at which one can consider them as a system of independent atoms. Evidently, this limit follows mainly from the atomic structure and corresponds to the pressure below which we can ignore excited atomic states and metallization. In reality, when the pressure is very high indeed, the electronic bands of the ground and excited states approach each other as the pressure increases. When these bands become close enough to an extent that metallic conductivity begins, electronic processes become important, and this scheme terminates. As said previously, for xenon, this transition to metallic conductivity is expected at pressures $130–150$ GPa [120–122]; for other inert gases the limiting pressures are higher, and the foregoing analysis is valid below these pressures.

Thus, the phase transition in a bulk ensemble of repelling atoms is similar to the phase transition in a condensed system of bound atoms, i.e., an order–disorder or solid–liquid transition. But in contrast to the latter, the phase transition

in a bulk ensemble of repelling atoms proceeds between two random distributions of atoms. In addition, according to experiments and computer simulations, a general statement by Stishov [156] is fulfilled, namely that the melting curve in the pressure – temperature phase diagram for a bulk ensemble of repelling atoms does not need terminate at a critical point, but may continue up to high temperatures and pressures, until other interaction effects will not act.

4. Configurational excitation in clusters with pairwise atomic interactions

4.1 Peculiarities of configurational excitation of clusters

We now consider the evolution of a cluster as motion of a point along a potential energy surface in a phase space of atomic coordinates. The potential energy surface for a cluster contains many minima separated by saddles; the number of local minima increases sharply with cluster size [11, 12, 14 – 16]. These include both the minima corresponding to geometrically distinct structures, which typically increase at least exponentially with the number of particles n, and the permutational isomers, which increase approximately as $n!$. Hence, one can (in principle) describe the cluster's evolution as a result of transitions between local minima of the potential energy surface, passages that correspond to saddle-crossing dynamics [10, 13, 18, 20]. Within the framework of this description, the cluster remains near a given minimum of the potential energy surface relatively long, since its average total kinetic energy is lower than typical saddle heights. We may characterize a configurational state of this system by the local minimum of the potential energy surface, near which the cluster is found for a time long compared with a typical oscillation period near this minimum. Because the dwell times around local minima are typically long compared with vibrational periods and even with vibrational relaxation times, we may suppose that the configurational cluster state is independent of the atomic (vibrational) kinetic energy. In other words, one can separate the configurational and vibrational cluster excitations as independent degrees of freedom.

This is the basis of our treatment in which we divide cluster excitation into configurational and vibrational parts and assume these parts to be independent. (Of course, they are ultimately coupled on sufficiently long time scales.) Next, to simplify the description of configurational excitation, we introduce a void as an elementary configurational excitation, so that any configurational excitation results from formation of one or more voids. Then one can express the parameters of the phase transition and other cluster properties through parameters associated with voids being formed. Therefore, our task is to find the void parameters and to express through them the parameters of the cluster phase transition.

Assuming the motion of cluster atoms to be classical, we represent the energy E of a cluster consisting of n atoms with a pair interaction between them in the form

$$E = U + K = \sum_{i,j} u(\mathbf{r}_{ij}) + \frac{m}{2} \sum_i \left(\frac{\mathrm{d}\mathbf{r}_i}{\mathrm{d}t} \right)^2 . \quad (4.1)$$

Here, U is the total potential energy, K is the total kinetic energy of atoms, and $u(\mathbf{r}_{ij})$ is the pair interaction potential between atoms at a distance $\mathbf{r}_{ij} = \mathbf{r}_i - \mathbf{r}_j$, so that $\mathbf{r}_i, \mathbf{r}_j$ are the atomic coordinates, and m is the atomic mass. This formula is the basis for the analysis of computer simulations of clusters. Let us consider the properties of two terms in this formula, taking into account that thermal equilibrium is established for atomic vibrations, as usually takes place. This allows us to introduce the vibrational temperature T, considering the motion of atoms as that of a set of harmonic oscillators. In particular, in the limit of high temperatures, when a typical atomic kinetic energy significantly exceeds a typical small-amplitude vibrational energy (or the Debye temperature), the Dulong – Petit law is valid, according to which

$$K = \frac{(3n - 6)\, T}{2} , \quad (4.2)$$

and we include in this expression the vibrational degrees of freedom for a cluster as a system of bound atoms. We will focus on conditions set in the limiting case $n \gg 1$. The global minimum of the complex potential energy surface corresponds to the cluster's ground state, i.e., its equilibrium state at zero temperature. Transitions from the global minimum to other local minima, corresponding to configurational excitations of the cluster, are responsible for a phase transition, whether from one solid form to another or from solid to liquid.

In analyzing the behavior of cluster atoms, we are guided first by the results of computer simulations of the Lennard-Jones cluster consisting of 13 atoms [8], in which this cluster is considered a member of a microcanonical ensemble of bound atoms [4], i.e., it is isolated and the total cluster energy is conserved during the cluster's evolution. There is a range of temperatures and pressures in which the distribution of short-term-average total kinetic energy of the cluster exhibits a bimodal distribution. In that range, one can treat the results of computer simulations [8] in terms of a dynamic equilibrium of two aggregate states. It was fulfilled partially in Refs [33, 76, 165], and below we give the results of this treatment. The structure of the ground state of this cluster [166] at zero temperature and the character of its configurational excitation in the lowest excited states are shown in Fig. 7a. The simplest configurational excitation corresponds to promotion of one atom from the shell of 12 atoms onto the hollow between three atoms on the cluster surface, as shown in Fig. 7b. For this transfer, an atom must overcome a barrier; likewise, transitions to other positions on the cluster surface are accompanied by overcoming the energy barriers. Figure 8 gives the energies of states for one-atom transitions at zero temperature and the values of barriers which separate them [167]. Increasing the energy facilitates transitions between different stable positions on the cluster surface, as well as
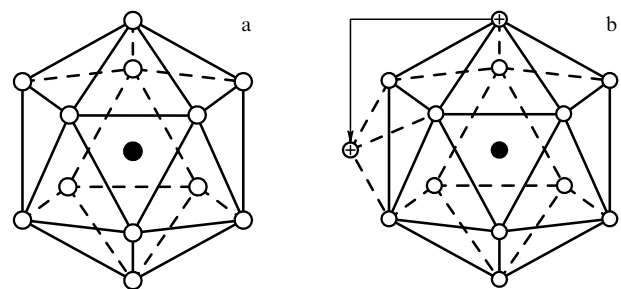

Figure 7. The structure of the icosahedral cluster consisting of 13 atoms in the ground configuration state [166] (a), and configurational excitation of this cluster (b).
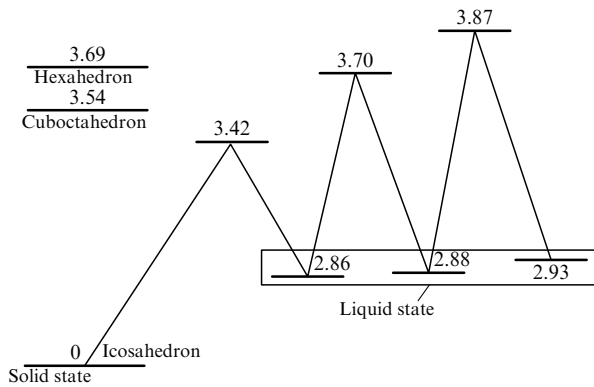
Figure 8. The lowest excited states of the Lennard-Jones cluster with 13 atoms, and the character of their formation through saddle points [167]. Values near levels indicate the excitation energies expressed in units of the binding energy D per one bond. The energies of the close-packed structures are taken from Ref. [11]. The lowest excited cluster states may be linked to the cluster's liquid state in which the clusters spend most of the time if they begin with sufficient excitation energy or temperature [8, 168–170].

Figure 9. Structures of the lowest excited states for the Lennard-Jones cluster consisting of 13 atoms [167], which correspond to the lowest local minima of the potential energy surface (a), and to the saddle structures (b) for this cluster. Excitation energies of these structures and energy barriers are expressed in the binding energies per one bond. Arrows indicate coincidence of projections of two or more atoms.

exchanges between states of a configurationally excited cluster. All the configurationally excited states of this cluster in the liquid state are connected with transitions of one atom at a time, so that the system may go through all permutations among the atoms of any attainable structure, as follows from the data in Fig. 9.

Let us represent formula (4.1) in the form

$$E = E_0 + E_{ex} = U'_{sol} + K_{sol} = \Delta E + U'_{liq} + K_{liq}, \qquad (4.3)$$

where E_0 is the binding energy of cluster atoms in the ground configuration state at zero temperature, E_{ex} is the total excitation energy, K_{sol} and K_{liq} are the total kinetic energies of atoms for the solid and liquid cluster states, respectively, U'_{sol} and U'_{liq} are the average potential energies of the cluster for a given aggregate state, and ΔE is an average excitation energy for producing the liquid aggregate state. Within the framework of this formulation, we join nearby local minima of the cluster's potential surface into one aggregate state, assuming transitions between local minima of the same aggregate state to be more effective than transitions between states which belong to different aggregate states. That is, we suppose that it is easier to move a void from one site to another than to create or destroy a void.

Figure 10 gives the probability that the Lennard-Jones cluster consisting of 13 atoms has a given total kinetic energy [8]. The bimodal character of this distribution at intermediate excitation energies testifies to the existence of two aggregate states, namely, the solid and the liquid. At low excitation energies, the solid aggregate state is only realized, whereas at high excitation energies only the liquid aggregate state exists. Of course, the total kinetic energy of atoms is averaged over time, so that oscillations due to vibrations of individual atoms are excluded from consideration. Thus, the time of such averaging must be brief compared to the typical time interval for transitions between aggregate states, but long compared with the time for coupling vibrational modes. This allows us to separate cluster aggregate states. For clusters in the size range from roughly 10 to several hundred atoms, averaging over many
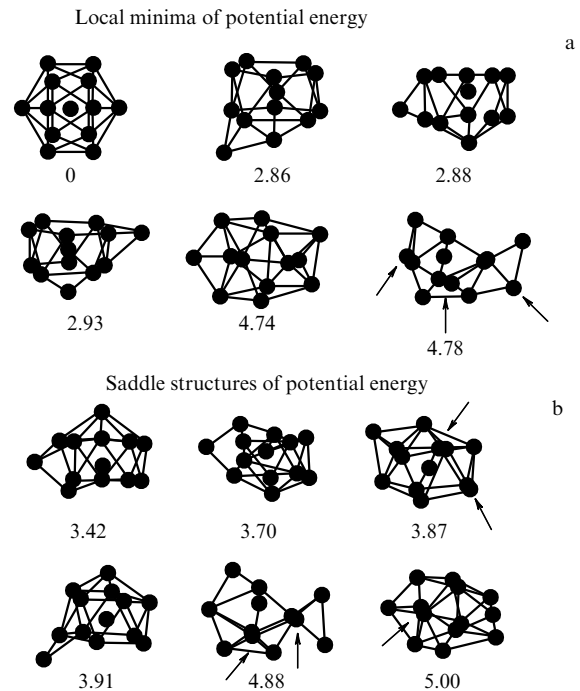
dozen vibrational periods accomplishes this and separates the time scales for thermal equilibration very conveniently from that for passage between aggregate states. Dynamic coexistence of aggregate states at intermediate excitation energies is simply the phenomenon that for part of the time a cluster is found in one aggregate state, and for the rest of the observation time it is found in another aggregate state. Clusters of many kinds exhibit the bimodal character shown in Fig. 10, i.e., residence times in each phase are long enough to establish properties we normally identify with a bulk phase, such as the diffusion coefficient and pair correlation function. Some clusters, e.g., Ar_{15}, pass between the phase-like forms too rapidly to develop such characteristic properties; these would appear in experiments to behave as a sort of slush in what would otherwise be the region of phase coexistence. This latter class of clusters has not yet been studied in depth. (In fact, clusters may exhibit dynamic coexistence of more than two phases [171, 172].)

We introduce the effective temperature for a given aggregate state of the cluster on the basis of a transformation of formula (4.2):

$$T = \frac{2}{3n-6} K = \frac{2K}{33}, \qquad (4.4)$$

where $n = 13$ is the number of cluster atoms, and we assume an atomic thermal energy is large in comparison with a typical excitation energy of atomic vibrations. The energy part η related to the kinetic energy of atoms is given by

$$\eta_{sol} = \frac{K_{sol}}{E_{ex}}, \quad \eta_{liq} = \frac{K_{liq}}{E_{ex} - \Delta E}. \qquad (4.5)$$
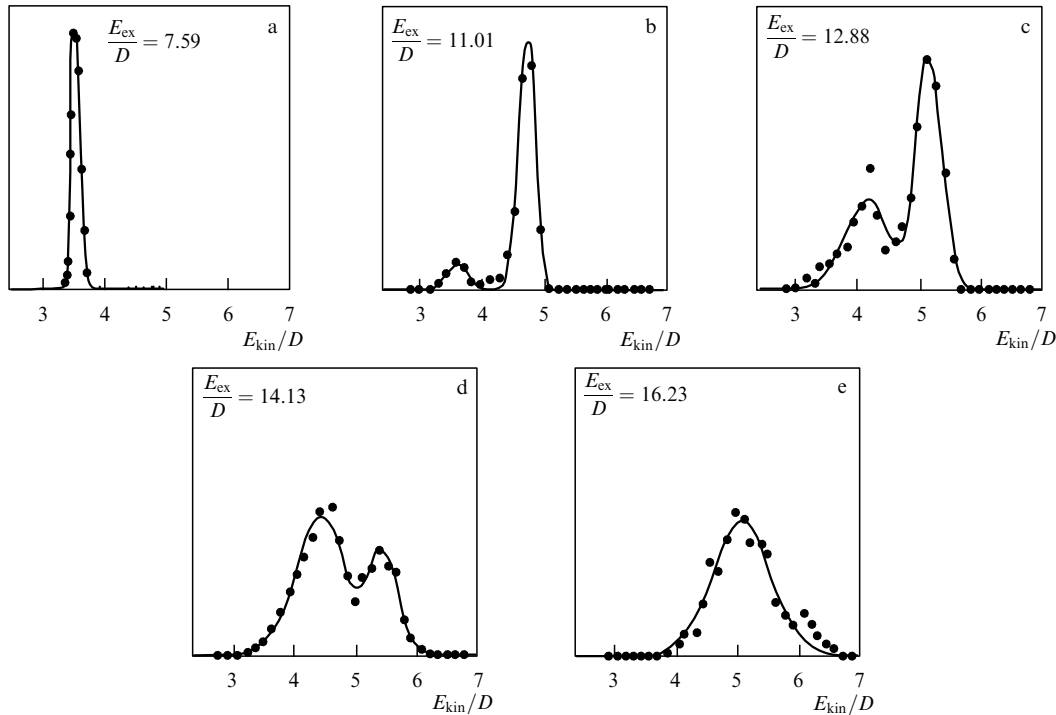
Figure 10. The distribution function of the total kinetic energy of atoms in the Lennard-Jones cluster consisting of 13 atoms. The range near the left maximum corresponds to the liquid state, and the right maximum with a range close to it relates to the solid state [8]. E_{ex} is the total binding energy of the atoms, and E_{kin} is the total kinetic energy of the atoms.

If atomic motion is representable as a combination of motions of harmonic oscillators, we have $\eta = 0.5$. Anharmonicity of the oscillations typically leads to a decrease in this value, and $\eta(E)$ decreases with an increase in E_{ex}. Figure 11 gives this dependence which was obtained [76] on the basis of computer simulations [8] for an isolated 13-atom cluster. Note that $\eta_{sol}(E_{ex}) = \eta_{liq}(E_{ex})$ within the limits of their accuracy, while this quantity has different values for the solid and liquid states at identical temperatures. This is because the value of η can be supposed first to be $\eta(E_{ex} = 0) = 0.5$ if the system were to be described in terms of harmonic oscillators, but in a real system it decreases monotonically with increasing excitation energy because of the increasing role of anharmonicity. Hence, the parameter η characterizes the influence of the anharmonicity on the atomic motion of an isolated cluster as the excitation energy increases.

From these data, we infer the excitation energy of the cluster's liquid state in the melting range:

$$\Delta E = \frac{K_{sol} - K_{liq}}{\eta(E_{ex})} = E_{ex}\left(1 - \frac{K_{liq}}{K_{sol}}\right) = 2.49 \pm 0.05 . \quad (4.6)$$

This suggests that the entropy jump ΔS_m at the temperature of equal free energies, the analogue of the bulk melting point $T_m = 0.29D$, is equal to $\Delta S_m = 8.6 \pm 0.2$. Figure 12 shows how the temperatures of the solid and liquid cluster states depend on the excitation energy for the Lennard-Jones cluster consisting of 13 atoms. These data are obtained on the basis of formula (4.4) applied to results of computer simulations [8] of this cluster. The effective cluster temperature T_{con} of the configurational excitation is determined from the equilibrium population ratio of the solid and liquid cluster states using the formula

$$\frac{w_{liq}}{w_{sol}} = \exp\left(-\frac{\Delta F}{T_{con}}\right) = \exp\left(-\frac{\Delta E}{T_{con}} + \Delta S\right), \quad (4.7)$$

where w_{sol} and w_{liq} are the probabilities for the cluster to be found in the solid and liquid states, respectively, and ΔF is the free energy jump at melting. It follows from Fig. 12 that the effective configurational temperature T_{con} tends to the solid temperature defined by formula (4.4) in the limit of low temperatures, and to the liquid temperature in the limit of high temperatures.
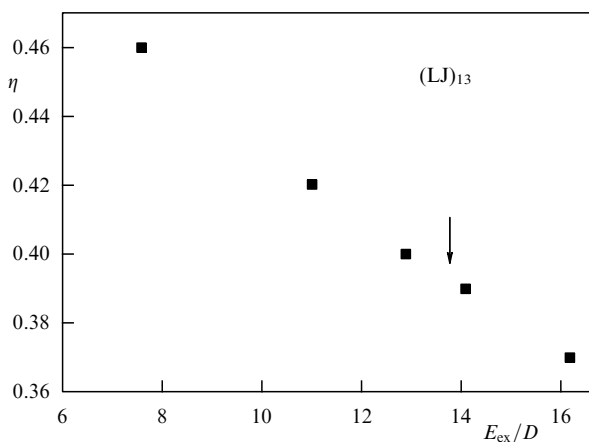

Figure 11. The dependence on the excitation energy for the energy part related to the kinetic energy of atoms for an isolated Lennard-Jones cluster consisting of 13 atoms. This quantity is identical for the solid and liquid cluster states. The arrow indicates the excitation energy of the phase transition, where $w_{sol} = w_{liq}$.
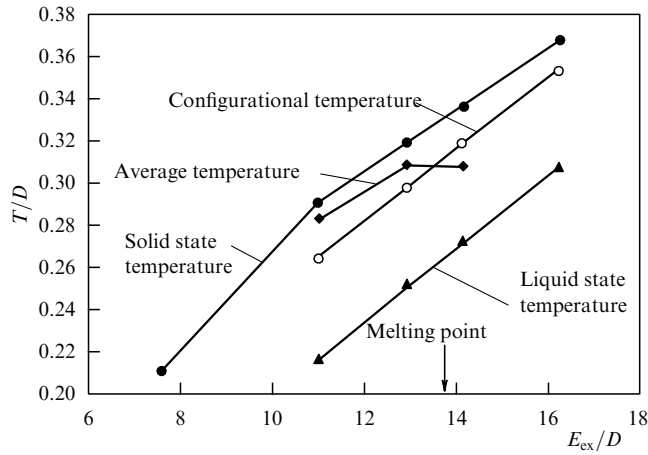
Figure 12. The translational temperatures for the solid and liquid cluster aggregate states, the average translational temperature according to formula (5.21a), and the configurational temperature T_{con} that follows from the ratio w_{liq}/w_{sol} and is given by formula (5.22). These temperatures relate to the Lennard-Jones cluster consisting of 13 atoms and are obtained on the basis of data from Fig. 10.

4.2 Approach of two aggregate states

A cluster consisting of bound atoms has many configurationally excited states. It is convenient to join them in groups, so that excited states with similar excitation energies are joined in one group. Often one can obtain in this manner two (or more) groups of configurationally excited states, so that the probability of finding a cluster located in one or the other of these states dominates the population distribution. In particular, in this way we find the solid and liquid aggregate states for the Lennard-Jones cluster consisting of 13 atoms (see Fig. 10). We next consider this form of the cluster distribution function, assuming the existence of two cluster aggregate states, i.e., supposing the probability of finding other configurational excitations with our cluster parameters to be small.

Let us consider an isothermal case in which the ensemble of clusters is located in a thermostat. This can be achieved experimentally by placing the clusters in a bath of helium atoms that collide with clusters in a chamber with metallic walls maintained at a desired temperature; such experiments have been carried out [173, 174]. In this way, the wall temperature becomes the cluster temperature. We introduce the liquid aggregate state probability [33, 76, 165]

$$w_{liq} = \frac{p}{1+p}, \quad p = \exp\left(-\frac{\Delta F}{T}\right) = \exp\left(\Delta S - \frac{\Delta E}{T}\right),$$
(4.8)

where T is the cluster temperature coinciding with the thermostat temperature, ΔE is the energy of configurational excitation, ΔS is the entropy jump as a result of melting, ΔF is the change in free energy, and we assume the cluster to be a member of canonical ensembles. The parameters ΔE and ΔS of the phase transition determine the behavior of the cluster heat capacity in the range of the phase transition. Using the average atomic kinetic energy for each aggregate state, we characterize each cluster aggregate state by a certain potential energy, i.e., we ignore the broadening of the energy of each cluster state due to fluctuations.

We determine below the cluster heat capacity and separate its resonance part related to the phase transition. We have, according to formula (4.3), the following relationship

$$E = \frac{K_{sol}}{\eta_{sol}} w_{sol} + \Delta E w_{liq} + \frac{K_{liq}}{\eta_{liq}} w_{liq},$$

and since the cluster is in a thermostat, $K_{sol} = K_{liq}$. Assuming $\eta_{sol} = \eta_{liq}$, we obtain the average cluster energy according to formula (4.1):

$$E = \frac{K_{sol}}{\eta_{sol}} + \Delta E w_{liq} = \frac{K_{sol}}{\eta_{sol}} + \Delta E \frac{p}{1+p}.$$
(4.9)

Hence, the cluster heat capacity consists of two parts:

$$C = \frac{dE}{dT} = C_0 + \frac{d(\Delta E w_{liq})}{dT},$$
(4.10)

where the first is given by

$$C_0 = \frac{d(K_{sol}/\eta_{sol})}{dT} = \frac{d(K_{liq}/\eta_{liq})}{dT},$$
(4.11a)

and the resonance part of the heat capacity is [33, 165]

$$C_{res} = \frac{d(\Delta E w_{liq})}{dT} = \frac{\Delta E^2}{T^2} \frac{p}{(1+p)^2}.$$
(4.11б)

Here, we assume that the energy of configurational excitation ΔE and the entropy jump ΔS are independent of the temperature. Formula (4.10) leads to the maximum C_{res}^{max} at the melting point T_m defined in this case through the equality $p(T_m) = 1$. We have

$$C_{res}^{max} = \frac{\Delta E^2}{4T_m^2} = \frac{\Delta S^2}{4}.$$
(4.12)

Let us introduce the temperature dependence of the entropy jump in the form [175]

$$\Delta S = \Delta S_0 + aT,$$
(4.13)

with ΔS_0 being the entropy jump at zero temperature. This gives, at the melting point, the relationship

$$a = \frac{\Delta S_m - \Delta S_0}{T_m},$$
(4.14)

where ΔS_m is the entropy jump at the melting point. Substituting this into formula (4.12), we get

$$C_{res}^{max} = \frac{\Delta S_m^2}{2} - \frac{1}{4}\Delta S_0 \Delta S_m.$$
(4.15)

This formula can be used for determining ΔS_m from other parameters, so we have [175]

$$\Delta S_m = \frac{\Delta S_0}{4} + \sqrt{\frac{\Delta S_0^2}{16} + 2C_{res}^{max}}.$$
(4.16)

Thus, we divide the entropy abrupt change at the phase transition into two parts, so that the first, ΔS_0, is due to configurational cluster excitation at zero temperature, and the second part $\Delta S_m - \Delta S_0$ is determined by the difference in

Table 10. Parameters of melting for atomic clusters and bulk systems. $(LJ)_n$ is a cluster consisting of n atoms with the Lennard-Jones interaction potential; D is the depth of the potential well.

Parameter	$(LJ)_{13}$	$(LJ)_{55}$	Bulk inert gases
T_m/D	0.29	0.31	0.58
$\Delta E/D$	2.5	16 ± 1	$0.98n$
ΔS_0	5.2	31 ± 2	$0.73n$
ΔS_m	8.6	48 ± 4	$1.68n$
$\Delta S_0/\Delta S_m$, %	60	65 ± 10	44

the entropies of the two aggregate states due to the thermal motion of atoms. Formula (4.16) connects these two contributions to the entropy at the melting point.

On the basis of computer simulations, one can find separately the entropy jumps ΔS_0 and ΔS_m at zero temperature and at the melting point; these are given in Table 10 for the clusters considered here. The statistical weight of configurational excitation of a cluster consisting of 13 atoms (see Fig. 7a [166]) is equal to $g_0 = 12 \times 15$, where the first factor is the number of surface atoms, and the second factor is the number of positions to which the promoted atom can go on the cluster surface, if the new vacancy and the excited atom are not adjacent. Correspondingly, the entropy jump for this transition is $\Delta S_0 = \ln g_0 = 5.2$. We note that the contribution $\Delta S - \Delta S_0$ from thermal vibrations to the total entropy jump ΔS increases with increasing temperature, as does the anharmonicity of vibrations in accordance with Fig. 11. Evidently, the vibrational anharmonicity makes a contribution to the entropy jump also.

Considering the approximation of two aggregate states [165], we have for the total partition function of a cluster, both isolated (at constant energy) and under isothermal conditions, the following relation

$$Z = Z_{sol} + Z_{liq} \,, \tag{4.17}$$

where Z_{sol} and Z_{liq} are the partition functions for the solid and liquid cluster states, respectively. This means that the probability is small for intermediate configurationally excited states which cannot be associated clearly with either the solid state or the liquid aggregate state. Introducing the parameter

$$p = \frac{Z_{liq}}{Z_{sol}} \,, \tag{4.18}$$

we obtain formula (4.8) for the probabilities w_{sol}, w_{liq} that the cluster will be found in the solid and liquid states, respectively [165]:

$$w_{sol} = \frac{1}{1+p} \,, \quad w_{liq} = \frac{p}{1+p} \,. \tag{4.19}$$

From the thermodynamic relation, we find

$$p = \exp\left[-\frac{\Delta E}{T_{con}} + S_{liq}(T_{liq}) - S_{sol}(T_{sol}) \right]$$
$$= \exp\left[-\frac{\Delta E}{T_{con}} + \Delta S \right] \,, \tag{4.20}$$

where $S_{sol}(T_{sol})$ and $S_{liq}(T_{liq})$ are the entropies of the solid and liquid states, respectively, at the corresponding temperatures. We assume thermodynamic equilibrium in each aggregate state for an isolated cluster, if the temperature T_{sol}

of the solid aggregate state and the temperature T_{liq} of the liquid state are different; T_{con} is an effective configurational temperature (see Fig. 12) that characterizes the rate of transitions between the solid and liquid states, and ΔE and ΔS are the indicated changes of thermodynamic parameters at the phase transition.

Although clusters exhibit bands of phase coexistence rather than the sharp transitions at melting points of bulk systems, we can, as mentioned above, define the melting point of a cluster by analogy with that of the bulk system as the temperature of equal free energies for the two phases. In this way, the melting point T_m is defined as

$$p(T_m) = 1 \,, \tag{4.21}$$

and hence $w_{sol} = w_{liq} = 1/2$ at this configurational temperature within the framework of the approach of two aggregate states. The effective cluster temperature of configurational excitation at thermodynamic equilibrium in each aggregate state tends to T_{sol} if $p \to 0$ ($w_{sol} = 1$) for an isolated cluster, and tends to T_{liq} in the limit $p \to \infty$, or when $w_{liq} = 1$ in accordance with Fig. 12. (It is sometimes useful to use the distribution measure $D = [w_{liq} - w_{sol}]/[w_{liq} + w_{sol}]$ simply because it varies only between -1 and $+1$ [10, 171, 172].)

Note that the caloric curves give the energy of the phase transitions ΔE as the energy difference between these curves at the melting point. But this leads to an additional error in comparison with the results of computer simulation at constant energy. Indeed, for the Lennard-Jones cluster with 13 atoms we have $\Delta E = 2.5D$. In the case of isothermal computer simulation, we find for the energy difference

$$\Delta E' = \Delta E + \frac{K_{liq}(T_m)}{\eta_{liq}(T_m)} - \frac{K_{sol}(T_m)}{\eta_{sol}(T_m)} = 3.7D \,, \tag{4.22}$$

so that strong anharmonicity of the liquid state increases the energy difference at the melting point by almost 50%. Thus, simplistic inference of parameters directly from isothermal computer simulation would lead to an additional error.

4.3 Voids in liquid clusters
In contrast to configurational excitation of a cluster consisting of 13 atoms, for which the liquid state corresponds to excitation of one void, many voids partake in the excitation of the liquid state for larger clusters. Therefore, the aggregate state of such a system may be a mixture of excitations of several voids. We base our treatment of configurational excitation on the results of computer simulations and assume the existence of two aggregate states [33, 76, 165]. In doing so, we use the dynamic coexistence of phases in clusters [8, 168 – 170] within a certain temperature range, i.e., part of the time the cluster is in one aggregate state, and the rest of the time in the other state. (Strictly speaking, clusters may exhibit more than two aggregate states at thermodynamic equilibrium; we consider such cases below.) In addition, while the cluster is residing in either aggregate state, vibrational equilibrium is established [21], so that the vibrational temperature for each aggregate state coincides with the thermostat temperature, if the cluster is in a canonical ensemble [4]. In this case, the probability w_{liq} that the cluster will be found in the liquid state is given by formula (4.8) [33, 165, 76]

Let us consider now configurational excitation for the Lennard-Jones cluster consisting of 55 atoms, $(LJ)_{55}$. Note that in contrast to a cluster with 13 atoms, the energy
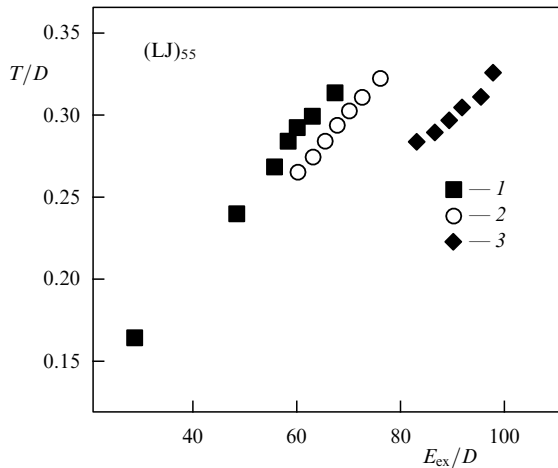
Figure 13. The caloric curve of the Lennard-Jones argon cluster consisting of 55 atoms [171, 172]: *1* — solid cluster, *2* — solid internal shell and liquid outer shell, and *3* — liquid cluster.

differences between excitations associated with promotion of different numbers of atoms for this and larger clusters need not be large, and such configurational excitations may include the formation of several or many voids. Next, large clusters can have several aggregate states; Fig. 13 exhibits such a possibility for $(LJ)_{55}$. One can see three aggregate states of this closed-shell icosahedral cluster composed of an external shell of 42 atoms, an internal shell of 12 atoms, and a central atom. In the lowest-energy aggregate state, both shells are solid; in the second aggregate state, the outermost shell is, in some sense, liquid and the inner shell is solid, while both atomic shells are liquid in the third aggregate state.

In analyzing the parameters of this cluster on the basis of numerical simulations, we first find the excitation energy of a surface atom by treating it as an atomic transition from the outer shell to the cluster surface and supposing that the excited atom is found far from a newly created vacancy. In this way, we neglect interactions between an excited atom and its vacancy. Then the excitation energy equals [76] $\Delta\varepsilon = \varepsilon_{56} - \varepsilon_{55}$, where ε_{55} and ε_{56} are the total binding energies of atoms for clusters consisting of 55 and 56 atoms, respectively According to calculations [88] for the ground state energies of these clusters, we have $\Delta\varepsilon = 2.64D$ at zero temperature. Direct calculations for lower excitations of this cluster [177] lead to a minimal excitation energy of $2.63D$. Therefore, an excited atom on the cluster surface can be treated as being far from the newly created vacancy. According to computer simulations [172, 178, 187], we have the following parameters of the $(LJ)_{55}$ cluster: $\Delta E = 14-17$, $T_{\mathrm{m}} = 0.30D$, and $C_{\mathrm{res}}^{\mathrm{max}} = 600-700$. This gives

$$\Delta S_{\mathrm{m}} = \frac{\Delta E}{T_{\mathrm{m}}} = 52 \pm 5 \,, \qquad (4.23)$$

and the mean number of atoms that leave the body of the cluster to form voids is estimated as

$$v \geqslant \frac{\Delta E}{\Delta\varepsilon} \approx 5 \qquad (4.24)$$

for this system.

To analyze the Lennard-Jones cluster consisting of 55 atoms, whose global minimum structure is a closed

icosahedron, we express the energy ΔE of configurational excitation in terms of the energy $\Delta\varepsilon$ of the excitation of an individual void as $\Delta E = v\Delta\varepsilon$, where v is the number of new voids. The data from computer simulations [172, 178] give us the entropy jump ΔS_0 at zero temperature separately for each number of new voids if, according to the above formula, we take $v = 5-7$. We assume that atoms can transfer not only from the icosahedron's vertices, but also from the edges; we ignore the difference in the energy changes when an atom goes from a vertex or from an edge to the cluster surface, and we assume that transferring atoms are not adjacent to the vacancies they leave. A new vacancy on a cluster edge or surface has 6 neighboring atoms, and a vertex vacancy has only 5. Thus, we find that $v \times (5-6)$ positions on the cluster surface are lost for atoms transferred from any of 80 positions on the cluster surface, if v transferring atoms on the cluster surface do not border vacancies in the cluster shell. From this we find the entropy jump for this configurational excitation of the cluster at zero temperature, which results from v atoms moving from the outermost cluster shell of 42 atoms. Atoms promoted to rest outside the outer shell are much more mobile than any other atoms and are therefore called 'floaters' [171, 172, 178]. The result for the entropy abrupt change in the course of configurational excitation takes the form

$$\Delta S_0 = \ln \, C_m^v C_{42}^v \,,$$

where

$$m = 80 - v \times (5-6)$$

is the number of positions for floaters on the cluster surface, when floaters do not border new vacancies. From this we have $\Delta S_0 = 28.2-28.7$ for $v = 5$, $\Delta S_0 = 31.2-32.0$ for $v = 6$, and $\Delta S_0 = 31.6-33.0$ for $v = 7$. This gives the average value

$$\Delta S_0 = 31 \pm 2 \,; \qquad (4.25)$$

and from formula (4.16) we obtain the entropy jump at the melting point:

$$\Delta S_{\mathrm{m}} = 45 \pm 2 \,. \qquad (4.26)$$

From formulas (4.23) and (4.26) for the entropy jump at the melting point, we find its average value $\Delta S_{\mathrm{m}} = 48 \pm 4$ given in Table 10. From this table follows that the contribution of thermal motion to the entropy jump at the melting point is almost identical for the Lennard-Jones clusters with 13 and 55 atoms. Thus, the above analysis shows that the entropy jumps at zero temperature and at the melting point are different; this fact is demonstrated in Table 10.

Considering a void as a relaxed vacancy, the isolated vacancy and void become equivalent at zero temperature if we neglect the vacancy–atom interaction. Real parameters of voids take into account this interaction and hence the influence of the thermal motion of atoms on configurational excitation. The lower the temperature, of course, the less the configurational excitation and the less the vibrational excitation as well. Evidently, the separation of the configurational excitation from thermal vibrations of atoms that we have used is valid only in the range from low to moderate temperatures, and is better for clusters with closed outer shells than for others. Therefore, we use the void concept especially for clusters with closed shells, such as those consisting of 7, 13,

19, 55, and 147 atoms. In these cases, there is a solid – liquid coexistence region of temperatures and pressures within which the probability distribution of total kinetic energy is distinctly bimodal [8, 179] for an isolated cluster (see Fig. 10). The occurrence and persistence of these two aggregate states substantiate our approach of two aggregate states [165], which is an analogue of the solid and liquid aggregate states for bulk systems.

In reality, one can observe several types of configurational excitations which correspond to the excitation of different cluster shells [178, 172, 171]. For clusters of about 50 or more atoms, the distribution may be trimodal over a narrow range, as it is for the 55-atom Lennard-Jones cluster. The intermediate aggregate state appears as a minority, and is generally called a 'surface-melted' state. However this is, in a sense, a misnomer because the atoms in the surface layer, while undergoing large-amplitude, anharmonic motion, move, according to simulations, in a very coherent manner around an average polyhedral structure. This state exhibits a liquid-like diffusion coefficient for its outer layer, but this is attributable to the 'floaters' which change places with surface atoms every few thousand vibrational periods [178].

Next, for some clusters with unfilled outer shells, thermodynamically stable states of configurational excitation may be absent, in particular, for Lennard-Jones clusters consisting of 8 and 14 atoms [179], because only a small entropy jump separates the states of these systems; this is much the same situation as occurs with excited states of atoms with open shells. Therefore, the real behavior of excitations in clusters with pair interactions between atoms may be more complicated than that within the framework of the void model of a cluster with two aggregate states. Nevertheless, this model is useful for understanding and describing clusters with a pairwise atomic interaction.

Thus, this analysis allows us to determine the average void parameters for clusters consisting of 13 and 55 atoms with closed atomic shells. It follows from this analysis that, although the configurational and thermal excitations are separated, thermal motion of atoms makes a contribution to the entropy jump in the transition between the solid and liquid aggregate states of clusters.

4.4 Voids in liquid inert gases
The phase transition in clusters is more complex than in bulk systems, and caloric curves representing the temperature dependences of the clusters' internal energies allow one to extract several types of phase transitions related to the melting of different cluster shells. (For example, see the caloric curves in Fig. 13 for the Lennard-Jones cluster consisting of 55 atoms.) As the number of cluster atoms increases, and the cluster is transformed into a bulk system, two types of phase transitions remain: the first relates to internal atoms, and the second includes surface atoms, as described above. In considering the melting of bulk systems, we concentrate on the phase transition involving internal atoms, when configurationally excited states of this system result from the formation of internal voids [25]. Here, we use this concept and determine the parameters of these voids.

Let us study the nature of elementary configurational excitations in bulk systems of bound atoms with pairwise atomic interactions in more detail. We consider this system as a very large cluster whose surface contains a relatively small number of atoms, small enough that we can ignore the surface phenomena in this system. The global minimum of the

potential energy surface for this cluster is typically a strict crystal lattice of atoms. In this sense, we consider systems large enough that their states of lowest energy are not polyhedral. The lowest configurational excitations in this system correspond to the formation of vacancies in which some atoms move to the cluster surface, and holes are formed inside the cluster. One can see that any configurational cluster excitation leads to an increase in its volume. When configurational excitation becomes extensive enough that neighboring vacancies can border on one another, the lattice cluster structure is lost. Elementary configurational excitations can then be represented as voids [25]. The shape and size of an elementary void vary in time, in contrast to an elementary vacancy in a lattice, so that one can use only average void parameters. Thus, considering a void as a developed vacancy and using real parameters of condensed inert gases, one can find the parameters of an average void [32, 34, 35].

Guided by condensed inert gases, we use the connection between the pair interaction potential of nearest atoms and the total energy of a condensed system of bound atoms (see Section 2.5). From this it follows, in particular, that the reduced pressure near the triple point is [33, 94] $(1.9 \pm 0.2) \times 10^{-3}$, and we ignore any pressure effects here. Hence, one can characterize excitation of this system by its entropy, and the cluster-free function depends on only one parameter. Figure 14 gives the dependence of the logarithm of the partition function for a configurationally excited cluster on the number of internal voids v, when this bulk cluster contains n bound atoms.

Thus, treating the configurational excitation of a bulk atomic system with pair interaction as the result of the formation of internal voids, we define the effective number of those voids as the consequence of relaxation of a specific number of initially formed vacancies in a solid from which this configurationally excited state arises [32 – 35]. The number of voids characterizes the degree of configurational excitation of this system which need not be in equilibrium with the thermal motion of the atoms. In order to prepare a system of bound atoms consisting of n atoms and v voids, we take a bulk solid cluster of $n + v$ atoms and remove v atoms to an unspecified place outside the cluster. This system is assumed to be large enough that almost all the removed atoms come from the inside of the system, and surface effects are negligible. Hence, this system contains n atoms and v internal voids after relaxation and, according to the definition, an individual void results from the relaxation of an
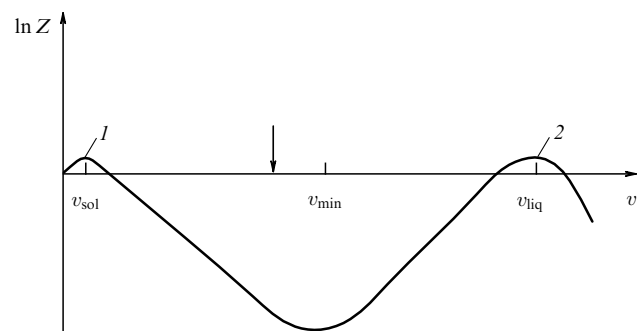

Figure 14. Logarithm of the atomic partition function for a macroscopic ensemble of bound atoms with a pair interaction as a function of the void concentration [32].

individual vacancy and its immediate environment. Because the number of voids can have any value, this system is not at thermodynamic equilibrium and will tend to equilibrium as a result of the diffusion of voids. Therefore, we consider this system during time intervals that are short in comparison with diffusion times of voids through the system. But still, during such intervals, thermodynamic equilibrium is established for the thermal vibrations of the atoms. Although the volume and shape of an individual void vary in time, here we use average parameters of individual voids, which depend only on the void concentration at a given temperature of atomic oscillations. We find the parameters of an individual void in the liquid state near the triple point on the basis of parameters of real inert gases. Additional information also follows from the fact of the existence of one thermodynamically stable configuration state of this system, which is the liquid state. Then, the cluster partition function must have the form depicted in Fig. 14.

Thus, considering configurational excitation of a macroscopic system of bound atoms with a pair interaction between atoms as a result of void formation, and neglecting surface effects for a bulk system, we will find the parameters of configurationalal excitation for the liquid state on the basis of real parameters of inert gases. We assume the total excitation to be expressible in terms of a sum of identical internal voids, i.e., elementary configurational excitations. An individual void is characterized by the statistical weight g_v and the average energy ε_v of its formation from the solid state. We establish the operations [33–36] for determining these parameters for condensed inert gases, a bulk system of bound atoms with interaction between nearest neighbors only, in a simplified form. The partition function of an excited bulk system consisting of n bound atoms includes a gas of v identical voids, so that we have for the partition function of this system:

$$Z_v = C_{n+v}^v \, g_v^v \exp\left(-v\,\frac{\varepsilon_v}{T}\right). \tag{4.27}$$

In the bulk limit $n \gg 1$, $v \gg 1$, we obtain

$$\ln Z_v = n \ln\left(1 + \frac{v}{n}\right) + v \ln\left(1 + \frac{n}{v}\right) + v \ln g_v - v\,\frac{\varepsilon_v}{T}$$

$$= v\left(\Delta S_v - \frac{\varepsilon_v}{T}\right), \tag{4.28a}$$

where

$$\Delta S_v = \frac{1}{x}\ln\left(1 + x\right) + \ln\left(1 + \frac{1}{x}\right) + \ln g_v\,, \quad x = \frac{v}{n}\,. \tag{4.28b}$$

It is convenient to reduce this expression to

$$\Delta S_v = 1 + \ln\frac{g_v}{x}\,, \tag{4.29}$$

and this change leads to an uncertainty below 7% if $x \leqslant 1/3$, which includes the entire transition range between solid and liquid states. We then derive the expression for the chemical potential of the atomic system:

$$\mu(x) \equiv \frac{1}{n}\ln Z_v = x\left(1 + \ln\frac{g_v}{x} - \frac{\varepsilon_v}{T}\right). \tag{4.30}$$

This simplification allows us to avail ourselves of the assumptions made above.

From this we get the partition function for the solid (crystalline) state ($v \ll n$, $g_v = 1$, $\varepsilon_v = \varepsilon_{\mathrm{sol}}$):

$$\ln Z_v = v\left(1 + \ln\frac{n}{v} - \frac{\varepsilon_{\mathrm{sol}}}{T}\right), \tag{4.31a}$$

and the minimum condition gives the number of voids (vacancies) in the solid state:

$$\frac{v_{\mathrm{sol}}}{n} = \exp\left(-\frac{\varepsilon_{\mathrm{sol}}}{T}\right), \tag{4.31b}$$

so that this concentration of voids is equal to $(1.9 \pm 0.2) \times 10^{-5}$ for inert gases near the triple point [33–35]. Below, we neglect the existence of vacancies for the solid state.

In the case of configurationally excited states, the above expression for the partition function of a void gas becomes analogous to the general expression (4.31a):

$$\ln Z_v = v\left(\Delta S_v - \frac{\varepsilon_v}{T}\right),$$

where ΔS_v is the entropy of an individual void. When considering the liquid state, we use the relation

$$v\varepsilon_v = n\Delta H_{\mathrm{fus}}\,, \tag{4.32}$$

where ΔH_{fus} is the enthalpy of the phase transition, and the values of the binding energy per individual void are listed in Table 11. Since the dependence on the number of voids for the function $\ln Z_v/v$ has a specific form (see Fig. 14) with two maxima (solid and liquid), this offers additional information for determining void parameters in the liquid.

The energy of void formation may be written in the form

$$\varepsilon_v = \varepsilon_0 - U\!\left(\frac{v}{n}\right), \quad \frac{U(x)}{\varepsilon_0} = \exp\left(-\frac{\alpha}{x}\right) - \exp\left(-\frac{k\alpha}{x}\right), \tag{4.33}$$

where α and k are the parameters. Table 11 lists values of some void parameters for the formation of one void in the liquid state from an initial solid state. We take as ε_0 the crystal sublimation energy per atom $\varepsilon_{\mathrm{sub}}$ near the triple point or the exponent $\varepsilon_{\mathrm{sol}}$ in the Clapeyron–Clausius law. In the latter case, the results of Table 11 are given in parentheses.

The equation at the melting point with $\ln Z_v = 0$ or $\mu(x_{\mathrm{liq}}) = 0$, where x_{liq} refers to the liquid state, has the form

$$1 + \ln\frac{g(v_{\mathrm{liq}})}{x_{\mathrm{liq}}} - \frac{\Delta H_{\mathrm{fus}}}{T_{\mathrm{m}} x_{\mathrm{liq}}} = 0\,, \quad x_{\mathrm{liq}} = \frac{v_{\mathrm{liq}}}{n}\,,$$

and the solution to this equation exists for

$$g(v_{\mathrm{liq}}) > g_{\mathrm{min}} = \exp\left(\frac{\Delta H_{\mathrm{fus}}}{T_{\mathrm{m}}} - 1\right). \tag{4.34a}$$

Next, from this equation and the definition of the fusion energy $\Delta H_{\mathrm{fus}} = \varepsilon(v_{\mathrm{liq}})\,x_{\mathrm{liq}}$ it follows that

$$g(v_{\mathrm{liq}}) = \frac{\Delta H_{\mathrm{fus}}}{\varepsilon_{\mathrm{liq}}}\exp\left(\frac{\varepsilon_{\mathrm{liq}}}{T_{\mathrm{m}}} - 1\right),$$

where $\varepsilon_{\mathrm{liq}} = \varepsilon(v_{\mathrm{liq}})$ is the energy of void formation for the liquid state at the melting point. Because g is a monotonic

Table 11. Reduced parameters of voids for bulk liquid rare gases [33–36].

Parameter	Ne	Ar	Kr	Xe	Average
T_{m}/D	0.581	0.587	0.578	0.570	0.579 ± 0.007
ε_0/D	6.1	6.5	6.7	6.7	6.5 ± 0.3
$\Delta H_{\mathrm{fus}}/D$	0.955	0.900	0.980	0.977	0.976 ± 0.017
g_{min}	1.9	2.0	2.0	2.0	2.0
g_{max}	1900	3700	4300	4100	3500 ± 1000
n/v_{liq}	3.12	3.13	3.14	3.13	3.13 ± 0.01
$\varepsilon(v_{\mathrm{liq}})/D$	3.00	3.09	3.05	3.05	3.05 ± 0.04
$\Delta S(v_{\mathrm{liq}})$	5.16	5.26	5.28	5.35	5.26 ± 0.08
$g(v_{\mathrm{liq}})$	55	62	63	68	62 ± 5
a	171	189	193	207	190 ± 15
$g(v_{\mathrm{min}})$	15	17	17	18	17 ± 1
U_{liq}/D	3.1	3.4	3.6	3.6	3.4 ± 0.2
$U_{\mathrm{liq}}/\varepsilon_0$	0.51	0.52	0.54	0.54	0.52 ± 0.01
$\Delta S(v_{\mathrm{min}})$	6.19	6.32	6.32	6.38	6.3 ± 0.1
$1 - T_{\mathrm{m}}\Delta S(v_{\mathrm{min}})/\varepsilon_0$	0.41	0.43	0.44	0.44	0.44 ± 0.02
α	0.165	0.159	0.151	0.151	0.158 ± 0.005
$\alpha n/v_{\mathrm{liq}}$	0.51	0.50	0.48	0.48	0.49 ± 0.02
k	3.26	3.38	3.56	3.58	3.44 ± 0.15

function of v_{liq}, and $\varepsilon_{\mathrm{liq}} < \varepsilon_0$, we obtain

$$g(v_{\mathrm{liq}}) < g_{\mathrm{max}} = \frac{\Delta H_{\mathrm{fus}}}{\varepsilon_0} \exp\left(\frac{\varepsilon_0}{T_{\mathrm{m}}} - 1\right). \qquad (4.34b)$$

Table 11 contains the values of g_{min} and g_{max}. It is important that the liquid state, i.e., a configurationally excited and thermodynamically stable state of a bulk system, exists only if the void statistical weight yields a minimum of the free energy in a certain range. In particular, if the only value of the statistical weight of a void that minimizes the free energy is that of an isolated vacancy in the crystal lattice, $g = 1$, then the liquid state of such a system is simply not stable. Likewise, the void density yielding a free energy minimum may be so high that the state to which it corresponds is a vapor. Only if the conditions are established under which there is a stable void density between these limits, can the liquid exist as a stable state. Because the void statistical weight increases with increasing vibrational temperature, atomic thermal motion is important for the existence of the liquid, and this aggregate state is not realized at low temperatures. (Helium is, of course, the exception.)

Note that at the melting point we have simultaneously

$$\mu(x_{\mathrm{liq}}) = \mu'(x_{\mathrm{liq}}) = 0. \qquad (4.35)$$

Taking

$$g_{\mathrm{v}} = 1 + a\,\frac{v}{n}, \qquad (4.36)$$

we obtain from equation (4.35) at the melting point:

$$\frac{\mathrm{d}U(x_{\mathrm{liq}})}{\mathrm{d}x} = 0, \qquad (4.37a)$$

or

$$\frac{\alpha}{x_{\mathrm{liq}}} = \frac{\ln k}{k - 1}, \qquad (4.37b)$$

and we assume $g(v_{\mathrm{liq}}) \gg 1$. Note that, just from its physical nature, the function $U(v/n)$ is monotonic, and from equation (4.37a) it follows that the model under consideration is valid only for $v \lesssim v_{\mathrm{liq}}$. We obtain one more equation by assuming

that a minimum of the function $\ln Z_{\mathrm{v}}$ (see Fig. 14) appears at the void concentration at which a test void finds a nearest-neighbor void. This gives $x_{\mathrm{min}} = 1/12$. Now, neglecting the second term in expression (4.33) for $U(x)$, and assuming $g(x_{\mathrm{min}}) \gg 1$, or $a \gg 12$, we obtain from the first equation (4.35) the equality $\mu'(x_{\mathrm{min}}) = 0$ yielding

$$(1 + 12\alpha)\exp(-12\alpha) = 1 - \frac{(1 + \ln a)T_{\mathrm{m}}}{\varepsilon_0}.$$

The corresponding values for inert gases are listed in Table 11. Of course, these values are close to those found previously [33–36], and the differences between them are due to the simplified scheme used now. In spite of its crudeness, the model allows us to determine the void parameters on the basis of the physical nature of the configurationally excited states.

We now analyze the results from another standpoint. Let us represent the entropy of the solid–liquid phase transition in accordance with formulas (4.13) and (4.14) as the sum of two parts:

$$\Delta S = \Delta S_0 + \Delta S_{\mathrm{th}}, \qquad (4.38a)$$

so that the first, configurational term accounts for the formation of internal voids, and the second term for the thermal motion of atoms. The first term is equal to

$$\Delta S_0 = n\ln\left(1 + \frac{v}{n}\right) + v\ln\left(1 + \frac{n}{v}\right), \qquad (4.38b)$$

and $\Delta S_0/n = 0.73$ for the above values of void parameters relating to condensed rare gases. Because the total entropy jump for the phase transition of rare gases is $\Delta S/n = 1.68$, we obtain for the contribution caused by phonons:

$$\Delta S_{\mathrm{th}} = 0.95.$$

The nature of this term is due to oscillations of atoms; it contributes 56% of the total entropy. As a result of the phase transition, the specific volume per atom increases, which increases the amplitude of each atom's vibrational motion. This leads to an entropy increase due to atomic motion. Expressed in terms of a harmonic oscillator model, this effect

leads to a decrease in the Debye temperature of the system. Let us assume for simplicity that the melting point exceeds the Debye temperature θ_D, so that we use the limiting expression for the entropy of a bulk system of n bound atoms [6]:

$$S_{osc} = 3n \ln \frac{T}{\theta_D} + 4n \,.$$

In this limit, taking $\Delta S_{th} = S_{ocs}$, we find that the melting transition increases the Debye temperature by about 40%. Comparing the contribution from thermal oscillations to the total entropy of Lennard-Jones clusters and bulk inert gases at their melting points, one can readily see that the vibrational contribution grows as the temperature drops. Indeed, if the reduced melting point T_m/D increases from 0.3 for the Lennard-Jones cluster consisting of 13 atoms to 0.58 for bulk rare gases, the contribution of atomic oscillations at the phase transition to the total entropy jump varies from 36% up to 56%. These values were included in Table 10.

4.5 Definition of the aggregate state and melting criteria

One can see the difference between the definition of the cluster liquid aggregate state we use here and that in classical thermodynamics in which the phase or aggregate state of bulk corresponds to a uniform, long-time average distribution of atoms in some bounded spatial domain. This means that the phase or aggregate state in classical thermodynamics includes many elementary configurational excitations, while in the case of a 13-atom cluster this state can result from one elementary configurational excitation. Of course, it is necessary to apply additional criteria to the liquid cluster state (or an excited aggregate state) for two-body correlations that are different for the solid and liquid states (see, for example, Refs [7–9]).

From this it follows that the cluster aggregate states have additional peculiarities differentiating them from bulk systems. One of the most important of these is dynamical coexistence of phases [7–9, 167]. This coexistence is partly a consequence of the time scales for phenomena at the nanoscale. In contrast to the time scales for bulk matter, those of clusters and nano-sized materials allow us to make observations that can be slow enough to obtain time averages over different phases or, if the observation times are somewhat shorter, as with dozens of nanoseconds or less, to distinguish clusters in specific, recognizable phases. Many, but not all, kinds of clusters exhibit a dynamic equilibrium like that of chemical isomers in a certain range of parameters near the melting point; each cluster is found part of the time in the solid state, and the rest of the time in the liquid state — in cases in which there are two distinguishable aggregate states. This situation means that the distinction between 'phase' and 'component' is blurred for clusters, and the Gibbs phase rule loses its applicability. Thus, we must be cautious in how we use classical thermodynamics when dealing with clusters, and in particular, we must be especially aware of hidden assumptions that are entirely valid on the bulk scale but not on the nanoscale. To understand the phase behavior of clusters and relate that to the phase transitions in bulk matter, we must slightly change the definition of aggregate states from the classical thermodynamic definition of states of macroscopic systems. Within the framework of this description, we consider the cluster aggregate state as a group of configurationally excited cluster states with similar excitation energies.

Thus, the nature of the solid–liquid phase transition in clusters with pairwise interaction between atoms is predominantly a result of configurational excitation. In practice, it is convenient to use the Lindemann criterion [26] as a diagnostic tool for this phase transition. According to this rule, the phase transition occurs at the temperature at which the relative amplitude of atomic oscillations reaches a characteristic value; specifically, melting is said to occur when the ratio of the root-mean-square amplitude of atomic oscillations to the distance between nearest neighbors is 0.10–0.15. Typically, in the range of this temperature, the ratio of distances increases sharply. With the development of numerical methods to simulate cluster dynamics, more precise criteria for the phase transition were introduced, which are based on pair correlations of positions of the cluster atoms. In particular, this correlation function can use the Etters–Kaelberer parameter [28–30] or the Berry parameter [9, 31]. These parameters are proportional to the fluctuations of the interatomic distance. These fluctuations give a somewhat more precise insight into how the solid and liquid states differ, and how the transition between them occurs over the range of their coexistence.

One can see in all the above discussions a paradox or apparent contradiction between the nature of the 'cause' of the phase transition and the parameters typically used to characterize this phenomenon. While the essence of the melting, i.e., the onset of fluidity in a dense medium, consists in configurational excitation and the introduction of voids in the system, the parameters for its description, such as the Lindemann criterion, are based on the atomic thermal motion. The former is the cause, and the latter is the effect.

The void concept for the configurational excitation of such systems, interpreted with the help of computer simulations and thermodynamic parameters of condensed inert gases, shows that the origin of this apparent paradox lies with the changes in thermal vibrations of atoms in the melting process and their consequent striking contribution to the entropy's abrupt change at the melting transition. Indeed, because of the lower density of atoms in the liquid state, the atomic thermal motion contributes to the entropy of the configurational transition in accordance with formula (4.13). As a result, the entropy jumps ΔS_0 and ΔS_m at zero temperature and at the melting point are quite different, as follows from the data in Table 10. This allows us to characterize the phase transition also by the value of the difference $\Delta S_m - \Delta S_0$ that is determined by the thermal motion of atoms. Thus, although the ideas of the Lindemann criterion and other melting criteria are not rooted in the cause of the transition, the criteria reflect correctly the consequences of this phenomenon.

We now formulate the steps we need to transfer the description of configurational excitation of clusters to the phase transitions in classical thermodynamics. In considering clusters with pairwise atomic interactions, we start from the potential energy surface (PES) in a many-dimensional space of atomic coordinates, in which cluster evolution is described as motion on this PES. A special characteristic of such a PES is the immensely large number of local minima. In the course of its evolution, a cluster dwells for some time interval near each PES minimum it visits, so that it has many oscillations in the phase space near each minimum until it moves on to a neighboring minimum. In this manner, we separate thermal motion of atomic oscillations from configurational excitation identified with each PES minimum. In the next step of the

analysis, in order to simplify the problem, we introduce an elementary configuration excitation, a void, and here we assume all single configurational excitations to be equivalent. One can see that this assumption is valid more or less, if we consider a void as a result of relaxation of an initially formed vacancy.

Then, basing our next step on the shell cluster model, we introduce groups of individual vacancies or groups of voids. Again, all states with the same number of voids fall into a class whose members we consider indistinguishable. Of course, interaction between voids (or interaction between atoms for a configurationally excited ensemble) violates this picture, and hence the isolated-void description of configurational excitation is an oversimplified model. In transition to bulk systems, if we restrict our discussion to internal voids, these voids all correspond to the same kind of configurational excitation, i.e., we deal with identical voids. In the next step of the transition to classical bulk thermodynamics, we form the liquid aggregate state of a bulk ensemble of bound atoms by excitation of a sufficient number of voids in the solid aggregate state. This state includes enough elementary configurational excitations, voids, to permit diffusive motion of the atoms, and therefore it is sufficient for the classical definition of the liquid phase that we can describe as a uniform distribution of atoms. In addition, we take as the liquid state the thermodynamically most favorable state that contains the optimal number of voids. This means the state with the lowest free energy with respect to the number of voids or the maximum of the partition function, as follows from Fig. 14. In this way, moving from the mechanical description of a bulk ensemble of bound atoms, one can transfer to its thermodynamic description at the nanoscale by incorporating some additional assumptions and avoiding some that may be tacit in the classical framework.

Thus, to go to classical thermodynamics, one can see that additional assumptions are required for this passage. Simultaneously, it leads to simplifications and gives a universal description of the phase transition within the framework of classical thermodynamics on the basis of some thermodynamical parameters. Returning back to a cluster, one can see that thermodynamic parameters can be used even when classical macroscopic thermodynamics is not applicable for clusters in principle. Indeed, employing the entropy S, the internal cluster energy E, the cluster free energy F, and other thermodynamic parameters is useful for configurationally excited clusters, although it requires additional analysis of the validity of some thermodynamic relations. Following this path to classical thermodynamics, we use the two-state approach to cluster aggregate states; it is also beneficial for describing clusters.

4.6 Voids as elementary configurational excitations of a macroscopic atomic system

According to definition, voids are elementary configurational excitations; we will now ascertain the strictness of this definition. A void is introduced as a perturbed or relaxed vacancy of a crystal lattice. Indeed, starting from a macroscopic crystal particle containing $n + v$ atoms, we remove from it v atoms and obtain a macroscopic cluster containing n atoms and v vacancies. Assuming the fraction of surface atoms in this cluster is relatively small, we suppose that practically all the vacancies are located inside. If neighboring vacancies border on this area, their interaction leads to compression of the cluster, and then vacancies convert into

voids. Of course, in contrast to vacancies, parameters of a void vary in time, so we deal with time-averaged parameters of voids. We assume the number of vacancies in the initial distribution is equal to the number of voids after relaxation, and therefore, in accordance with the character of relaxation, the average void parameters, such as the energy and entropy of their formation, the average void volume, etc., differ from the parameters for vacancies.

Let us consider this problem from another standpoint. The basic property of a system of atoms with a pairwise interaction is separation of its ground electronic state from the first electronically excited state by a wide energy gap, and therefore we deal with the ground electronic state only. The total electronic energy and the electron–nuclear and nuclear–nuclear potential energy contributions to the total energy of the ground state determine the effective potential energy surface in the space of atomic coordinates. This is, of course, the Born–Oppenheimer approximation. Consequently, the evolution of this macroscopic system of atoms may be represented as a motion along the potential energy surface in a many-dimensional space of atomic coordinates. A characteristic property of virtually any potential energy surface for a many-particle system is its large number of local minima in this space [19]. The system of atoms spends almost all its time in regions near the local minima of the potential energy surface; only a small part of the time is consumed in transitions between neighboring local minima. Local minima of the potential energy surface characterize stable atomic configurations; we associate these stable configurations with configurational excitations from the ground configurational state. Each configuration of atoms has a specific number of voids.

Let us follow this connection. When the number of voids v is very small compared with the number of atoms n, so that neighboring voids do not border on one another, the elementary configurational excitations are better described as vacancies than as voids, and the volume per atom is equal to the volume per void. Correspondingly, all permutations of atoms and voids, when they form a crystal lattice, lead to stable configurations of atoms with the same energy of configurational excitation. In other words, any configuration of atoms and voids corresponds to a certain local minimum of the potential energy surface. Then the energy of configurational excitation, as well as variations in the total volume of the system relative to that of the ground state, is proportional to the number of vacancies v. The same relates to the entropy variation associated with configurational excitation of the atomic system.

Relaxation of this atomic system in the case where the number of voids is not small leads to some compression and moves the atomic system to a stable configuration. Assuming that each initially created distribution of vacancies in the crystal lattice gives rise to its own configuration of atoms after relaxation, we suppose that each initial distribution of atoms and vacancies corresponds to a certain local minimum of the potential energy surface to which it relaxes. There is likely to be some short-range order in the atomic distribution because each final state yields a stable configuration. Thus, considering a void as an elementary configurational excitation, we infer that voids are independent, and each set of voids leads to a certain stable distribution of atoms — a local minimum of the potential energy surface. This was used above in the course of determining void parameters for a liquid aggregate state of inert gases.

5. Thermodynamics of clusters near the phase transition

5.1 The hierarchy of times for atomic relaxation in clusters

We now analyze the character of equilibrium in a cluster, basing our discussion on the two-state approach to cluster aggregate states [165]. This extends the thermodynamic concept of the aggregate states from bulk to clusters. We assume the existence of local stability and thermal equilibration for two aggregate states, solid and liquid. Although clusters may exhibit several aggregate states in equilibrium, for example, associated with the melting of different cluster shells [171, 172], the model we use here supposes that in a given range of parameters the cluster can be found only in two aggregate states. The character of cluster equilibrium is determined by typical times for processes proceeding within the cluster. A typical time τ_{eq} to establish thermal equilibrium between bound atoms is equal (on the order of magnitude) to

$$\tau_{eq} \sim \frac{1}{\omega_D} , \qquad (5.1)$$

where ω_D is the Debye frequency, roughly inversely proportional to a period of cluster atomic oscillations ($\sim 10^{-14}$ s at room temperature). The typical dwell time of a cluster in the vicinity of the free energy minimum, τ_{ag}, associated with each aggregate state has long been compared with τ_{eq}:

$$\tau_{eq} \ll \tau_{ag} , \qquad (5.2)$$

because transitions between aggregate states require the cluster to overcome a significant free energy barrier. We consider a cluster of bound atoms as a member of a microcanonical ensemble, if one can neglect the interaction between the cluster and environment, that is

$$\tau_{ag} \ll \tau_{th} , \qquad (5.3)$$

where τ_{th} is the typical time for the exchange of energy between the cluster and its environment; for shorter times, the cluster can be considered an isolated particle. Let us introduce a typical time of cluster observation τ, so that in the case of an isolated cluster, when it is a microcanonical ensemble of atoms, we have

$$\tau_{ag} \ll \tau \ll \tau_{th} . \qquad (5.4)$$

This hierarchy of cluster times leads to a particular pattern of cluster behavior. Indeed, during τ_{eq} thermal equilibrium is established for the vibrational motion of the cluster atoms, so that the thermal motion of atoms can be characterized by the temperature [21]. Because of criterion (5.2), and because the two states have the same energy but occur at different levels on the potential energy surface, this temperature is different for the two aggregate states of an isolated cluster. Hence, we introduce different temperatures of atoms for the solid (T_{sol}) and liquid (T_{liq}) aggregate states. In particular, in the Dulong–Petit limit, assuming thermal motion of atoms to be a combination of harmonic vibrations (the parameter η in formula (4.5) is $\eta = 1/2$), for the cluster energy according to formula (4.4) we obtain

$$E = (3n - 6) T_{sol} = \Delta E + (3n - 6) T_{liq} , \qquad (5.5)$$

where n is the number of cluster atoms, and ΔE is the fusion energy, so, from this, we have for an isolated cluster:

$$\Delta T = T_{sol} - T_{liq} = \frac{\Delta E}{3n - 6} . \qquad (5.6)$$

Along with these temperatures, one can introduce a general cluster temperature T for a long time $\sim \tau$ that can be expressed in terms of the average energy of an individual cluster atom if an average is taken for a time $\sim \tau$ long enough for the cluster to change its aggregate state many times. We return below to the question of the meaning of temperature in noncanonical ensembles.

5.2 Entropy of an isolated cluster near the phase transition

Let us consider a microcanonical ensemble of large isolated clusters, with pairwise interaction between atoms, from the standpoint of thermodynamics and elucidate the conditions of validity of thermodynamics for its description. At issue is the question of what commonly held, implicit assumptions may be inapplicable to such systems, even though the basic principles of thermodynamics remain perfectly applicable. We continue to separate configurational and vibrational degrees of freedom. Moreover, we again use the two-state approach for cluster aggregate states, in which configurationally excited states belong either to the solid aggregate state or to the liquid aggregate state. In this way, we divide cluster configurational states into solid and liquid categories and ignore other configurational states, assuming that the probability of their realization is small. (We could choose situations, sometimes only in narrow ranges of temperature or pressure, in which this would be violated.) Under these conditions, one can determine some cluster parameters and compare them with the observed values when an isolated cluster can be characterized by two temperatures, T_{sol} and T_{liq}, depending on the aggregate cluster state.

We start by determining the cluster's entropy under the above conditions using a general expression for the entropy (see, for example, Ref. [6])

$$S = -\langle \ln P \rangle = -\sum_i P_i \ln P_i , \qquad (5.7)$$

where i is a cluster state, and P_i is the probability that the cluster is found in this state (with, of course, normalizing condition $\sum_i P_i = 1$). Because the configurational and vibrational degrees of freedom are separated, we have

$$P_j = w_{sol} X_j , \quad P_k = w_{liq} Y_k , \qquad (5.8)$$

where the probabilities of the solid and liquid states w_{sol} and w_{liq} are given by formulas (4.8) and (4.19), respectively, X_j is the probability of the j-th vibrational state for the solid aggregate state, and Y_k is the probability of the k-th vibrational state if a cluster is in the liquid aggregate state. The normalization conditions for the probabilities give

$$w_{sol} + w_{liq} = 1 , \quad \sum_j X_j = \sum_k Y_k = 1 . \qquad (5.9)$$

Substituting formulas (5.8) into Eqn (5.7), we find the entropy of a cluster with two aggregate states [175]:

$$S = -w_{sol} \sum_j X_j \ln(w_{sol} X_j) - w_{liq} \sum_k Y_k \ln(w_{liq} Y_k)$$
$$= w_{sol} S_{sol} + w_{liq} S_{liq} + S_{ph} , \qquad (5.10)$$

where

$$S_{\text{sol}} = -\sum_j X_j \ln X_j, \quad S_{\text{liq}} = -\sum_k Y_k \ln Y_k \qquad (5.11a)$$

are the entropies of the corresponding aggregate states, and the entropy due to configurational excitation is defined as

$$S_{\text{ph}} = -\sum_i x_i \ln x_i = -w_{\text{sol}} \ln w_{\text{sol}} - w_{\text{liq}} \ln w_{\text{liq}}$$
$$= \ln(1+p) - \frac{p}{1+p} \ln p. \qquad (5.11b)$$

Here, x_i is the probability of the cluster being in a given aggregate state, and we use formulas (4.19) for this quantity. Note that this expression is valid under the assumption that the cluster is observed in long-term equilibrium, i.e., during a time of observation it can be located many times in each aggregate state. Thus, expressions (5.11) for the cluster entropy are a sum of terms corresponding to the solid and liquid aggregate states, as well as of the term that accounts for configurational excitation.

One can divide the entropy variation into two parts: $dS = dS_{\text{th}} + dS_{\text{con}}$, so that the first part is connected with atomic vibrations, and the other one refers to the phase transition. Then we obtain [175]

$$dS_{\text{th}} = w_{\text{sol}} \, dS_{\text{sol}} + w_{\text{liq}} \, dS_{\text{liq}}, \qquad (5.12a)$$

$$dS_{\text{con}} = dS_{\text{ph}} + S_{\text{sol}} \, dw_{\text{sol}} + S_{\text{liq}} \, dw_{\text{liq}}$$
$$= \ln \frac{w_{\text{sol}}}{w_{\text{liq}}} \, dw_{\text{liq}} + \Delta S \, dw_{\text{liq}}. \qquad (5.12b)$$

Here, we included the constraint that $w_{\text{liq}} + w_{\text{sol}} = 1$ or $dw_{\text{liq}} + dw_{\text{sol}} = 0$, and $\Delta S = S_{\text{liq}} - S_{\text{sol}}$ is the entropy jump resulting from the phase transition. One can see that the variation dS_{con} does not depend on the thermal motion of atoms, while dS_{th} is determined by these degrees of freedom. Thus, the phase transition gives an additional contribution to the total cluster entropy and its variation.

5.3 Temperature of an isolated cluster near the phase transition

The internal cluster energy E is the sum of two parts for the vibrational and configurational degrees of freedom:

$$E = E_{\text{th}} + E_{\text{con}} = E_{\text{th}} + \Delta E w_{\text{liq}}, \qquad (5.13)$$

the second term based on the two-aggregate approach and the assumption being that the energy ΔE of configurational excitation is independent of the vibrational (and electronic) excitation energy. When a cluster is a member of a microcanonical ensemble, i.e., it is isolated, all its parameters are considered at $E = \text{const}$. We next find an effective 'translational' cluster temperature T that refers to thermal motion (or vibrations) of atoms and follows from the thermodynamic relation

$$dE_{\text{th}} = T \, dS_{\text{th}}, \qquad (5.14)$$

where dS_{th} is given by formula (5.12a), determining the appropriate contribution to the microcanonical entropy.

The hierarchy of times according to relations (5.2) and (5.4) leads to the two-temperature thermal regime of an isolated cluster, so that the temperature of atomic motion at

a given cluster energy E is either T_{sol} or T_{liq}, depending on its aggregate cluster state. We can apply definition (5.14) to each aggregate state separately, or to the long-time average over both aggregate states. In the first case we have

$$\frac{1}{T_{\text{sol}}} = \frac{dS_{\text{sol}}}{dE_{\text{th}}}, \quad \frac{1}{T_{\text{liq}}} = \frac{dS_{\text{liq}}}{dE_{\text{th}}}, \qquad (5.15)$$

where both entropies are microcanonical. Let us find the temperature for a long-time average on the basis of formula (5.14). For simplification we make an additional assumption: because within the range of the phase transition the caloric curves are approximately parallel lines, we suppose that the heat capacity in the absence of the phase transition does not depend on the cluster energy E over the transition range:

$$C_0 = \frac{dE_{\text{th}}}{dT_{\text{sol}}} = \frac{dE_{\text{th}}}{dT_{\text{liq}}}, \qquad (5.16)$$

where C_0 is the heat capacity far from the phase transition.

From this we obtain at each cluster energy:

$$T_{\text{sol}} = \overline{T} + \frac{\Delta T}{2}, \quad T_{\text{liq}} = \overline{T} - \frac{\Delta T}{2} \qquad (5.17a)$$

and

$$\overline{T} = \frac{T_{\text{sol}} + T_{\text{liq}}}{2}, \quad \Delta T = T_{\text{sol}} - T_{\text{liq}}. \qquad (5.17b)$$

In addition, we assume for simplicity that

$$\Delta T \ll \overline{T}. \qquad (5.18)$$

The data in Table 12, based on computer simulations for the Lennard-Jones cluster consisting of 13 atoms [8], show the validity of criterion (5.18), and the small parameter $\Delta T / \overline{T}$ used above is equal to 0.2 for this cluster. This small parameter determines the accuracy of using a single translational cluster temperature. Note that the heat capacity near the melting point does not show a large increase for this cluster, and the heat capacity is positive at all temperatures. This contrasts with the report of a negative heat capacity for larger clusters near the melting point [180, 181], based on experiments with sodium clusters [173, 174, 182, 183]. A more precise test of the use of the above approach with Lennard-Jones clusters requires examining the behavior of a larger system, e.g., a closed-shell icosahedral structure consisting of 55 or 147 atoms. We discuss this point below.

Table 12. The parameters of an isolated Lennard-Jones cluster consisting of 13 atoms at the melting point. The data were obtained on the basis of Ref. [8].

Parameter	Value
E_{m}	13.6
ΔE	2.46
$\eta(E_{\text{m}})$	0.39
T_{sol}	0.32
T_{liq}	0.26
T_{m}	0.29
$Z(T_{\text{m}})$	0.46
ΔE	8.5
C_{max}	18

Note. Bond dissociation energy D is adopted as an energy unit.

We apply formula (5.14) as the definition of the temperature of cluster atoms, and use formula (5.12a) for the entropy variation dS_{th} that corresponds to the thermal motion of atoms of a cluster possessing two aggregate states. Note that this is not a unique definition of the effective temperature of a microcanonical system, and different definitions may give different results, even different signs [184]. Our chosen definition gives

$$\frac{1}{T} = \frac{w_{sol}}{T_{sol}} + \frac{w_{liq}}{T_{liq}} \,. \qquad (5.19)$$

From this we obtain the effective cluster temperature on the basis of our chosen definition, if criterion (5.18) holds true:

$$T = \overline{T} + \frac{\Delta T}{2} \frac{1-p}{1+p} \,. \qquad (5.20)$$

It follows from the analysis of Section 5.1 that an isolated cluster with two aggregate states can be considered in the two-temperature approach if the criterion (5.2) holds true, i.e., a typical time τ_{eq} for thermodynamic equilibration of the atomic thermal motion in each aggregate state is short compared with the dwell time τ_{ag} of the cluster in each aggregate state. However, if we observe a cluster over a time long compared with τ_{ag}, we can model the cluster with two aggregate states as a cluster with one aggregate state, the average of the two states observable by shorter-time observations, and introduce in this way a single average cluster temperature T. This means that we consider the cluster within the framework of classical thermodynamics; in this case, one can find the cluster temperature from expression (5.14) in which the entropy and the internal energy dE_{th} relate to the thermal motion of atoms, as they do in formulas (5.15):

$$T = w_{sol}\, T_{sol} + w_{liq} T_{liq} \,. \qquad (5.21a)$$

This temperature definition may be used in the context of conventional statistical physics, i.e., on the basis of a very long-time average. On the basis of formulas (5.9) and (5.17), in the limit (5.18) this expression gives

$$T = \overline{T} + \frac{\Delta T}{2} \frac{1-p}{1+p} \,. \qquad (5.21b)$$

We see that there is no difference between the thermodynamic (5.20) and kinetic (5.21b) temperatures for a cluster with two aggregate states in the limit (5.18) under consideration if we restrict the discussion to the first expansion term over this small parameter.

Note that, because the vibrational and configurational degrees of freedom are separated, one can introduce separately the temperature T_{con} of configurational excitation on the basis of a formula analogous to Eqn (4.7):

$$T_{con} = \frac{\Delta E}{\Delta S + \ln(w_{sol}/w_{liq})} \,, \qquad (5.22)$$

where we resorted to expression (5.13) for dE_{con}, and (5.12b) for dS_{con}. Also, we continue to use the approach of two aggregate states and assume that the energy of configurational excitation ΔE is independent of the vibrational energy. At the melting point, the temperature of configurational excitation $T_{con} = \Delta E/\Delta S$ coincides with that defined by

formulas (5.14) and (5.15) at thermodynamic equilibrium. The melting point corresponds to the relation $\Delta F = 0$, where ΔF is the change in the cluster's free energy at the phase transition.

Thus, the 'proper' cluster temperature is a parameter of an atomic system at thermodynamic equilibrium. An isolated cluster, especially if it resides near the point of exact phase equilibrium, is not a system in thermodynamic equilibrium and may be characterized by two temperatures. But if the difference of the solid and liquid temperatures is relatively small, one can consider this cluster a near-equilibrium system with one temperature. However, it is sometimes possible to distinguish the effective temperatures for different phases of clusters in microcanonical ensembles.

Up to this point, we have defined the temperature of a microcanonical system in terms of the entropy derivative of the energy, as in equation (5.14). We reiterate that to do this one must use the *microcanonical* entropy, not the canonical entropy, for which the classical relation $dE/dS = 1/T$ is valid for canonical systems in equilibrium. Alternatively, one can define the temperature of the ensemble in terms of the mean kinetic energy per degree of freedom, E_{kin}, as $T = 2\langle E_{kin}\rangle/(3n-6)$. In common with the previous definitions of microcanonical temperature, especially in the range of coexisting phases, we may take this average over times short enough to see the individual aggregate phase states, or over a time long enough to capture only a single average aggregate state. It is precisely the differences among these definitions that resolve the apparent paradoxes of negative heat capacities [184].

5.4 Heat capacity of an isothermal cluster near the phase transition

We define the cluster heat capacity on the basis of formula (4.10) as

$$C = \frac{dE}{dT} \,, \qquad (5.23)$$

where dE refers to the total cluster energy including both the vibrational motion of atoms and configurational excitation, whereas the translational cluster temperature T characterizes thermal motion of atoms only. This definition applies to both cases, whether the cluster is in a canonical ensemble in accordance with the criterion

$$\tau_{ag} \gg \tau_{th} \qquad (5.24)$$

or is in a microcanonical ensemble according to criterion (5.3). In the case of a canonical ensemble, the cluster temperature is identical for both aggregate states. Then, introducing the average energy E_{con} of configurational excitation, $E_{con} = \Delta E w_{liq}$, where the energy ΔE of configurational excitation is assumed to be a constant in the range of the phase transition, we obtain, from formulas (4.10) and (4.11), the cluster heat capacity

$$C = C_0 + \frac{dE_{con}}{dT} = C_0 + \frac{\Delta E^2}{T^2} \frac{p}{(1+p)^2} \,. \qquad (5.25)$$

The contribution to the heat capacity C_0 due to vibrational motion is assumed to be independent of the temperature. For a large cluster consisting of $n \gg 1$ atoms, the quantities C_0 and ΔE are proportional to n, and the height of the resonance or maximum increases as $\sim n^2$, but its width is $\sim 1/n$. Thus, the

heat capacity consists of two parts: the first is the conventional vibrational contribution, and the second is due to configurational excitation. This part produces the resonance-like peak at the temperature of equal free energies, and the heat capacity near the phase transition temperature can be represented in the form

$$C = C_0 + C_{max} \exp\left[-\alpha(T - T_m)^2\right],$$
$$C_{max} = \frac{\Delta E^2}{4 T_m^2} = \left(\frac{\Delta S}{2}\right)^2, \quad \alpha = \frac{\Delta E^2}{4 T_m^4} = \left(\frac{\Delta S}{2 T_m}\right)^2. \quad (5.26)$$

This relation is valid under the condition $\Delta E \gg T_m$. One can see that the 'resonance' or peak corresponds to a narrow range of temperatures $\Delta T \sim \alpha^{-1/2} \sim T_m/\Delta S \ll T_m$. For a bulk system of bound atoms, this contribution tends to infinity at its maximum. Indeed, the ratio of the second term in formula (5.25) to the first is $\sim n^2$. Hence, determination of the heat capacity of a large cluster reveals its melting point with high accuracy.

5.5 Heat capacity of an isolated cluster near the phase transition

For an isolated cluster in a microcanonical ensemble, we may assume that the caloric curve far from the melting point can be approximated by two straight lines. One can expect two forms of the caloric curves near the melting point, as shown in Fig. 15: in case 1, the cluster heat capacity is positive at any temperature, and in case 2 it is negative near T_m. In principle, both cases are possible. Based on their experimental study of sodium clusters consisting of hundreds atoms, Haberland and coworkers [180, 181] infer that the case of the negative cluster heat capacity near T_m is more representative. Initially, the accuracy of the experimental data [173, 174, 182, 183] left open the possibility of questioning that inference, but more recent, independent measurements have made the case for some microcanonical negative heat capacities much more plausible [185, 186]. All these experiments, in effect, base the evaluation of temperature on the kinetic energy of the particles of the clusters. It is easy to understand how this definition allows for negative heat capacities.

Below, we analyze this problem using our simplified approach within the framework of the statistical and thermodynamic analyses. We introduce a general tempera-
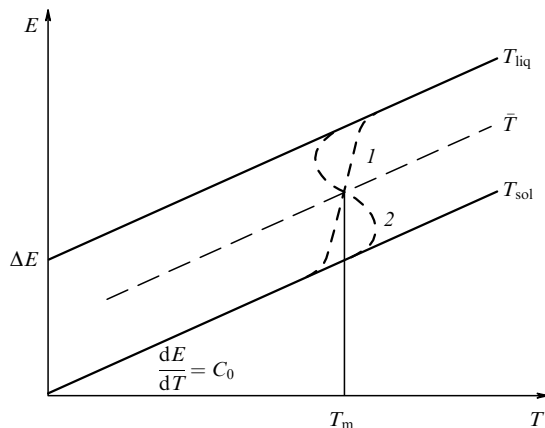

Figure 15. Caloric curves of an isolated cluster with two aggregate states in the one-temperature approach [175]: *1* — the case of positive heat capacity, and *2* — the case of negative heat capacity near the melting point.

ture for an isolated cluster, which can be found both in the solid and liquid states, and assume the energy of configurational excitation to be small compared to the thermal excitation of the cluster. Considering this problem in terms of two aggregate states, with the additional simplifying assumption that the separate caloric curves for the solid and liquid states are parallel straight lines, we have from Fig. 15 or formula (5.21a) for the cluster's translational temperature

$$dT = dT_{sol} - \Delta T\, dw_{liq}. \quad (5.27a)$$

Let us introduce the energy of thermal excitation $dE_{th} = C_0\, dT_{sol} = C_0\, dT_{liq}$, which is responsible for the cluster's shift along one caloric curve in Fig. 15, and the energy of configurational excitation $dE_{con} = \Delta E\, dw_{liq}$, which is responsible for displacement between two caloric curves. Then, we arrive at the total energy change dE of an isolated cluster in the following form

$$dE = dE_{th} + dE_{con} = C_0\, dT_{sol} + \Delta E\, dw_{liq}. \quad (5.27b)$$

Under these conditions, when equilibrium is established at each new energy, every small increase in energy near the melting point goes in part to the excitation of thermal (vibrational) motion, and in part to configurational excitation. If a new small portion of energy induces configurational excitation, i.e., a small part of the injected thermal energy excites configurational degrees of freedom, the effective cluster temperature defined by the average kinetic energy of atoms decreases when there is an increase in the total cluster energy. Another way to picture this is in terms of the means the population distributes itself over the potential energy surface. The solid corresponds to a region of a deep and rather narrow potential well. The liquid corresponds to a broad region of high potential energy, like a high, uneven range. If the density of available states is significantly higher in the liquid region and increases with energy faster than the density of states in the solid region, then increasing the energy of the microcanonical ensemble will move systems from the deep well of the solid to the high plain of the liquid. But the mean kinetic energy in the high plain is necessarily less than that in the deep well for this constant-energy system. Hence, the temperature defined as mean kinetic energy drops as energy is added, and the heat capacity, so defined, is negative for this case. This is known as an 'S-bend' in the cluster caloric curve. Such cluster behavior is obtained both on the basis of theoretical analysis [184, 187–192] and experiments [173, 174, 182, 183, 186].

If we use two temperatures to describe an isolated cluster, the translational and configurational, and employ formulas (5.27) for the change of the translational temperature T and the total cluster energy E, we find for the heat capacity of an isolated cluster:

$$C = \frac{dE}{dT} = C_0\, \frac{1 + X}{1 - X}, \quad X = \Delta T\, \frac{dw_{liq}}{dT_{sol}}. \quad (5.28)$$

To deduce this formula, we took account of the relation $\Delta E = C_0 \Delta T$. From this it follows that the cluster heat capacity can be negative near the melting point, where $X > 1$.

This view of the problem of heat capacities of clusters puts it outside the traditional thermodynamic context for two reasons. First, we introduced a time scale for observation

that allowed us to distinguish the two coexisting phases. This, however, is in much the same spirit as the widely used approach of 'local thermal equilibrium', in which one can use thermodynamics for regions local in space or time, even though the entire system is out of equilibrium. (Typically, one applies this approach to steady-state flows.) In particular, for the time hierarchy of Eqns (5.2) and (5.4), we describe a cluster with two aggregate states as having two different translational temperatures. Second, the translational cluster temperature does not coincide with the configurational one. This is another kind of separation, again associated with time scale separability, in which two sets of degrees of freedom interact so weakly that it becomes possible to determine their population distributions separately and, hence, to assign each of them its own temperature — provided those distributions correspond to a temperature at all. In reality, the vibrational or translational temperature is sure, in this context, to be associated with a thermal distribution. The distribution of population among configurational states may not actually correspond as closely to a thermal distribution. However, we assume here that in the cases we are considering the distribution is close enough to thermal to allow us to assign an effective configurational temperature. Hence, it is not appropriate to describe a microcanonical ensemble with two phases in dynamic equilibrium in terms one would use for a system in thermodynamic equilibrium, with a single temperature. The negative heat capacity exhibited in several such systems is a reflection of changes of population distributions, but not of thermodynamic conditions [175].

6. Kinetics of voids in some phenomena

6.1 Freezing point for bulk inert gases

Condensed inert gases, like other bulk ensembles of bound atoms with pairwise interactions, have two aggregate states, liquid and crystalline. At each temperature except that of thermodynamic phase equilibrium, one of these states is stable, and the other is metastable. Relaxation of configurationally excited states will then transfer the ensemble of atoms into a stable or metastable state. We will consider this process at temperatures below the melting point from the standpoint of configurational excitation of an ensemble of bound atoms.

Indeed, taking a void as an elementary configurational excitation, one can utilize minima of the free energy or maxima of the partition function as functions of the number of voids inside the system (Fig. 16) to define the aggregate states. (As for condensed inert gases, here we ignore the pressure term in the free energy expression.) At the melting point, the minimum values of the free energy (or maxima of the partition function) for the solid and liquid states coincide. But as the temperature decreases, the liquid minimum of the free energy curve rises with respect to the solid minimum and the curve itself becomes flatter. As a result, there is a critical temperature at which the liquid minimum disappears. This temperature is called the 'freezing limit' and corresponds to the lowest point of the caloric curve for which the liquid state has any stability, as shown in Fig. 17 for argon [37].

Below the freezing limit, apart from the defects that occur in any solid at equilibrium at a temperature above 0 K, any configurationally excited state of an ensemble of bound atoms is unstable. This means that relaxation of such a state leads to a state with free energy near that of the global
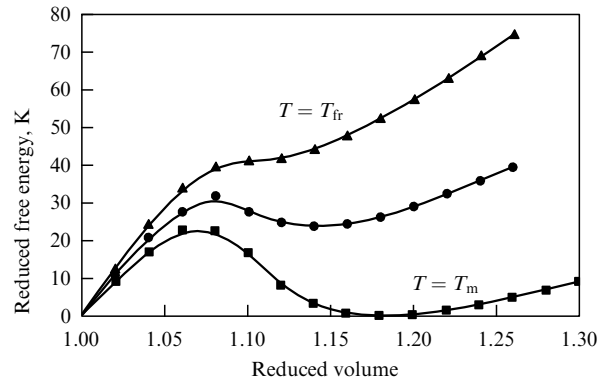

Figure 16. The dependence of the reduced free energy of bulk argon on the volume per atom [37].
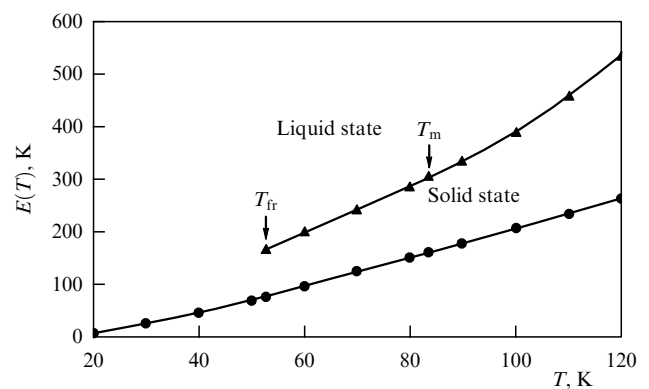

Figure 17. The caloric curves of bulk argon [37].

minimum. The number of voids is small in such a state and diffusion is slow, as in normal solids. The transition of a bulk system to this state occurs through the departure of voids from the system, via their transport and evaporation. From the standpoint of the landscape of the potential energy surface, this process is a series of successive transitions between neighboring local minima of the surface. But any transition between local minima is an activation process, and the rate of such a transition decreases with decreasing temperature according to the Arrhenius law. Hence, configurationally excited states of such a cold, solid body are characterized by a long lifetime that grows with decreasing temperature. According to the usual definition [38, 193–195], a glassy state of a system of bound atoms is a thermodynamically unstable state that has an arbitrarily long lifetime if the kinetic temperature tends to zero. The rate of decay of this state is expressed by the Arrhenius exponential decay formula due to the thermal barrier or barriers associated with this transition. Using the analogy with this definition, we will consider configurationally excited states of an ensemble of bound atoms at low temperatures as glassy-like or glassy states.

6.2 Kinetics of the cooling process and formation of glassy states

Let us consider the process of formation of a glassy state for a bulk condensed inert gas as it cools, or the decay of such a state as it is warmed. We suppose that the transition to a new aggregate state in a homogeneous system occurs adiabati-

cally, so that the rate of the configurational transition coincides with the rate of variation of the imposed temperature. In the case under consideration, the configurational transition results in the diffusion of internal voids to the boundary of the system or from it to the interior. A typical time τ_d of the void diffusion process is estimated as

$$\tau_d \sim \frac{l^2}{D_v}, \tag{6.1}$$

where l is a typical size of the object or a typical distance from an internal point of the object to its boundary, and D_v is the diffusion coefficient of voids inside the object. Since the displacement of voids is determined by a reverse displacement of atoms, the diffusion coefficient of voids can be evaluated in the following way

$$D_v \sim \omega_D a^2 \exp\left(-\frac{E_a}{T}\right), \tag{6.2}$$

where ω_D is the Debye frequency, a is the lattice constant, T is a current temperature, and E_a is the activation energy for the void displacement that results from the displacement of atoms and depends on the concentration of voids or vacancies inside the object. The effective activation energy drops if the concentration of voids increases.

Assuming the rate of the temperature variation dT/dt is constant, we obtain for a typical time τ_c of the cooling process:

$$\frac{1}{\tau_c} \sim \frac{1}{\Delta T} \frac{dT}{dt} \sim \frac{E_a}{T^2} \frac{dT}{dt}, \tag{6.3}$$

where $\Delta T = T^2/E_a$ is the transition temperature range in which the diffusion coefficient varies sharply. Defining the temperature T_g of the glassy transition by the relation $\tau_d(T_g) = \tau_c$, we obtain, from formulas (6.1) and (6.3), the sought-for (implicit) relationship

$$T_g = E_a \left[\ln\left(\frac{\omega_D a^2}{l^2} \frac{T_g^2}{E_a(dT/dt)}\right) \right]^{-1}. \tag{6.4}$$

Formula (6.4) connects the parameters of processes that are responsible for the glassy transition. This formula is valid for both cooling and heating processes.

In considering the glassy state of our systems as containing frozen voids, we distinguish two methods of preparing such glassy states. The first, which we discussed previously, results from fast cooling of the liquid state; in the second method, the glassy state is prepared by depositing atoms on a very cold target. The initially deposited atoms, too cold to diffuse rapidly to a relaxed structure, form an amorphous body whose structure is precisely the glassy state of this system. This amorphous structure may transform into a crystal as a result of relaxation; naturally this transition is facilitated by increasing the temperature, still keeping it below the melting point. This mode of forming a glassy state was realized in an experiment [196] in which amorphous argon was prepared by depositing an argon stream on a copper substrate at a temperature of 10 K. Note that the triple point of bulk argon is $T_{tr} = 83.7$ K (Table 8), and its freezing point is 52 K [165]. Amorphous argon is formed under these experimental conditions if the deposition rate is less than 3×10^{-9} cm s^{-1}. We refer to this amorphous structure of argon as a glassy state. Subsequent heating induces an
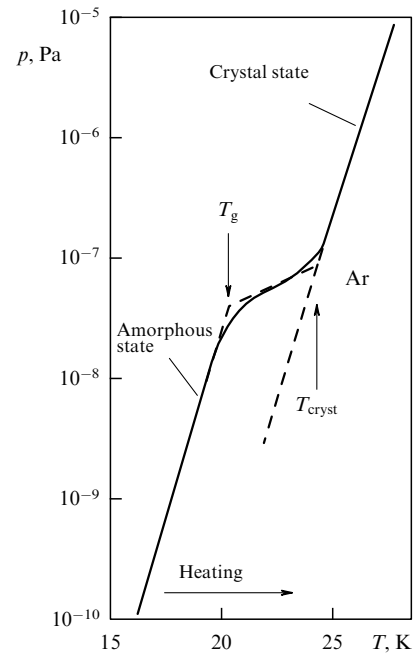

Figure 18. The temperature dependence of the saturated vapor pressure above heated amorphous argon film formed by deposition of the argon flux on a copper substrate at a temperature of 10 K [196], and its approximation by the limiting cases [38] referred to as the glassy-like and crystal argon states.

annealing transition to the crystalline state, as shown in Fig. 18 [38, 196].

Let us now examine the nature of transitions involving the aggregate or glassy-like states of a bulk system of bound inert gas atoms, as voids in this system diffuse to its boundary or from it. The rate of transition between one aggregate state and another or the rate of relaxation in the glassy state of this system is expressed through the diffusion coefficient D_v of voids, which is connected with the self-diffusion coefficient of atoms D_a by the relation

$$D_v = \frac{v}{n} D_a. \tag{6.5}$$

As an activation process, diffusion of voids is characterized by an activation energy. In the solid state, the relative number of vacancies is estimated by

$$\frac{v}{n} \sim \exp\left(-\frac{\varepsilon_v}{T}\right),$$

where ε_v is the energy of vacancy formation. Hence, the activation energies for the self-diffusion coefficients of atoms E_a, for which the data in Table 13 are taken [197], and the diffusion coefficients of voids-vacancies (E_{sol}) differ from those of the solid crystal by the energy ε_v of formation of an individual vacancy ($E_a = E_{sol} + \varepsilon_v$). In the case of the liquid state, for which $v \sim n$, the activation energies for these diffusion processes are identical. The parameters of the atomic self-diffusion coefficients in liquid inert gases, given in Table 13 [198–200], include the activation energies for the diffusion of voids in the solid (E_{sol}) and liquid (E_{liq}) states. The diffusion coefficient of voids for the solid aggregate state of inert gases is assumed to have the form

$$D_v = d_{sol} \exp\left(-\frac{E_{sol}}{T}\right), \tag{6.6a}$$

Table 13. Parameters of void diffusion in condensed inert gases.

Parameter	Ne	Ar	Kr	Xe	Average
D, K	42	143	200	278	
E_a, K	480 ± 20	1900 ± 100	2500 ± 100	3700 ± 100	
E_a/D	11.4 ± 0.5	13.3 ± 0.7	12.5 ± 0.5	13.3 ± 0.4	12.6 ± 0.9
E_{sol}/D	5.3 ± 0.5	6.8 ± 0.7	5.8 ± 0.5	6.6 ± 0.4	6.1 ± 0.7
d_{sol}, 10^{-4} cm^2 s^{-1}	3	3	2	1	
E_{liq}, K	113	352	402	607	
E_{liq}/D	2.69	2.46	2.01	2.18	2.3 ± 0.3
ε_{liq}/D	2.1	2.0	2.1	2.1	2.1 ± 0.1
d_{liq}, 10^{-3} cm^2 s^{-1}	2.7	3.7	1.5	2.2	
$l^2|(dT/dt)_{lim}|$, K cm^2 s^{-1}	0.014	0.11	0.16	0.22	

and for the liquid aggregate state it is

$$D_v = d_{liq} \exp\left(-\frac{E_{liq}}{T}\right). \tag{6.6b}$$

The parameters of these formulas are listed in Table 13. The energy parameters are measured in units of the energy D of breaking one bond. Comparison of the activation energies of the diffusion process for voids and energies of formation of vacancies and voids shows a correspondence between these values. Therefore, the activation energy of the void diffusion process may be expressed through the energy of void formation, whose values are given in Table 11.

Note that the quantity ε_{liq} in Table 13 differs from the quantity $\varepsilon(v_{liq})$ in Table 11. Indeed, $\varepsilon(v_{liq})$ is the average energy of void formation, if we start from the crystal state. In contrast to this quantity, ε_{liq} is the energy of formation of a new void if the system is found in the liquid state. Within the framework of the model under consideration, the latter is approximately equal to

$$\varepsilon_{liq} = \varepsilon(v_{liq}) - \Delta H_{fus}.$$

One can utilize various parameters of the system in order to distinguish the solid and glassy-like states; for this purpose, guided by the experiment [196], we use the saturated vapor pressure over a plane surface of the system. According to the Clapeyron–Clausius law, the saturated vapor pressure is given by [4, 6]

$$p(v, T) = p_v \exp\left(-\frac{\varepsilon(v)}{T}\right), \tag{6.7}$$

where $\varepsilon(v)$ is the mean binding energy of a surface atom in a system with a given concentration of internal voids; equivalently, it is the sublimation energy per atom for a bulk system, with a given concentration of voids v inside. We assume that the saturated vapor pressures may refer to any concentration of voids, and are identical at the triple point, as they must be for the solid and liquid states. This gives for the pre-exponential coefficient:

$$p_v = p_0 \exp\left(\frac{\varepsilon(v) - \varepsilon_{sol}}{T_{tr}}\right), \tag{6.8}$$

where ε_{sol} is the binding energy per atom for the solid state, with $\varepsilon_{sol} = \varepsilon(0)$, p_0 is the pre-exponential factor in formula (6.7) for the solid state, and T_{tr} is the triple-point temperature. It follows from this formula that the pre-exponential factor in formula (6.7) drops as the density of voids increases. Of course, formula (6.8) is correct for the liquid state.

From this we have

$$\frac{p(v, T)}{p_{sol}(T)} = \exp\left[(\varepsilon_{sol} - \varepsilon(v))\left(\frac{1}{T} - \frac{1}{T_{tr}}\right)\right], \tag{6.9}$$

where $p_{sol}(T)$ is the saturated vapor pressure over the solid surface at a given temperature. In particular, for the metastable liquid state at a temperature T below the triple point, formula (6.9) yields

$$\frac{p_{liq}(T)}{p_{sol}(T)} = \exp\left[\Delta H_{fus}\left(\frac{1}{T} - \frac{1}{T_{tr}}\right)\right], \tag{6.10}$$

where ΔH_{fus} is the specific fusion enthalpy.

Along with the temperature of the glassy transition, which is given by formula (6.4) and characterizes the equality of the rate of heating and the process of void diffusion, we introduce the temperature T_* from which the subsequent growth of the saturated vapor pressure can proceed. For the heating of an amorphous state of an inert gas, this temperature is defined by the relation

$$p(v, T_g) = p_{sol}(T_*),$$

and according to formula (6.9) we obtain

$$\varepsilon(v)\left(\frac{1}{T_g} - \frac{1}{T_{tr}}\right) = \varepsilon_{sol}\left(\frac{1}{T_*} - \frac{1}{T_{tr}}\right). \tag{6.11}$$

Let us apply these formulas to analyze the results of the experiment [196] (see Fig. 18) in which amorphous argon was prepared by deposition of an argon stream on a copper substrate at a temperature of 10 K. The triple point of bulk argon is $T_{tr} = 83.7$ K. Warming the deposited material leads to an annealing transition to the crystalline state [38, 196]. The typical film thickness in this experiment was 10 μm, thus exceeding the distance between nearest neighbors in bulk condensed argon by more than three orders of magnitude. Hence, this film can be considered to be bulk condensed argon. A heating rate of $dT/dt \approx 2$ K min^{-1} leads to the glassy transition at $T_g = 20 \pm 1$ K, and the saturated vapor pressure starts to grow from the temperature $T_* = 24 \pm 1$ K. The results of this experiment are compared with the above formulas in Table 14, if we assume that the amorphous state

Table 14. Comparison between theoretical and experimental evidence for bulk condensed argon.

	T_g, K	T_*, K	$\varepsilon(v)$, K	E_a, K
Experiment [196]	20 ± 1	24 ± 1	730 ± 90	330 ± 20
Theory for liquid	21	23	790	350

has the same concentration of voids as the liquid state and we treat experimental data on the basis of formulas (6.4) and (6.11). In addition, the parameter l in formula (6.1) is the thickness of the deposited film. This comparison shows the identity of the amorphous state of argon obtained by deposition of atoms on a cold target and the glassy-like state that we have described as a frozen liquid state at low temperatures.

In treating the experimental data [196], we also found the ratio between the binding energies in the glassy and solid states: $\varepsilon_v/\varepsilon_{sol} = 0.78 \pm 0.10$. Note that the ratio of the binding energies ε_{liq} and ε_{sol} of the liquid and solid states is $\varepsilon_{liq}/\varepsilon_{sol} = 0.85 \pm 0.10$ for inert gases on average [24, 111], and is 0.86 ± 0.02 for argon. One can see that the binding energy per atom in the glassy state ε_v implied by this experiment coincides with the binding energy per atom ε_{liq} for the liquid state within the limits of the accuracy of these data. We obtain a striking analogy between the glassy and liquid states, although they exist in different temperature ranges. Hence, from this analysis for the simplest bulk systems of bound atoms it follows that the glassy and crystal-to-liquid phase transitions have a common feature: both involve a change of configurational excitation. The difference between these phenomena is that thermal excitation of bound atoms influences the latter phase transition, whereas thermal motion of atoms is not so important for glassy-like states because of the low temperatures at which they exist.

Thus, the void concept of configurational excitation for simple ensembles of bound atoms describes simultaneously the formation of both the liquid aggregate states and the glassy-like states. These voids are formed inside bulk systems or on the surface of medium-sized or moderately large clusters. Thermal vibrations of atoms influence significantly the entropy of configurational excitation close to the melting point, and are not important for the glassy-like states, since these exist only at low temperatures where this influence is weak. We can again apply the concept of time scale separation to characterize and validate the glassy-like states, as well-defined states with specifiable thermodynamic properties.

6.3 Glassy states of clusters

Let us once again use the concept of shell structure for the ground and slightly excited configurational states of clusters. If the clusters are not very large (e.g., in the nanoscale range), those with a finite number of locally stable, configurationally excited states form these states by the transition of atoms from closed cluster shells to the surface to become floaters. Such changes correspond to the formation of voids in the outer shell that may diffuse into the cluster. Annihilation of the simplest voids results in transitions of atoms from the cluster surface to the outermost shell. This glassy-like state may also be considered from the standpoint of the concept of cluster configurational excitation as a result of the transition of the potential energy surface of this cluster to local minima. Because neighboring local minima of the cluster's configurational energy are separated by energy barriers, transitions from the ground cluster shell to excited configurations have an activation character. Thus, the void concept of the liquid and glassy-like states can be combined with our understanding of the evolution of clusters as transitions between local minima of the potential energy surface of clusters. Joining these concepts is important for a more detailed understanding of cluster behavior.

By analogy with a bulk system of bound atoms, we define the glassy-like state of clusters as a configurationally excited cluster state at low temperatures, low enough that diffusion is on a slow, solid-state scale, rather than on a liquid-like scale. Guided by systems of inert gas atoms, we will again consider clusters bound by pair interactions of atoms. Such a cluster, like the bulk solid state, may have more than one excited aggregate state [171, 172] which corresponds to the melting of different cluster shells. As the cluster size increases, only two liquid aggregate states remain distinguishable, the surface and volume liquid aggregate states. Because of the difference in the binding energies for the internal and surface atoms, these liquid states may be separated and distinguished experimentally [201, 202]. Previously, we restricted ourselves to the volume liquid state of bulk inert gases, while below we consider excited cluster states in which the liquid or amorphous character is restricted to the outermost shell.

We adhere to the principle of detailed balance that connects the rates of cluster excitation v_{ex} and quenching v_q as a result of the thermal motion of bound atoms [33, 203–205]; this has the form

$$v_{ex} = v_q\, g \exp\left(-\frac{\Delta\varepsilon}{T}\right), \tag{6.12}$$

where g is the ratio of the statistical weights for excited and ground states, and $\Delta\varepsilon$ is the cluster excitation energy. In particular, for the rate of excitation of a classical atom in the cluster consisting of 13 atoms we take

$$v_{ex} = 12\omega_D \exp\left(-\frac{E_b}{T}\right) \alpha, \tag{6.13}$$

where ω_D is the Debye frequency, a typical frequency of atomic oscillations; the factor 12 takes into account that each surface atom can partake in this transition; E_b is the barrier energy for this transition from the ground state, and α is the geometrical factor, i.e., the range of solid angles for atomic motion that determines this transition. For simplicity, we take $12\alpha = 1$, which gives an estimate for the cooling rate at which the excited cluster state may be frozen:

$$\frac{dT}{dt} > \frac{T_m^2}{E_a}\, \frac{\omega_D}{g} \exp\left(-\frac{E_a}{T_m}\right). \tag{6.14}$$

We used formula (6.4) and accounted for the probability of quenching being maximal at the melting point; the activation energy is $E_a = E_b - \Delta\varepsilon \approx 0.56D$ [8] in the case of the 13-atom cluster.

Comparing criterion (6.14) with the criterion for the formation of the glassy state in a bulk system of bound atoms, $T_g < T_m$, where T_g is given by formula (6.4), we find two aspects of the difference of these criteria for bulk systems and clusters. First, the activation energy is higher for a bulk system because more energy is required to change the position of an internal crystal atom than to move a surface atom. In particular, we have $\exp(E_a/T_m) = 400$ in the case of bulk argon, while this value is only 8 for the Lennard-Jones cluster consisting of 13 atoms. Second, the criterion (6.4) for the formation of the glassy state of a bulk system contains an additional large factor l^2/a^2 in comparison with the cluster; this factor is responsible for the diffusion of voids to the boundary. Although small and moderate-sized clusters exhibit no volume diffusion, but instead have excited surface
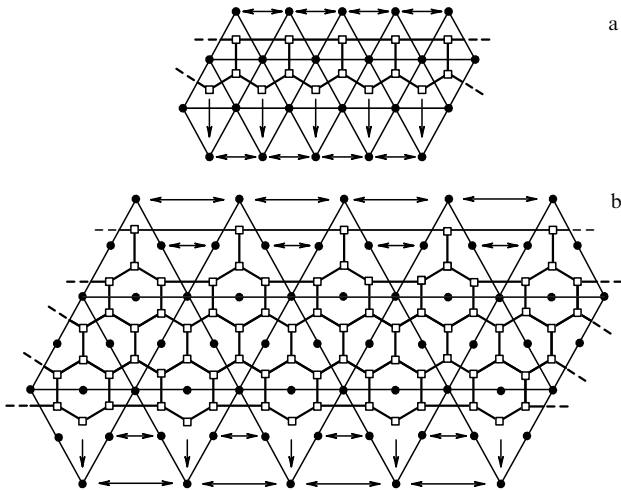
Figure 19. The developed view of the surface of the icosahedron cluster with the closed layers consisting of 13 (a) and 55 (b) atoms [39]. Solid circles are the surface cluster atoms, the open squares are positions of an atom located on the cluster surface; migrations of this atom over the cluster surface are shown by solid lines, while boundaries of the surface cluster triangles are denoted by fine solid lines. Arrows show transitions of a test atom into the ground state, while double arrows relate to the same atom of a three-dimensional structure, and dotted lines indicate the ways for the transformation into the three-dimensional cluster.

atoms, motion of voids over the cluster surface can include many configurations, as demonstrated by Fig. 19 [39], where possible positions are shown for atoms on the surface of clusters with closed shells. Then, instead of the factor l^2/a^2 in formula (4.6) for macroscopic systems, we obtain the quantity g^2 for a configurational state with excited surface atoms, for which the statistical weight g of an excited atom on the surface characterizes the diffusion of atoms over the cluster surface. Hence, configurational entropy is typically significant for a cluster with voids. On the other hand, one can reach high rates of cooling dT/dt with clusters by inserting a cluster into a cold gas, which provides frequent collisions with the responsive cluster surface.

Let us now estimate the critical density of a cold gas that would provide fast enough cooling of the cluster to 'freeze in' its excited configurational state. We apply to a simple model for an exchange of energy between a colliding atom and a cluster [24, 33], so that the average energy of an atom before collision is $3T_0/2$, where T_0 is the gas temperature expressed in energy units (as $k_B T$); after the collision, the atomic energy is $3T/2$, where T is the cluster temperature. Then, the heat balance equation of the cluster takes the form

$$c_p \frac{dT}{dt} = \frac{3}{2}(T_0 - T) N v_T \sigma, \qquad (6.15)$$

where c_p is the cluster's heat capacity, N is the density of gas atoms, v_T is the average atomic velocity, and σ is the cross section for atom–cluster collisions. Assuming the cluster atoms behave classically, we use the Dulong–Petit formula $c_p = 3n$ for the heat capacity, where n is the number of cluster atoms. The liquid drop cluster model for collision processes [24, 33, 111] yields

$$\sigma = \pi r_W^2 n^{2/3},$$

where r_W is the Wigner–Seitz radius. Under these conditions, the criterion (6.14) takes the form

$$\frac{dT}{dt} > n^{1/3} \frac{T_m^2}{E_a(T_m - T_0)} \frac{\omega_D}{v r_W^2} \exp\left(-\frac{E_b}{T_m}\right), \qquad (6.16)$$

where $v = \sqrt{2\pi T_0/m}$, and m is the atomic mass; we used relations (6.14) and $E_b = E_a + \Delta\varepsilon$. As a specific example, we apply this estimate to the argon (Lennard-Jones) cluster consisting of 13 atoms ($T_m = 44$ K) [155] and inserted into helium gas at a temperature of 20 K. Then, formula (6.16) gives the density of helium atoms:

$$N \gg 3 \times 10^{17} \text{ cm}^{-3},$$

a criterion that may be fulfilled in reality.

This example demonstrates the possibility of conserving a cluster's configurational excitation by cooling it rapidly enough. Since excited configurational states of metallic clusters may be detected, for example, by collisional ionization of such clusters with a metallic surface or perhaps by photoionization, one can check the possibility of forming the glassy-like cluster state when a liquid metallic cluster is inserted into a cold gas. Determination of radial density distributions for clusters bound primarily by pair interatomic interactions may also become a way to probe densities of vacancies [202]. Thus, the configurational excitation of small clusters, via passage of surface atoms from the outermost closed shell to the cluster's surface, is an analog of the formation of a bulk glassy state with frozen surface voids. In fact, configurationally excited cluster states are analogs of glassy-like states, if their lifetime is long enough, and such states may be formed by the evolution of thermodynamically stable or metastable states.

Simulations show that it should also be possible to prepare some glassy states of clusters by the quenching that occurs when a cluster strikes a surface, exchanging momentum extremely efficiently and rapidly with that surface, and then atoms from the substrate evaporate and quench the cluster faster than its vibrations can equilibrate with the substrate. It had been found from simulations [206] that some alkali halide clusters consisting of many dozens or hundreds of particles could be quenched to a glassy state if they could be cooled from the liquid state at a rate of 10^{13} K s^{-1}. It was then shown by Cheng and Landman [207] that this cooling rate could be achieved if sodium chloride clusters were to strike solid argon at moderately high energy. The momentum transfer between argon and NaCl clusters is very efficient, and the nearby argon substrate atoms evaporate at a high rate.

On the basis of the above analysis, the glassy state concept can be carried over from complex (i.e., bulk macroscopic) systems to simple ones, specifically to atomic clusters. According to its definition [38], the glassy state is a thermodynamically unstable configurational state of an ensemble of bound atoms formed by fast cooling of the system, for which extremely slow cooling of this ensemble would yield a true first-order phase transition by overcoming an activation energy. For glasses to relax to ordered solids, this transition involves the change of positions of some constituent particles, so that finally the system takes on a crystalline structure as it undergoes 'infinitely' slow cooling. One more peculiarity of this transition is the difference in densities of the structures for the initial and final states.

Therefore, together with the restructuring of the atomic positions, voids must diffuse outside the system or into the system.

This approach is complementary to a more traditional free-volume model, in which detailed attention is directed toward the change in available free volume as a system goes between liquid and glass [208–210]. Here, our emphasis is on the change of the kinetics with temperature, specifically on the way how reducing temperature inhibits passage over saddles when the free volume remains relatively unchanged. In this sense, this treatment differs in emphasis but is not inconsistent with a model that emphasizes relatively small but perhaps important changes in the volumes of vacancies at the glass transition.

Focusing on simple bulk systems of bound atoms such as condensed inert gases, we find no need to invoke the restructuring of chemical bonds in such systems, as apparently takes place in real glasses [38]. Rather, the transport of voids proceeds by analogy with glasses, with an activation character. In the case of clusters, cold systems exhibiting a finite number of locally stable, configurationally excited states formed by the transition of atoms from closed cluster shells to the surface conform to the model of a glassy state. This corresponds to the formation of surface voids, and the annihilation of voids results in the transition of atoms from the cluster surface to its outermost, unfilled shell. From the other standpoint, these atomic transitions result from transitions between local minima of the potential energy surface of this cluster. Because neighboring local minima of the cluster's configurational energy are separated by energy barriers [10, 18, 19], transitions from the ground cluster structure to excited configurations show an activation character. Thus, known excited structures of simple systems of bound atoms conform to the definition of the glassy state. Being based on the nature of the glassy-like states of simple systems as a result of the formation of voids, one can analyze these states in more detail.

6.4 Growth of a solid nucleus in liquid as a result of void transport

The void concept of configurational excitation may be used for the analysis of nucleation phenomena in condensed systems. In contrast to the previous problems, in this case we obtain a nonuniform distribution of voids in a space, and therefore it is necessary to analyze the stability of such a distribution. For definiteness, we consider the growth of a spherical solid nucleus of a current radius r_0 in a liquid. In terms of voids, the void concentration for this distribution is close to zero inside the nucleus and is close to the liquid value outside it. Hence, a gradient of void concentration occurs in this case, and the transport of voids causes the nucleus to grow. Thus, we consider the growth of a favorable phase in a macroscopic ensemble of atoms with a pairwise interaction as a result of void transport. Evidently, such a consideration is valid when we deal with many elementary configurational excitations — voids, and therefore we refer below to bulk systems of bound atoms.

The void flux in the one-dimensional case is given by the equation

$$j = -D_v N \frac{dc}{dx} + w_v Nc . \qquad (6.17)$$

Here, x is a coordinate, N is the density of atoms, c is the concentration of voids defined as the number of voids per given number of atoms, D_v is the diffusion coefficient of voids

in this system, and w_v is the drift velocity of voids. Note that transport coefficients of voids are connected with transport coefficients of atoms in this system, namely, with D_a, the self-diffusion coefficient of atoms, by formula (6.5), and with w_a, the drift velocity of atoms. Indeed, the atomic flux j_a is equal to the void flux and is directed oppositely. Hence, we have

$$D_v = \frac{D_a}{c} , \quad w_v = \frac{w_a}{c} . \qquad (6.18)$$

The drift velocity of atoms and voids is determined by the force $d\mu/dx$ that acts on an atom because the atomic chemical potential μ varies in space (correspondingly, a force acting per individual void is $d\mu/c\,dx$). On the basis of the Einstein relation between the mobility and diffusion coefficient, assuming the gradient of μ to be relatively small (except, perhaps, at the boundary of the nucleus), we find

$$w_a = \frac{D_a}{T} \frac{d\mu}{dx} \qquad (6.19)$$

and the same relation holds between the transport coefficients of voids. On the basis of this formula, let us represent the void flux (6.17) in the form

$$j = -D_v N \frac{dc}{dx} \left(1 + \frac{c}{T} \frac{d\mu}{dc} \right) , \qquad (6.20)$$

while the dependence $\mu(c)$ is depicted in Fig. 20. The values of the void diffusion coefficients for the solid and liquid aggregate states of inert gases are collated in Table 13 in accordance with formulas (6.6).

Applying the one-dimensional result (6.17) to the growth of a spherical nucleus, we get for the total flux of voids J through a sphere of a radius r:

$$J = 4\pi r^2 j(r) = -4\pi r^2 D_v N \frac{dc}{dr} \left(1 + \frac{c}{T} \frac{d\mu}{dc} \right) , \qquad (6.21)$$

and one can consider the total flux to be independent of r, since voids are not formed in space. We can reduce this problem to the previous one-dimensional case by a change in the variable
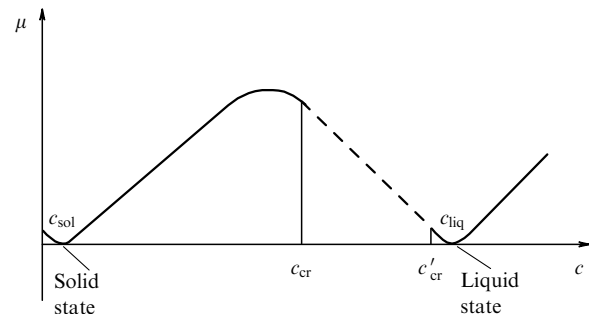
$$x = \frac{1}{4\pi r} . \qquad (6.22)$$

Figure 20. The dependence of the chemical potential on the void concentration for a system of bound atoms with a pair interaction between atoms and a void gas inside it. The void concentrations $c_{sol} \approx 0$ and c_{liq} correspond to the solid and liquid aggregate states, the maximum of the chemical potential corresponds to the void concentration c_{max}, and the range between c'_{cr} and c_{cr} is not stable, i.e., small uniformities lead to an instability that separates the system into two phases. This dependence relates to the melting point.

We now consider the nucleation process at pressures comparable to that at the triple point in inert gases. In this case, one can neglect the pressure term in the expressions for the Helmholz free energy F and Gibbs free energy G of the system, i.e., take $F = G$, so that these thermodynamic parameters are determined by the entropy term. Correspondingly, the chemical potential of this system consisting of n atoms assumes the form

$$\mu(c) = -\frac{T \ln Z}{n} = c \left[\varepsilon(c) - T s(c) \right] . \tag{6.23}$$

Here, Z is the partition function of the void gas, $\varepsilon(c)$ is the energy of formation of one void at a given void concentration, $s(c)$ is the entropy of formation of one void, $g(c)$ is the statistical weight of an individual void, and the energy of formation of one vacancy is $\varepsilon_0 = \varepsilon(0)$. The dependence (6.23) is portrayed in Fig. 20. It follows from this dependence and formula (6.21) that the spatial distribution for the void concentration is unstable for concentrations of voids at which

$$1 + \frac{c}{T} \frac{\mathrm{d}\mu}{\mathrm{d}c} < 0 , \tag{6.24}$$

so that the transport of voids is directed opposite to a void gradient. Table 15 lists the values of the critical void concentration c_{cr} near the liquid minimum that is the boundary of the void stability. In accordance with formula (6.24), this concentration satisfies the relation

$$\left(\frac{\mathrm{d}\mu}{\mathrm{d}c} \right)_{c_{\mathrm{cr}}} = -\frac{T}{c_{\mathrm{cr}}} . \tag{6.25}$$

Thus, an evolving surface arises on the boundary separating the solid nucleus and its liquid environment, and the void concentration varies discontinuously at this boundary. This creates a tension on the liquid environment to shrink. As a result, voids move outside the dividing surface, and the solid nucleus expands as the void-free region grows. Because the chemical potential has different values in the two regions — that is, $\mu_{\mathrm{sol}} \approx \mu(c_{\mathrm{sol}})$ and $\mu_{\mathrm{liq}} \approx \mu(c_{\mathrm{liq}})$ on different sides of this surface, the surface is unstable and moves. We connect the motion of the growing sphere with the drift of atoms or voids. Indeed, let us introduce the effective difference in the chemical potentials $\Delta\mu(r)$ at a given distance r from the nuclear center:

$$\Delta\mu = \mu_{\mathrm{liq}} - \mu_{\mathrm{sol}} = \int_{r_0}^{\infty} F(r) \, \mathrm{d}r \tag{26}$$

and $r \geqslant r_0$, where r_0 is the current nuclear radius. From this it is inferred that the drift velocity of atoms on the basis of formula (6.18) may be represented as

$$w_{\mathrm{a}} = \frac{r_0}{r^2} \frac{D_{\mathrm{liq}}}{T} \left(\mu_{\mathrm{liq}} - \mu_{\mathrm{sol}} \right) ,$$

and the total atomic flux towards the solid nucleus through a sphere located a distance r from it is equal to

$$J = 4\pi r^2 w_{\mathrm{a}} N = 4\pi r_0 N \, \frac{D_{\mathrm{liq}}}{T} \left(\mu_{\mathrm{liq}} - \mu_{\mathrm{sol}} \right) .$$

Evidently, this flux does not depend on r, despite its appearance in formula (6.26).

This atomic flux is equal to the void flux outside the solid nucleus. As a result of void drift, the solid nucleus expands so that

$$J = 4\pi r_0^2 \, \frac{\mathrm{d}r_0}{\mathrm{d}t} \, N c_{\mathrm{liq}} .$$

This gives the rate of growth of the nuclear radius:

$$\frac{\mathrm{d}r_0}{\mathrm{d}t} = \frac{D_{\mathrm{liq}}}{r_0 \, c_{\mathrm{liq}}} \, \frac{(\mu_{\mathrm{liq}} - \mu_{\mathrm{sol}})}{T} , \tag{6.27}$$

where D_{liq} is the diffusion coefficient of voids in the liquid state.

We now evaluate the rate of growth of the solid nucleus in the case in which the current temperature T is close to the melting point T_{m}. We then have $\mu_{\mathrm{liq}} - \mu_{\mathrm{sol}} = (T_{\mathrm{m}} - T)s$, where s is the transition entropy per atom, and formula (6.27) yields

$$\frac{\mathrm{d}r_0^2}{\mathrm{d}t} = \frac{\delta_{\mathrm{sol}}}{c_{\mathrm{liq}}} \, \frac{(T_{\mathrm{m}} - T)}{T} \exp \left[-\alpha_{\mathrm{sol}} \frac{(T_{\mathrm{m}} - T)}{D} \right] ,$$
$$\delta_{\mathrm{sol}} = \frac{1}{2} D_{\mathrm{liq}}(T_{\mathrm{m}}) s , \quad \alpha_{\mathrm{sol}} = \frac{E_{\mathrm{liq}} D}{T_{\mathrm{m}}^2} . \tag{6.28}$$

Table 15 contains the values of parameters δ_{sol} and α_{sol} for inert gases, as well as some other parameters.

In considering this problem, we do not include any contribution of surface effects to the chemical potential. Therefore, we neglect the critical phenomena that occur during nucleation and are responsible for the first appearance of growing nuclei [6, 38]. Rather, any current nuclear radius invoked here is assumed to exceed the critical radius significantly. Next, we have concentrated on the growth of a solid nucleus inside a liquid that results from a force induced by a difference between the chemical potentials for the solid and liquid aggregate states. This force acts on each void independently and compels it to move from the dividing surface. Hence, the rate of expansion of the solid nucleus does not depend on the void concentration and is determined by the friction of moving voids, so that the frictional force is expressed through the diffusion coefficient of voids in this system. Therefore, the growth of the liquid nucleus in a solid will proceed by the same scenario, and the rate of an increase in the radius of the liquid nucleus inside a solid, by analogy with formula (6.28), is given by

$$\frac{\mathrm{d}r_0^2}{\mathrm{d}t} = \frac{\delta_{\mathrm{liq}}}{c_{\mathrm{sol}}} \, \frac{(T_{\mathrm{m}} - T)}{T} \exp \left[-\alpha_{\mathrm{liq}} \frac{(T_{\mathrm{m}} - T)}{D} \right] ,$$
$$\delta_{\mathrm{liq}} = \frac{1}{2} D_{\mathrm{sol}}(T_{\mathrm{m}}) s , \quad \alpha_{\mathrm{liq}} = \frac{E_{\mathrm{sol}} D}{T_{\mathrm{m}}^2} . \tag{6.29}$$

For condensed inert gases, the parameters of this formula are listed in Table 15. One can see that the growth rate for the solid nucleus is lower than that for the liquid, because the void diffusion coefficient in solids is lower than in liquids.

Table 15. The parameters of growth of a solid nucleus in liquid inert gases.

	c_{liq}	c'_{cr}	δ_{sol}, 10^{-5} cm^2 s^{-1}	α_{sol}	δ_{liq}, 10^{-8} cm^2 s^{-1}	α_{liq}
Ne	0.31	0.25	8.2	8.0	$10 \times 10^{\pm 0.4}$	16 ± 2
Ar	0.32	0.25	17	7.2	$1 \times 10^{\pm 0.5}$	20 ± 2
Kr	0.32	0.26	14	6.3	$3 \times 10^{\pm 0.4}$	17 ± 2
Xe	0.31	0.25	17	6.8	$0.4 \times 10^{\pm 0.3}$	20 ± 1

Thus, considering an ensemble of bound atoms as consisting of atoms and voids, one can treat the nucleation process as a result of the transport of atoms or voids inside this system. From the standpoint of the behavior of the system's potential energy surface, an elementary displacement of a void is a transition of the system between two neighboring local minima of the potential energy surface. We conclude that a thermodynamic instability of configurational excitations occurs when the degree of configurational excitation varies in space to make the aggregate state change from solid to liquid. This implies the impossibility of a continuous transition between the solid and liquid aggregate states by varying the density of voids. Therefore, in the spatial coexistence of solid and liquid states that occurs in nucleation processes, the dividing surface forms and separates the solid and liquid phases. When a nucleus of a new phase grows inside an old phase, the difference of the chemical potentials on two sides of the breaking surface creates a force that acts on voids of an old phase and compels them to move such that the nucleus of the new phase grows. Because the displacements of voids and atoms in this system are mutually connected, the rate of the nucleus's growth is expressed through the coefficient of self-diffusion of atoms in this system.

7. Conclusions

Analyzing the phase transition for the simplest ensembles of finite and infinite numbers of bound atoms allows us to understand many details of this phenomenon. Concentrating on the order – disorder or solid – liquid phase transition in clusters and macroscopic systems of bound atoms with pairwise atomic interactions, we start from the standpoint of classical thermodynamics with each aggregate state characterized by certain thermodynamic parameters. The complex topographies of the potential energy landscapes for these systems, with their many, many local minima, allow us to view these atomic systems from another standpoint. Indeed, in this space the system undergoes many oscillations in the vicinity of any one minimum of the potential energy surface and then occasionally transfers to a neighboring minimum. This allows us to separate the thermal motion of a system, corresponding to vibrations around any of the energy minima, from configurational excitation that specifies a given energy minimum. This leads to a redefinition of the aggregate state as a group of configurationally excited states with similar excitation energies. Together with concepts of classical thermodynamics, separation of vibrational and configurational degrees of freedom provides the basis for our treatment.

Analyzing the phase transitions and the behavior of systems near the melting point from this standpoint, we obtain new details and new connections to related phenomena for these systems with the simplest character of atomic interactions. In addition, this analysis allows us to follow the passage from clusters to bulk systems. Basing on the simplified form of configurational excitation in which the elementary configurational excitation corresponds to the formation of one void, we demonstrate that the liquid state which is metastable below the melting point can be realized in this form only above the freezing limit, the lowest temperature for which the liquid has local stability, equivalent to the spinodal limit. Below the freezing limit, excitation of voids gives a thermodynamically unstable or glassy state, and the

void concept permits us to analyze the liquid and glassy states from a common standpoint. Next, nucleation phenomena in condensed matter, which correspond to the growth of a new condensed phase in an old one, may be represented as a result of void transport. In this way, one can relate various phenomena in a condensed system within the framework of the void concept.

It should be noted that any phase transition includes simultaneously many atomic particles and therefore analytic methods based on single-atom models are not suitable for its analysis. Therefore, all the results are based either on experimental data or on computer simulation of this phenomenon. Hence, new results of this type lead to improvements in the void concept of the phase transitions and adjacent phenomena.

References

1. Huang K *Statistical Mechanics* (New York: Wiley, 1963)
2. Brout R *Phase Transitions* (New York: W.A. Benjamin, 1965)
3. Kubo R *Statistical Mechanics* (Amsterdam: North-Holland, 1965)
4. Ter Haar D *Elements of Thermostatistics* 2nd ed. (New York: Holt, Rinehart and Winston, 1966)
5. Feynman R P *Statistical Mechanics* (Reading, Mass.: W.A. Benjamin, 1972)
6. Landau L D, Lifshitz E M *Statisticheskaya Fizika* (Statistical Physics) Pt. 1 (Moscow: Nauka, 1976) [Translated into English (Oxford: Pergamon Press, 1980)]
7. Berry R S, Jellinek J, Natanson G *Phys. Rev. A* **30** 919 (1984)
8. Jellinek J, Beck T L, Berry R S *J. Chem. Phys.* **84** 2783 (1986)
9. Berry R S et al. *Adv. Chem. Phys.* **90** 75 (1988)
10. Berry R S, in *Theory of Atomic and Molecular Clusters* (Ed. J Jellinek) (Berlin: Springer-Verlag, 1999) p. 1
11. Hoare M R, Pal P *Adv. Phys.* **20** 161 (1971); **24** 645 (1975)
12. Hoare M R *Adv. Chem. Phys.* **40** 49 (1979)
13. Ball K D, Berry R S *J. Chem. Phys.* **111** 2060 (1999)
14. Stillinger F H, Weber T A *Phys. Rev. A* **25** 978 (1982)
15. Corti D S et al. *Phys. Rev. E* **55** 5522 (1997)
16. Stillinger F H, Weber T A *Phys. Rev. A* **28** 2408 (1983)
17. Becker O M, Karplus M *J. Chem. Phys.* **106** 1495 (1997)
18. Wales D J et al. *Adv. Chem. Phys.* **115** 1 (2000)
19. Wales D J *Energy Landscapes* (Cambridge: Cambridge Univ. Press, 2003)
20. Komatsuzaki T, Berry R S *J. Chem. Phys.* **110** 9160 (1999)
21. Vekhter B et al. *J. Chem. Phys.* **106** 4644 (1997)
22. Bragg W, Williams H J *Proc. R. Soc. London Ser. A* **145** 699 (1934)
23. Ziman J M *Models of Disorder* (Cambridge: Cambridge Univ. Press, 1979)
24. Smirnov B M *Statistical Physics and Kinetic Theory of Atomic Systems* (Moscow: IVT RAN, 2001)
25. Reiss H, Frisch H L, Lebowitz J L *J. Chem. Phys.* **31** 369 (1959)
26. Lindemann F A *Z. Phys.* **11** 609 (1910)
27. Hansen J-P, Verlet L *Phys. Rev.* **184** 151 (1969)
28. Etters R D, Kaelberer J *Phys. Rev. A* **11** 1068 (1975)
29. Etters R D, Kaelberer J B *J. Chem. Phys.* **66** 5112 (1977)
30. Kaelberer J B, Etters R D *J. Chem. Phys.* **66** 3233 (1977)
31. Zhou Y et al. *J. Chem. Phys.* **116** 2323 (2002)
32. Smirnov B M *Zh. Eksp. Teor. Fiz* **112** 1847 (1997) [*JETP* **85** 1010 (1997)]
33. Smirnov B M *Clusters and Small Particles: in Gases and Plasmas* (New York: Springer-Verlag, 2000)
34. Smirnov B M *Neorg. Mater.* **35** 672 (1999) [*Inorg. Mater.* **35** 562 (1999)]
35. Smirnov B M, in *Nucleation Theory and Applications: Research Workshop, Dubna, Russia, April 1999* (Eds J W P Schmelzer, G Röpke, V B Priezzhev) (Dubna: JINR, 1999) p. 355

36. Berry R S, Smirnov B M, in *Nucleation Theory and Applications*: *Research Workshop, Dubna, Russia, April 2002* (Eds J W P Schmelzer, G Röpke, V B Priezzhev) (Dubna: JINR, 2002) p. 340

37. Berry R S, Smirnov B M *Zh. Eksp. Teor. Fiz.* **120** 889 (2001) [*JETP* **93** 541 (2001)]

39. Berry R S, Smirnov B M *Zh. Eksp. Teor. Fiz.* **122** 298 (2002) [*JETP* **95** 255 (2002)]

40. Berry R S, Smirnov B M *J. Chem. Phys.* **118** 5979 (2003)

41. Ashcroft N W, Mermin N D *Solid State Physics* (New York: Holt, Rinehart and Winston, 1976)

42. Echt O, Sattler K, Recknagel E *Phys. Rev. Lett.* **47** 1121 (1981)

43. Echt O et al. *Ber. Bunsenges. Phys. Chem.* **86** 860 (1982)

44. Ding A, Hesslich J *Chem. Phys. Lett.* **94** 54 (1983)

45. Harris I A, Kidwell R S, Northby J A *Phys. Rev. Lett.* **53** 2390 (1984)

46. Phillips J C *Chem. Rev.* **86** 619 (1986)

47. Harris I A et al. *Chem. Phys. Lett.* **130** 316 (1986)

48. Miehle W et al. *J. Chem. Phys.* **91** 5940 (1989)

49. Farges J et al. *Surf. Sci.* **106** 95 (1981)

50. Kim S S, Stein G D *J. Colloid. Interface Sci.* **87** 180 (1982)

51. Farges J et al. *J. Chem. Phys.* **78** 5067 (1983)

52. Farges J et al. *J. Chem. Phys.* **84** 3491 (1986)

53. Lee J W, Stein G D *J. Phys. Chem.* **91** 2450 (1987)

54. Farges J et al. *Adv. Chem. Phys.* **70** 45 (1988)

55. Bartell L S *Chem. Rev.* **86** 491 (1986)

56. Van de Waal B W *J. Chem. Phys.* **98** 4909 (1993)

57. Easter D C et al. *Chem. Phys. Lett.* **157** 277 (1989)

58. Easter D C, Whetten R L, Wessel J E *J. Chem. Phys.* **94** 3347 (1991)

59. Beck S M, Hecht J H *J. Chem. Phys.* **96** 1975 (1992)

60. Martin T P et al. *J. Chem. Phys.* **100** 2322 (1994)

61. Martin T P *Phys. Rep.* **273** 199 (1996)

62. Smirnov B M *Usp. Fiz. Nauk* **162** (12) 97 (1992) [*Sov. Phys. Usp.* **35** 1052 (1992)]

63. Ino S *J. Phys. Soc. Jpn.* **27** 941 (1969)

64. Smirnov B M *Usp. Fiz. Nauk* **162** (1) 119 (1992) [*Sov. Phys. Usp.* **35** 37 (1992)]

65. Smirnov B M *Usp. Fiz. Nauk* **163** (10) 29 (1993) [*Phys. Usp.* **36** 933 (1993)]

66. Doye J P K, Wales D J, Berry R S *J. Chem. Phys.* **103** 4234 (1995)

67. Kittel Ch *Introduction to Solid State Physics* (New York: Wiley, 1986)

68. Landau L D, Lifshitz E M *Kvantovaya Mekhanika: Nerelyativistskaya Teoriya* (Quantum Mechanics: Non-Relativistic Theory) (Moscow: Nauka, 1974) [Translated into English (Oxford: Pergamon Press, 1977)]

69. Wang S-W, Falicov L M, Searcy A W *Surf. Sci.* **143** 609 (1984)

70. Raoult B et al. *Philos. Mag. B* **60** 881 (1989)

71. Smirnov B M *Teplofiz. Vys. Temp.* **33** 700 (1995)

72. Kihara T, Koba S *J. Phys. Soc. Jpn.* **7** 348 (1952)

73. Bunn Ch *Crystals* (New York: Academic Press, 1964)

74. Leibfried G *Gittertheorie der mechanischen und thermischen Eigenschaften der Kristalle* (Handbuch der Physik, Bd. VII, Teil 2) (Berlin: Springer, 1955)

75. Mackay A L *Acta Cryst.* **15** 916 (1962)

76. Smirnov B M *Usp. Fiz. Nauk* **164** 1165 (1994) [*Phys. Usp.* **37** 1079 (1994)]

77. Smirnov B M *Chem. Phys. Lett.* **232** 395 (1995)

78. Smirnov B M *Phys. Scripta* **51** 402 (1995)

79. Lennard-Jones J E *Proc. R. Soc. London Ser. A* **106** 636 (1925)

80. Jones J E, Ingham A E *Proc. R. Soc. London Ser. A* **107** 463 (1924)

81. Northby J A et al. *Z. Phys. D* **12** 69 (1989)

82. Xie J et al. *J. Chem. Phys.* **91** 612 (1989)

83. van de Waal B W *J. Chem. Phys.* **90** 3407 (1989)

84. Berry R S, Smirnov B M, Strizhev A Yu *Zh. Eksp. Teor. Fiz.* **112** 1082 (1997) [*JETP* **85** 588 (1997)]

85. Smirnov B M, Strizhev A Yu, Berry R S *J. Chem. Phys.* **110** 7412 (1999)

86. Berry R S, Smirnov B M *Zh. Eksp. Teor. Fiz.* **117** 562 (2000) [*JETP* **90** 491 (2000)]

87. Berry R S, Smirnov B M *J. Chem. Phys.* **113** 728 (2000)

88. Northby J A *J. Chem. Phys.* **87** 6166 (1987)

89. Van de Waal B W *Z. Phys. D* **20** 349 (1991)

90. Aziz R A, Slaman M J *Chem. Phys.* **130** 187 (1989)

91. Aziz R A, Slaman M J *J. Chem. Phys.* **92** 1030 (1990)

92. Dham A K et al. *Mol. Phys.* **67** 1291 (1989)

93. Dham A K et al. *Chem. Phys.* **142** 173 (1990)

94. Smirnov B M *Usp. Fiz. Nauk* **171** 1291 (2001) [*Phys. Usp.* **44** 1229 (2001)]

95. Beck T L, Doll J D, Freeman D L *J. Chem. Phys.* **90** 5651 (1989)

96. Leitner D M, Doll J D, Whitnell R M *J. Chem. Phys.* **94** 6644 (1991)

97. Leonas V B *Usp. Fiz. Nauk* **107** (3) 29 (1972) [*Sov. Phys. Usp.* **15** 266 (1972)]

98. Sena L A *Edinitsy Fizicheskikh Velichin i Ikh Razmernosti* (Units of Physical Quantities and Their Dimensions) (Moscow: Nauka, 1977) [Translated into English (Moscow: Mir Publ., 1972)]

99. Okun' L B *Fizika Elementarnykh Chastits* (Physics of Elementary Particles) (Moscow: Nauka, 1984)

100. Krainov V P *Qualitative Methods in Physical Kinetics and Hydrodynamics* (New York: American Institute of Physics, 1992)

101. Moses A J *The Practising Scientist's Handbook* (New York: Van Nostrand Reinhold Co., 1978)

102. Reid R C, Prausnitz J M, Poling B E *The Properties of Gases and Liquids* 4th ed. (New York: McGraw-Hill, 1987)

103. Rabinovich V A et al. *Thermophysical Properties of Neon, Argon, Krypton, and Xenon* (Washington, DC: Hemisphere Publ. Corp., 1988)

104. Emsley J *The Elements* 2nd ed. (Oxford: Clarendon Press, 1991)

105. Barin I *Thermochemical Data of Pure Substances* 2nd ed. (Weinheim: VCH, 1993)

106. Lide D R (Ed.) *Handbook of Chemistry and Physics* 79th (London: CRC Press, 1998–1999)

107. Smirnov B M *Phys. Scripta* **58** 595 (1998)

108. Schuberth E, Creuzburg M, Müller-Lierheim W *Phys. Status Solidi B* **76** 301 (1976)

109. Bostanjonglo O, Kleinschmidt B *Z. Phys. A* **21** 276 (1977)

110. Sonnenblick Y et al. *Chem. Phys. Lett.* **52** 276 (1977)

111. Smirnov B M *Physics of Ionized Gases* (New York: John Wiley, 2001)

112. Smirnov B M *Physics of Atoms and Ions* (New York: Springer-Verlag, 2003)

113. Bernal J D *Nature* **183** 141 (1959)

114. Scott G D *Nature* **178** 908 (1960)

115. Bernal J D, Mason J *Nature* **188** 908 (1964)

116. Hoover W G, Ree F H *J. Chem. Phys.* **49** 3609 (1968)

117. Rintoul M D, Torquato S *Phys. Rev. Lett.* **77** 4198 (1996)

118. Rintoul M D, Torquato S *Phys. Rev. E* **58** 532 (1998)

119. Hirschfelder J O, Curtiss Ch F, Bird R B *Molecular Theory of Gases and Liquids* (New York: Wiley, 1954)

120. Goettel K A et al. *Phys. Rev. Lett.* **62** 665 (1989)

121. Reichlin R et al. *Phys. Rev. Lett.* **62** 669 (1989)

122. Eremets M I et al. *Phys. Rev. Lett.* **85** 2797 (2000)

123. Boehler R et al. *Phys. Rev. Lett.* **86** 5731 (2001)

124. Jephcoat A P et al. *Phys. Rev. Lett.* **59** 2670 (1987)

125. Cynn H et al. *Phys. Rev. Lett.* **86** 4552 (2001)

126. Belonoshko A B, Ahuja R, Johansson B *Phys. Rev. Lett.* **87** 165505 (2001)

127. Weitz D A, Oliveria M *Phys. Rev. Lett.* **52** 1433 (1984)

128. Weitz D A et al. *Phys. Rev. Lett.* **53** 1657 (1984)

129. Weitz D A et al. *Phys. Rev. Lett.* **54** 1416 (1985)

130. Keefer K D, Schaefer D W *Phys. Rev. Lett.* **56** 2376 (1986)

131. Aubert C, Cannell D S *Phys. Rev. Lett.* **56** 738 (1986)

132. Dimon P et al. *Phys. Rev. Lett.* **57** 595 (1986)

133. Wilcoxon J P, Martin J E, Schaefer D W *Phys. Rev. A* **39** 2675 (1989)

134. Pusey P N, van Mengen W *Nature* **320** 340 (1986)

135. Pusey P N, van Mengen W *Phys. Rev. Lett.* **59** 2083 (1987)

136. Pusey P N et al. *Phys. Rev. Lett.* **63** 2753 (1989)

137. Zhu J et al. *Nature* **387** 883 (1997)

138. Chu J H, Lin I *Phys. Rev. Lett.* **72** 4009 (1994)

139. Thomas H et al. *Phys. Rev. Lett.* **73** 652 (1994)

140. Hayashi Y, Tachibana K *Jpn. J. Appl. Phys.* **33** L804 (1994)

141. Melzer A, Trottenberg T, Piel A *Phys. Lett. A* **191** 301 (1994)

142. Tsytovich V N *Usp. Fiz. Nauk* **167** 57 (1997) [*Phys. Usp.* **40** 53 (1997)]

143. Nefedov A P, Petrov O F, Fortov V E *Usp. Fiz. Nauk* **167** 1215 (1997) [*Phys. Usp.* **40** 1163 (1997)]

144. Morfill G E et al. *Phys. Plasma* **6** 1769 (1999)

145. Shukla P K, Mamun A A *Introduction to Dusty Plasma Physics* (Bristol: IOP Publ., 2001)
146. Fortov V E et al. *Usp. Fiz. Nauk* **174** 495 (2004) [*Phys. Usp.* **47** 447 (2004)]
147. Morfill G E et al. *Phys. Scripta* **T107** 59 (2004)
148. Ichimaru S *Rev. Mod. Phys.* **54** 1017 (1982)
149. Kremer K, Robbins M O, Grest G S *Phys. Rev. Lett.* **57** 2694 (1986)
150. Meijer E J, Frenkel D *J. Chem. Phys.* **94** 2269 (1991)
151. Fortov V E, Yakubov I T *Neideal'naya Plazma* (Nonideal Plasma) (Moscow: Energoatomizdat, 1994) [Translated into English (New York: Plenum, 2000)]
152. Hamaguchi S, Farouki R T, Dubin D H E *Phys. Rev. E* **56** 4671 (1997)
153. Vaulina O, Khrapak S, Morfill G *Phys. Rev. E* **66** 016404 (2002)
154. Khrapak S A et al. *Phys. Rev. E* **66** 046414 (2002)
155. Rytkönen A, Valkealahti S, Manninen M *J. Chem. Phys.* **106** 1888 (1997)
156. Stishov S M *Usp. Fiz. Nauk* **114** 3 (1974) [*Sov. Phys. Usp.* **17** 625 (1975)]
157. Van Vitzenburg W, Stryland J C *Can. J. Phys.* **46** 811 (1968)
158. Crawford R K, Daniels W B *Phys. Rev. Lett.* **21** 367 (1968)
159. Stishov S M, Fedosimov V I *Pis'ma Zh. Eksp. Teor. Fiz.* **14** 326 (1971) [*JETP Lett.* **14** 217 (1971)]
160. Cheng V M, Daniels W B, Crawford R K *Phys. Lett. A* **43** 109 (1973)
161. Zha C-S et al. *J. Chem. Phys.* **85** 1034 (1986)
162. Jephcoat A P, Beresin S, in *Proc. US-Japan Conf. Mineral Physics, Washington, 1997*
163. Alder B J, Hoover W G, Young D A *J. Chem. Phys.* **49** 3688 (1968)
164. Hoover W G, Gray S G, Johnson K W *J. Chem. Phys.* **55** 1128 (1971)
165. Berry R S, Smirnov B M *J. Chem. Phys.* **114** 6816 (2001)
166. Khanna S N, Jena P *Phys. Rev. Lett.* **69** 1664 (1992)
167. Wales D J, Berry R S *J. Chem. Phys.* **92** 4283 (1990)
168. Natanson G, Amar F, Berry R S *J. Chem. Phys.* **78** 399 (1983)
169. Berry R S, Jellinek J, Natanson G *Chem. Phys. Lett.* **107** 227 (1984)
170. Davis H L, Jellinek J, Berry R S *J. Chem. Phys.* **86** 6456 (1987)
171. Kunz R E, Berry R S *Phys. Rev. Lett.* **71** 3987 (1993)
172. Kunz R E, Berry R S *Phys. Rev. E* **49** 1895 (1994)
173. Schmidt M et al. *Phys. Rev. Lett.* **79** 99 (1997)
174. Schmidt M et al. *Nature* **393** 238 (1998)
175. Berry R S, Smirnov B M *Zh. Eksp. Teor. Fiz.* **125** 414 (2004) [*JETP* **98** 366 (2004)]
176. Berry R S *Chem. Rev.* **93** 2379 (1993)
177. Wales D J *Chem. Phys. Lett.* **166** 419 (1990)
178. Cheng H-P, Berry R S *Phys. Rev. A* **45** 7969 (1992)
179. Beck T L, Jellinek J, Berry R S *J. Chem. Phys.* **87** 545 (1987)
180. Haberland H, in *Metal Clusters* (Ed. W Ekardt) (Chichester: Wiley, 1999)
181. Haberland H, in *Atomic Clusters and Nanoparticles*: *Les Houches, Session LXXIII, 2 – 28 July 2000* (Eds C Guet et al.) (Berlin: Springer-Verlag, 2001)
182. Schmidt M et al. *Phys. Rev. Lett.* **86** 1191 (2001)
183. Schmidt M et al. *Phys. Rev. Lett.* **87** 203402 (2001)
184. Berry R S *Israel J. Chem.* **44** 211 (2004)
185. Gobet F et al. *Phys. Rev. Lett.* **89** 183403 (2002)
186. Reyes-Nava J A, Garzón I L, Michaelian K *Phys. Rev. B* **67** 165401 (2003)
187. Bixon M, Jortner J *J. Chem. Phys.* **91** 1631 (1989)
188. Labastie P, Whetten R L *Phys. Rev. Lett.* **65** 1567 (1990)
189. Wales D J *Mol. Phys.* **78** 151 (1993)
190. Wales D J, Berry R S *Phys. Rev. Lett.* **73** 2875 (1994)
191. Umirzakov I H *Phys. Rev. E* **60** 7550 (1999)
192. Mülken O, Stamerjohanns H, Borrmann P *Phys. Rev. E* **64** 047105 (2001)
193. Eitel W *The Physical Chemistry of the Silicates* (Chicago: Univ. of Chicago Press, 1954)
194. Bondi A *Physical Properties of Molecular Crystals, Liquids, and Glasses* (New York: Wiley, 1968)
195. Feltz A *Amorphe und glasartige anorganische Festkörper* (Berlin: Akademie-Verlag, 1983)
196. Kouchi A, Kuroda T *Jpn. J. Appl. Phys.* **29** L807 (1990)
197. Smirnov B M *Usp. Fiz. Nauk* **125** 331 (1978) [*Sov. Phys. Usp.* **21** 522 (1978)]
198. Naghizadeh J, Rice S A *J. Chem. Phys.* **36** 2710 (1962)
199. Bewilogua L, Gladun L, Kubsch B *J. Low Temp. Phys.* **4** 299 (1971)
200. Schmidt W F *Liquid State Electronics of Insulating Liquids* (Boca Raton: CRC Press, 1997)
201. Harms J, Toennies J P, Dalfovo F *Phys. Rev. B* **58** 3341 (1998)
202. Harms J et al. *Phys. Rev. B* **63** 184513 (2001)
203. Smirnov B M *Plasma Chem. Plasma Proc.* **13** 673 (1993); *Usp. Fiz. Nauk* **163** (10) 29 (1993) [*Phys. Usp.* **36** 933 (1993)]
204. Smirnov B M *Usp. Fiz. Nauk* **164** 665 (1994) [*Phys. Usp.* **37** 621 (1994)]
205. Smirnov B M *Usp. Fiz. Nauk* **170** 495 (2000) [*Phys. Usp.* **43** 453 (2000)]
206. Rose J P, Berry R S *J. Chem. Phys.* **98** 3246 (1993)
207. Cheng H-P, Landman U *Science* **280** 1304 (1993)
208. Cohen M H, Grest G S *Ann. New York Acad. Sci.* **371** 199 (1981)
209. Fox T G (Jr), Flory P J *J. Appl. Phys.* **21** 581 (1950)
210. Fox T G (Jr), Flory P J *J. Phys. Chem.* **55** 221 (1951)